ISSN 1980-9743

Soils and Rocks

Soils and Rocks

An International Journal of Geotechnical
and Geoenvironmental Engineering

Volume 33, N. 1
January-April 2010

Soils and Rocks Volume 33, N.1 2010

Soils and Rocks is an International Journal of Geotechnical and Geoenvironmental Engineering published by

ABMS - Brazilian Association for Soil Mechanics and Geotechnical Engineering
Av. Prof. Almeida Prado, 532, IPT/DEC-Prédio 54
05508-901 São Paulo, SP
Brazil

ABGE - Brazilian Association for Engineering Geology and the Environment
Av. Prof. Almeida Prado, 532, IPT/DIGEO- Prédio 59
05508-901 São Paulo, SP
Brazil

SPG – Portuguese Geotechnical Society
LNEC, Avenida do Brasil, 101
1700-066 Lisboa
Portugal

Issue Date: *April 2010*

Issue: *3,200 copies*

Manuscript Submission: *For review criteria and manuscript submission information, see Instructions for Authors at the end.*

SOILS and ROCKS

An International Journal of Geotechnical and Geoenvironmental Engineering

Editor Ennio Marques Palmeira - University of Brasília, Brazil

Co-editor Ricardo Oliveira - COBA, Portugal

Soils and Rocks publishes papers in English in the broad fields of Geotechnical Engineering, Engineering Geology and Geo-environmental Engineering. The Journal is published in April, August and December. Subscription price is US$ 90.00 per year. The journal, with the name "Solos e Rochas", was first published in 1978 by the Graduate School of Engineering-Federal University of Rio de Janeiro (COPPE-UFRJ). In 1980 it became the official magazine of the Brazilian Association for Soil Mechanics and Geotechnical Engineering (ABMS), acquiring the national character that had been the intention of its founders. In 1986 it also became the official Journal of the Brazilian Association for Engineering Geology and the Environment (ABGE) and in 1999 became the Latin American Geotechnical Journal, following the support of Latin-American representatives gathered for the Pan-American Conference of Guadalajara (1996). In 2007 the journal acquired the status of an international journal under the name of Soils and Rocks, published by the Brazilian Association for Soil Mechanics and Geotechnical Engineering (ABMS), Brazilian Association for Engineering Geology and the Environment (ABGE) and Portuguese Geotechnical Society (SPG).

Soils and Rocks

1978,	1 (1, 2)
1979,	1 (3), 2 (1,2)
1980-1983,	3-6 (1, 2, 3)
1984,	7 (single number)
1985-1987,	8-10 (1, 2, 3)
1988-1990,	11-13 (single number)
1991-1992,	14-15 (1, 2)
1993,	16 (1, 2, 3, 4)
1994-2009,	17-31 (1, 2, 3)
2010,	**32 (1,**

ISSN 1980-9743 CDU 624.131.1

ISSN 1980-9743

SOILS and ROCKS

An International Journal of Geotechnical and Geoenvironmental Engineering

Publication of

ABMS - Brazilian Association for Soil Mechanics and Geotechnical Engineering

ABGE - Brazilian Association for Engineering Geology and the Environment

SPG - Portuguese Geotechnical Society

Volume 33, N. 1, January-April 2010

Table of Contents

Articles

Soils and Rocks
v. 33, n. 1

Deep Rock Foundations of Skyscrapers

L. Ribeiro e Sousa, David Chapman, Tiago Miranda

Abstract. In the case of skyscrapers, the suitable bearing surfaces occur at considerable depth in rock formations, and when it is uneconomical to excavate the overlying weak material, socketed shafts are required for the foundations. In selecting a suitable foundation system, several factors must be taken into consideration. In this article problems associated to deep building foundations in rock formations are explained, as well as the actual evolution of skyscrapers. Geomechanical characterization in terms of deformability and strength of rock masses is analyzed in detail. The design processes of rock-socketed shafts are briefly explained and the foundations of some important buildings in New York and Chicago are presented with the available geotechnical information. Some conclusions on deep rock foundations of skyscrapers are presented.

Keywords: foundations, rock masses, skyscrapers, rock-socketed shafts, design values, settlements.

1. Introduction

The function of a building foundation is to transfer structural loads from a building safely into the ground. The foundation is a critical segment in the construction and performance of a skyscraper; statistics have shown that the most frequent cause of building collapse is an inappropriately built foundation. Therefore, the foundation must be properly designed and constructed. Its stability depends on the behavior of the ground on which it rests under the pressure of structural loads. This is affected by the foundation design and the ground characteristics.

The majority of foundations on rock are spread footings at the ground surface, but in the case of skyscrapers this type of footing may not be suitable. In these situations the suitable bearing surfaces often occur at considerable depths. Removal of the overlying weak material is likely to be uneconomical and socketed shafts are required. In selecting a suitable foundation system for a building, various factors must be taken into consideration including the ground conditions, load transfer pattern, shape and size of the building, site constraints, and the presence of underground structures or environmental issues.

The scope and the purpose of this article are to analyze deep rock foundations of skyscrapers and to provide explanations for caisson foundation design parameters based on general considerations about rock formations. Following this brief Introduction, Section 2 explains different deep rock foundations and evolution of the skyscrapers. Site and geomechanical characterization, in terms of deformability and strength, is analyzed in detail in Section 3. Section 4 shortly explains design processes for rock-socketed shafts and finally, Section 5 analyzes some tall buildings using standard expressions namely regarding settlements. Conclusions are presented in Section 6, as well as acknowledgements and cited references.

2. Evolution of Deep Rock Foundations

2.1. Types of deep foundations

Foundations on rock can be classified into spread footings, socketed shafts and tension foundations. The geotechnical information required for the design of all types of foundations consists of structural geology, geotechnical rock mass properties and ground water conditions (Wyllie, 1999).

Deep rock foundations transfer the load at a point far below the substructure. Deep foundations are used when adequate ground capacity is not available close to the surface and loads must be transferred to firm layers substantially below the ground surface. The common deep foundation systems for buildings are piles and caissons or shafts.

A pile is a column inserted in the ground to transmit the structural loads to a strong soil or rock deep underground. Piles are used in areas where near-surface soil conditions are poor. They are generally made of concrete, steel or a combination of both.

A caisson or shaft is a box or casing filled with concrete and forms a structure similar to a non-displacement pile but larger in diameter. Caisson foundations are used when soil or rock of adequate bearing strength is found below surface layers of weak materials. A caisson is also similar to a column footing in that it spreads the load from a column over a large area of soil so that the allowable stress in the soil is not exceeded. The lower ends of the caissons transfer the building load into the ground (Fig. 1). Ec represents the deformability modulus of the concrete.

There are different types of caissons, namely: i) *Bored* - some soil is removed and a caisson is set into the

L. Ribeiro e Sousa, Professor, Lachel Felice & Associates, P.O. Box 1059, 07962 Morristown, NJ, USA and Civil Engineering Department, University of Porto, Rua Dr. Rodrigo Frias s/n, 4200-465 Porto, Portugal. e-mail: ribeiro.e.sousa@gmail.com.
David Chapman, Engineering Consultant, Lachel Felice & Associates, P.O. Box 1059, 07962 Morristown, NJ, USA. e-mail: dchapman@lachel.com.
Tiago Miranda, Assistant Professor, Geotechnics Group, Civil Engineering Department, University of Minho, Campus of Azurém, 4800-058 Guimarães, Portugal. e-mail: tmiranda@civil.uminho.pt.
Submitted on May 26, 2008; Final Acceptance on December 8, 2008; Discussion open until September 30, 2010.

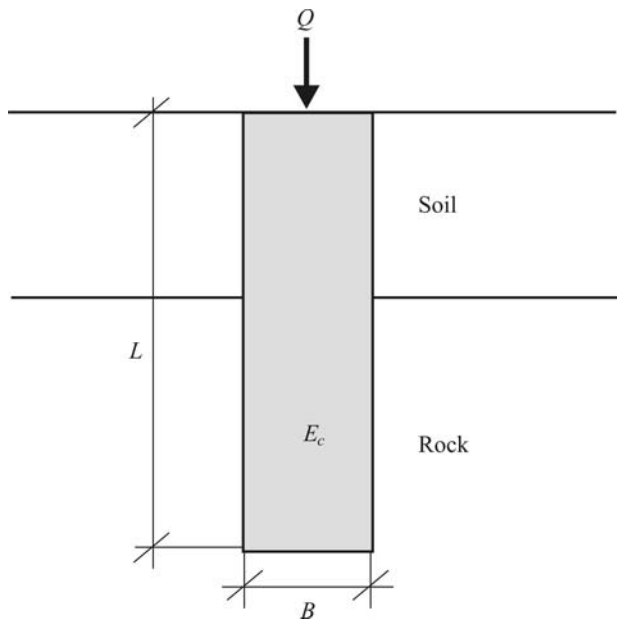

Figure 1 - Caisson or shaft foundation socket into rock.

hole; ii) *Socketed* - a socketed caisson is one that is drilled into rock at the bottom rather than belled; its bearing capacity comes from both its end bearing and frictional forces between the sides of the caisson and the rock; iii) *Box* - a box caisson is a structure with a closed bottom designed to be sunk into prepared foundations below water level; they are unsuitable for sites where erosion can damage the foundations, but they can be placed successfully on natural firm foundation material, on crushed rock placed after dredging soft material, or on a pile foundation; iv) *Pneumatic* - pneumatic caissons are usually used in riverbed work; a concrete box built with an airtight chamber at the bottom is constructed on ground; the air is compressed in the chamber, balancing with the ground water pressure to prevent the ground water from getting into the box and as soil is excavated and removed, the box is gradually sunk into the ground; steel shafts are connected to the pressurized working chamber as access for workers and excavation machinery.

2.2. Evolution of skyscrapers

The worldwide trend is towards living in megacities. It is estimated by 2030 that two thirds of the world population will be urbanized. Therefore a new generation of megacities is predicted to develop in the next twenty years. To accommodate this population the construction of tall buildings is expected to be a major tendency in those megacities (Binder, 2006).

The construction of tall buildings started at the end of the 19th century, particularly in the cities of New York and Chicago. Table 1 presents a list of the buildings that were each considered the tallest building in the world for a some period of time. Until the end of the 1990's all the tallest buildings were constructed in the United States.

Table 1 - Buildings that held the title of the tallest Building in the world (library.thinkquest.org).

Years	Building	Location	Height	Observations
1890-94	NY World Building	New York	94 m	Demolished 1955
1892-94	Masonic Temple	Chicago	92 m	Demolished 1939
1894-99	Manhattan Life Insurance Building	New York	106 m	Demolished 1930
1899-08	Park Row Building	New York	119 m	3,900 piles driven to sand and granite. 29 stories
1908-09	Singer Building	New York	187 m	Demolished 1968
1909-13	Metropolitan Life Insurance Company	New York	213 m	-
1913-30	Woolworth Building	New York	241 m	-
1930	40 Wall Street	New York	283 m	70 storey skyscraper
1930-31	Chrysler Building	New York	319 m	-
1931-72	Empire State Building	New York	381 m to roof	102 storey skyscraper
1972-73	World Trade Center (Twin Towers)	New York	417 m to roof	Designed with columns grouped around the perimeter and within core
1972-98	Sears Tower	Chicago	442 m to roof	-
1998-04	Petronas Twin Towers	Kuala Lum-pur	403 m to roof	The foundations are the deepest in the world
2004-08	Taipei Financial Centre	Taipei	509 m to top	Foundations with deepest dolomite bedrock
2008-	Burj Dubai	Dubai	800 m+	Underway

Nowadays the top four tallest buildings are lead by the tall skyscraper in Taiwan's capital followed by the twin Petronas Towers in Kuala Lumpur, Malaysia. The alignment also shows Chicago's Sears Tower in third place, with Shanghai's Tower in fourth as it is shown in Fig. 2.

The Taipei 101 tower has 101 stories above ground and five underground. Details of the foundation are shown in Fig. 3. The rock formations are dolomites. The building holds several records, namely the distance from the ground to the structural top (509 m), the ground to the roof (449 m) and the fastest ascending elevator speed. However the longest distance from ground to antenna is still held by Sears Tower with 527 m.

The Petronas Twin towers are the tallest twin towers in the world, owned by Malaysia's national oil company. They are supported by deep foundations of varying lengths consisting of rectangular cast-in places piles that extend to 130 m below grade with ground improvement up to 162 m depth. The challenges of the foundation were to be built on karstic bedrock (DFI, 2008).

However, several spectacular new buildings are planned for construction in the near future as shown in Table 2.

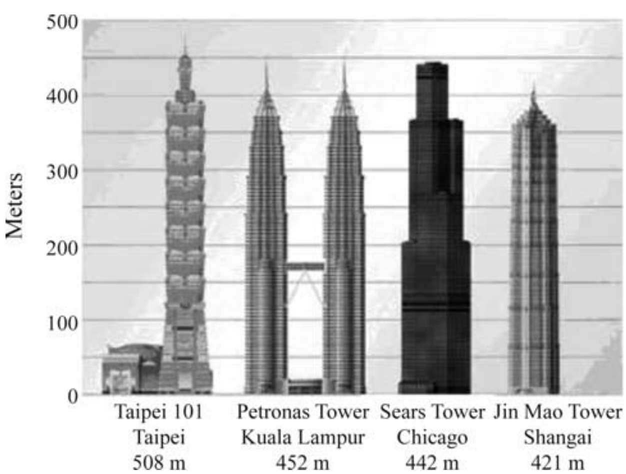

Figure 2 - Worlds top four tallest buildings (library.thinkquest.org).

The Palm tower also designated by Al Burj tower, a proposed skyscraper in Dubai, United Arab Emirates, will stand as the highest with about 643 m high to roof, and 808 m to antenna (Fig. 4). The site for the tower is an offshore island, which posed an unusual challenge to building. The Al Burj tower is built in reinforced concrete and is very slender in form. The 160-story tower has a hotel in the base, apartments from the 20th to the 110th story and offices above. The foundation evaluation was complicated by highly variable weak rock and high design loads. The designer developed an Osterberg load test program, testing several combinations of barrettes and bored piles from 50 to 75 m in depth (STS, 2006).

However, there are big changes coming in rankings. In the CBTUH Conference held in 2008, in its view of

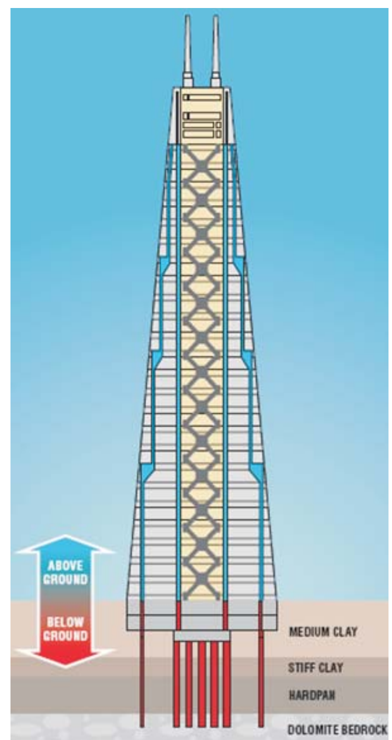

Figure 3 - Dolomite foundations of Taipei 101 tower (STS, 2006).

Table 2 - Tallest buildings in the near future.

Year of completion	Building	Location	Height	Observations
2009	Freedman Tower	New York	417 m to roof; 541 m to antenna	-
2009	Burj Dubai	Dubai	643 m to roof; 808 m to antenna	Foundation with 192 piles descending to a depth of more 50 m
2009	Trump Int. Hotel & Tower	Chicago	-	Bearing capacity of 25.9 MPa
2009	China Building TV Tower	Guan-gzhou	610 m	The base footprint is triangular
2011	Chicago Spire	Chicago	610 m to roof	Bearing capacity of 28.7 MPa
2012	Moscow Tower	Moscow	612 m	130-story tower

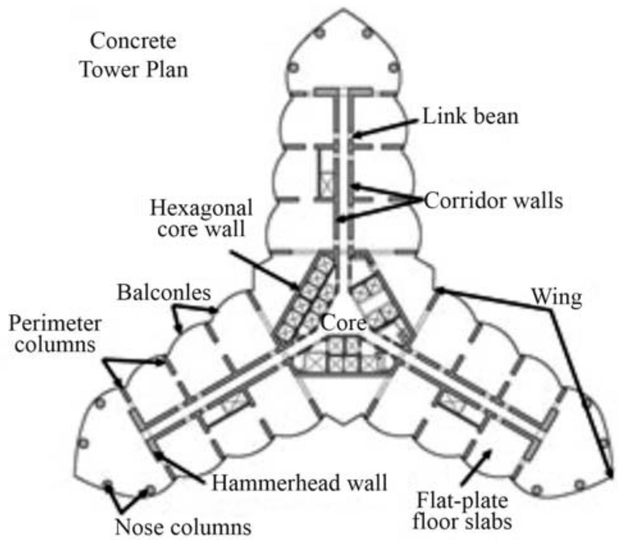

Figure 4 - Concrete tower plan of Al Burj tower (Reina, 2006a).

Figure 5 - Location of Chicago Spire near the lake (Hampton, 2007).

2020, there are proposals of 1,050 m Al Burj in Dubai and 1,001 m Burj Mubarak al-Kabir in Subiya, Kuwait (Post, 2008a, b).

In the Middle East, numerous skyscrapers are under construction as shown in Table 3. At the end of 1999, the 321 m Burj Al Arab, in Dubai, became the world's tallest hotel and in 2000; the Emirates Tower, also in Dubai, was finished, a twin-tower project composed of a 355 m office tower and a 309 m hotel (Binder, 2006).

In the USA special mention is made of the Chicago Spire which will be a 610 m tall twisting spire designed by architect-engineer Santiago Calatrava. The splendid spire, to overlook Lake Michigan, would easily top the 442 m high Sears tower as the US tallest building. Figs. 5 and 6 give images of the proposed tower. The building is located at Lake Shore Drive and the groundbreaking was on June 25, 2007. The predicted completion is in the year 2011 and the building will provide a floor area of about 278,700 m^2 (Hampton, 2007).

Calatrava's latest concept in skyscrapers is an all-concrete building of square-shaped floors that stack onto each other in two-degree horizontal offsets. The finished effect is an approximately 488 m tall structure that twists 360° from bottom to top. Each floor would have four concave sides and cantilevered corners. A tapering concrete core would resist wind and gravity loads, while 12 shear walls radiating from the core would provide additional support. The tower is composed by 300 condos and placed in the top a luxury hotel (Hampton, 2007).

After the tragedy of September 11, 2001, an imaginative outcropping of design has emerged in order to rebuild the World Trade Centre site in New York.

The official proposal comprehends 7 tall buildings. The Freedom tower designed by Norman Foster & Partners will be the most impressive. Figure 7 shows an image of the tower to be finished in 2009. The building heights are 417 m to the roof and 541 m to the antenna. It has a sloping roof on a 70-story building, and an open-air superstructure, windmills and suspension cables (Stephens, 2004).

Table 3 - Tallest buildings in the Middle East.

Name	City	Country	Year	Storys	Height (m)
Burj Dubai	Dubai	UAE	2009	150+	700+
Abraj Al Bait	Makkah	Saudi Arabia	2008	76	485
Burj Al Alam	Dubai	UAE	2009	108	484
Dubai Towers	Doha	Qatar	2008	86	445
Princess Tower	Dubai	UAE	2009	102	414
Al Hamra Tower	Kuwait City	Kuwait	2009	77	412
23 Marina	Dubai	UAE	2008	90	389
Najd Tower	Dubai	UAE	2008	82	375
The Torch	Dubai	UAE	2008	80	345

In Europe, the first skyscraper was built at Antwerp, Belgium, in 1932: the 26-storey Torengebouw that remained until the 1950s. Until the early 1970s, many high buildings in Europe were hotels. Moscow's 34 storey Ukraina hotel constructed in 1957 remains Europe's tallest hotel. Nowadays, Europe is not known as a tall buildings zone, however some important tall buildings have been constructed as referred in the publication of Binder (2006).

Figure 6 - Detailed view of Chicago Spire (DFI, 2008).

Figure 7 - Location of Freedom tower (Stephens, 2004).

In Moscow, several impressive tall buildings are under construction. Special reference is made to the proposed 520,800 m^2 Moscow Tower, sited a few kilometers from Red Square, which would provide office, residential and conference space. This skyscraper in Moscow will be potentially the Europe's tallest building. It was designed by Norman Foster & Partners. The building is a 130-story tower and its basement will be over 30 m deep in alternating clay and limestones.

3. Site and Geomechanical Characterization

3.1. General

Due to the variability of rock formations, the evaluation of geotechnical properties is one of the issues with the largest degree of uncertainty. This fact is a consequence of the complex geological processes involved and to the inherent difficulties of geomechanical characterization (ASCE, 1996; Sousa *et al.*, 1997; Miranda, 2003). The evaluation of the geomechanical parameters is mainly carried out through *in situ* and laboratory tests and also by the application of empirical methodologies (Bieniawski, 1989; Barton, 2000; Hoek, 2006).

In situ tests for the deformability characterization are normally carried out by applying a load in a certain way and measuring the correspondent deformations of the rock mass. Shear and sliding tests for strength characterization are normally performed in low strength surfaces. These strength tests are expensive and the strength parameters evaluation of the rock mass is normally carried out indirectly by the Hoek and Brown (H-B) strength criteria normally associated with the GSI empirical system.

Laboratory tests affect only a small rock volume and consequently it is necessary to perform a considerable number of tests in the rock and in the discontinuities in order to characterize the variability of the determined geomechanical parameters. Laboratory tests such as the determination of uniaxial compressive strength (UCS), point-load and discontinuities tests are also very important for the empirical methodologies.

Based on experience, it can be said that it is necessary to obtain direct geomechanical information from the site and it is not adequate to extrapolate from other situations. Only generic considerations can be made in order to obtain answers to the problem of deep foundations without site-specific geomechanical information.

However, the knowledge of the intact rock properties is always important. Some results obtained from a compilation of rock properties performed by Judd (1969) are presented in Table 4.

One of the goals of the study conducted by Judd (1969) was to establish rock property values that can be correlated with an acceptable correlation coefficient, and then minimize the types of tests required for design and construction of engineering structures.

The study indicated that there appears to be some usable degree of linear correlations between the rock properties determined by dynamic loads and its unconfined compressive strength, and with elastic properties measured by static load tests and its impact toughness.

Table 4 - Rock properties obtained from Judd (1969).

Rock	Properties	Values		
		Mean	Max.	Min.
Dolomite	Mod. def. (GPa)	29.0	73.6	2.1
	UCS (MPa)	214	365	20
	Permeab. (see 1)	1	2	1
	Poisson ratio	0.12	0.25	0.01
Basalt	Mod. def. (GPa)	38.8	75.9	1.7
	UCS (MPa)	23.4	45.5	2.1
	Permeab. (see 1)	2	3	1
	Poisson ratio	0.16	0.42	0.01
Breccia	Mod. def. (GPa)	12.3	17.7	5.4
	UCS (MPa)	11.0	29.3	0.8
Diorite	Mod. def. (GPa)	69.7	106.7	33.8
	UCS (MPa)	203.4	333.1	84.1
	Permeab. (see 1)	1	1	1
	Poisson ratio	0.25	0.32	0.15
Gneiss	Mod. def. (GPa)	51.4	103.4	7.2
	UCS (MPa)	178.6	304.8	35.9
	Permeab. (see 1)	1	2	1
	Poisson ratio	0.21	0.35	0.10
Granite	Mod. def. (GPa)	28.3	79.4	0.3
	UCS (MPa)	161.4	353.1	35.2
	Permeab. (see 1)	1	2	1
	Poisson ratio	0.16	0.26	0.05
Limes-tone	Mod. def. (GPa)	38.4	81.4	0.1
	UCS (MPa)	75.2	260.7	1.4
	Permeab. (see 1)	2	4	1
	Poisson ratio	0.22	0.48	0.01
Sand-stone	Mod. def. (GPa)	7.1	90.3	0.1
	UCS (MPa)	62.7	328.3	2.1
	Permeab. (see 1)	3	4	1
	Poisson ratio	0.12	0.50	0.01

(1) 1 = 0.001-1 x 10^{-8} m/s; 2 = 1-100 x 10^{-8} m/s; 3 = 100-100,000 x 10^{-8} m/s; 4 > 100,000 x 10^{-8} m/s.

Typical *in situ* load-deformation behavior of the rock mass is completely different from that observed in laboratory tests, mainly due to the presence of discontinuities in the rock mass. Rock masses exhibits characteristics of the rock material and discontinuities, which tend to make the deformability and strength properties of the rock foundations highly direction dependent (Kulhawy & Goodman, 1987).

To characterize rock masses for major building foundations, extensive and specialized exploration programs have to be conducted. They consist normally of vertical borings or even large-diameter shafts which allow a direct examination of the sidewalls and provide access for obtaining high-quality undisturbed samples. Extensive laboratory testing is done and *in situ* testing is carried out to measure the strength and deformability properties of the rock mass (Kulhawy and Carter, 1992a; ASCE, 1996; Sousa *et al.*, 1997).

3.2. Deformability properties

The mechanical characterization of the rock masses formations can be carried out through representative amounts of *in situ* tests. They are in general expensive and subject to significant uncertainties. A good site characterization together with the use of empirical methodologies should be used in the assessment of the design values for geomechanical parameters.

The characterization is also made through laboratory tests on the intact rock and on the discontinuities. The main question is related to their representativeness due to the small volume involved in the tests. Table 5 gives a summary of the primary *in situ* and laboratory tests of rock formations and intact rocks (Rocha, 1971; Baguelin *et al.*, 1978; ASCE, 1996).

Considering the evaluation of the deformability parameters, *in situ* tests can involve small volumes as in the case of the dilatometers or pressuremeters, or large volumes as in case of Large Flat Jacks (LFJ) tests or Plate Load Tests (PLT). Figure 8 presents approximate values of the involved volumes reporting experience in several projects.

In situ tests performed inside a borehole involve small volumes of the rock masses and they can be grouped in two main types, depending on the way the pressure is applied to the walls of the borehole (Baguelin *et al.*, 1978; Sousa *et al.*, 1997):

• Application of pressure through a flexible membrane adapted to the walls of the hole with an axyssimetrical pressure. Using dilatometers, as it is the case of the BHD dilatometer used in Portugal, radial deformations are measured while for the pressuremeter a volumetric deformation is measured. The last is more suitable to be used in soft rocks.

• Application of the pressure through rigid plates in two circumferential arches, which corresponds to a more complex load situation and consequently has more associ-

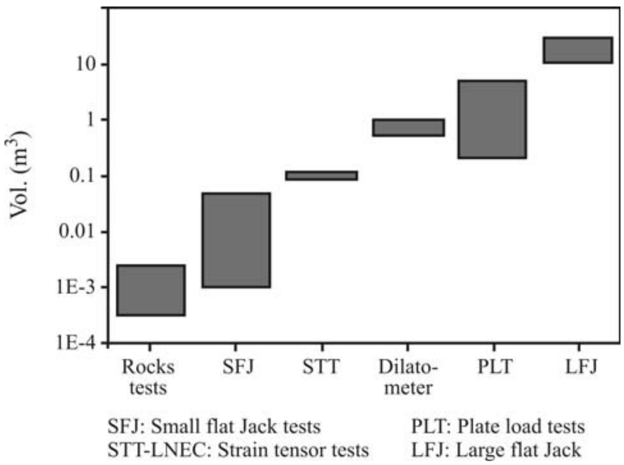

Figure 8 - Approximate volumes involved for different tests (Miranda, 2007).

ated interpretation challenges, as it is the case of Goodman jack dilatometer.

In situ tests in a gallery or at the surface can involve larger volumes, being therefore more representative. Not considering radial load tests and biaxial or triaxial *in situ* tests, the primary *in situ* tests are the following:

• PLT – the load is applied by means of a jack and the rock displacements are measured at the surface or in boreholes behind each loaded area.

• LFJ tests – the load is applied in the walls of one or more opened slots. There are also the SFJ tests that involve a smaller area but allow in addition determining the *in situ* stress state components.

• Seismic tests between boreholes and galleries – these tests allow determining the dynamic modulus measuring S and P wave's velocities. The values obtained are different from the static ones due to difference in time and deformation level applied during the tests. They can involve considerable volumes and can be correlated with the static tests results.

There are no universal rules to define which tests should be carried out for a given situation since each test presents advantages and drawbacks. A good plan should rely on engineering experience and the particular project issues. For rock masses presenting high anisotropy levels, tests should be carried out in order to define the parameters that characterize that anisotropy. This can be carried out by computing indexes which relate rock properties (for instance the uniaxial compressive and point load strengths and longitudinal wave velocity) perpendicular and parallel to planes of anisotropy.

In order to quantify the rock mass deformability the number of *in situ* tests should be rationalized. Excluding the situation of important faults involved, a methodology combining a small number of large scale tests with a larger number of small scale tests should be adopted (Sousa *et al.*, 1997):

Table 5 - *In situ* and laboratory tests for Rock Mechanics (adapted from ASCE, 1996).

Purpose of tests	*In situ* tests	Laboratory tests
Deformability	Geophysical (refraction) Dilatometer/pressuremeter LFJ and SFJ PLT Borehole jacking Chamber pressure	Uniaxial compression Triaxial compression Swelling Creep
Strength	Direct shear Rock pressuremeter Uniaxial compression Borehole jacking	Uniaxial compression Direct shear Triaxial compression Direct tension Brazilian Point load
Permeability	Constant head Falling head Well pumping Pressure injection	Gas permeability Water content Porosity Absorption
Stress conditions	Hydraulic fracturing Overcoring SFJ Pressuremeter-dilatometer	Overcoring biaxial Overcoring triaxial
Others	Anchor-rockbolt loading	Unit weight Rebound Sonic waves Abrasion resistance

• Zoning of the rock mass considering the available geotechnical information and the use of empirical systems.

• For each zone, small scale *in situ* tests should be executed in boreholes or galleries. They should be in sufficient number in order to assure a good characterization of the rock mass. The location of the tests can be chosen randomly in order to obtain a representative mean value of the deformability modulus or in zones in which lower values are expected.

• For each zone, *in situ* large scale tests can be executed in a smaller number. The results should be calibrated with the values obtained in the small scale tests. Depending on the deformability values, three different situations can be considered, as indicated in Table 6.

Empirical classification systems are also used for the purpose of deformability characterization of rock masses.

Table 6 - Evaluation of large scale tests needs.

Situation	E (GPa)	Large scale tests
I	$E \geq 10$	Advisable
II	$5 \leq E < 10$	Necessary
III	$0.1 \leq E < 5$	Necessary with high precision

Several proposals have been made in the literature (Miranda, 2007). The systems present several drawbacks and intrinsic limitations that should be known by the design engineers for their correct use. The empirical systems with wider application for the preliminary calculation of geomechanical parameters are the RMR, Q and GSI systems. Table 7 presents some of the more representative analytical expressions developed by several authors, as well as their limitations and references.

Also, Data Mining (DM) techniques can be applied in order to obtain new models for geomechanical characterization. A methodology was developed and applied to the granite rock mass formations of the Venda Nova II underground hydroelectric scheme (Lima *et al.*, 2002). The available data was mainly obtained through the application of the most widely used empirical systems and from the results traditional laboratory and *in situ* tests (LFJ, SFJ and dilatometers). Concerning the empirical classification systems applications, and for the underground powerhouse complex, data was organized in a database composed of 1230 examples and with 22 attributes. Several new models were established for these homogeneous granite formations (Miranda, 2007).

The developed models were updated with information obtained through large scale tests (LFJ tests) in a generic Bayesian framework, and finally through the observed behavior of the underground structures during construction (Miranda, 2007; Miranda *et al.*, 2008).

In many cases, the displacements of rock foundations control the design. Several models have been established for foundations on rock assuming the idealization of the discontinuous rock mass as an isotropic or anisotropic elastic continuum (Kulhawy and Carter, 1992b; Yufin *et al.*, 2007).

For these models, and for engineering purposes, it is useful to define a modulus reduction factor α, which represents the ratio of deformability modulus between rock mass and a smaller element of the rock material. Figure 9 represents the modulus reduction factor *vs.* the RMR coefficient. The correlation is based on values referenced in Bieniawski (1975), regarding foundations of dams, bridges, tunnels and power plants, and experimental results from the Venda Nova II hydroelectric scheme (Lima *et al.*, 2002; Placencia, 2003; Miranda, 2007), the Miranda II hydroelectric scheme (Sousa *et al.*, 1999), the Porto Metro (Miranda, 2003) and the Socorridos hydroelectric scheme (Cafofo, 2006) were added.

The curve that better fits the experimental results is represented by the Eq. (1):

$$\alpha = 0.083\, e^{[0.0269\, RMR]} \tag{1}$$

3.3. Strength properties

For the determination of the rock mass strength parameters, large scale *in situ* and laboratory tests for the in-

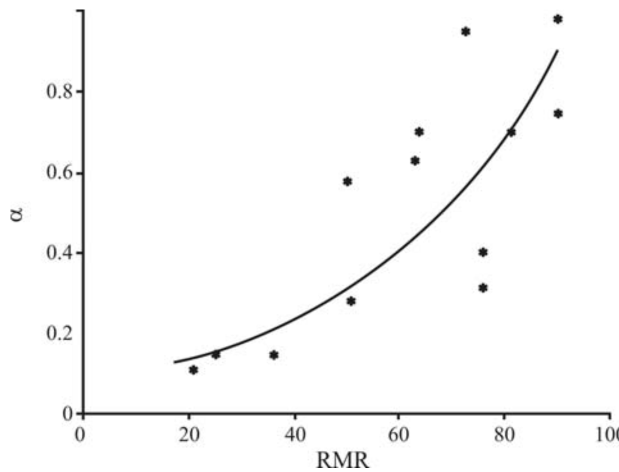

Figure 9 - Modulus reduction factor *vs.* RMR.

tact rock and discontinuities can be executed. The main *in situ* tests are: sliding or shearing on discontinuities, in the fault filling materials and along other low strength surfaces and at the rock mass/concrete interfaces. The primary laboratory tests for intact rock strength evaluation are (Rocha, 1971; ASCE, 1996): uniaxial compression, triaxial, diametral linear (Brazilian test), point load, uniaxial tension, shear and tension (Table 5).

In this context the use of empirical systems represents an important tool for the prediction of strength parameters for a given failure criterion. The GSI (Geological Strength Index) system was specially developed to obtain rock mass strength parameters (Hoek, 2006). The system uses the qualitative description of two fundamental parameters of the rock mass: its structure, and the condition of its discontinuities. This system has also been used for evaluation of heterogeneous rock masses in Porto Metro and tunnels in Greece and other difficult rock mass conditions like flysch (Marinos & Hoek, 2005; Babendererde *et al.*, 2006).

Normally, the calculation of the GSI value is based on correlations with modified forms of the RMR and Q indexes, taking into consideration the influence of groundwater and orientation of discontinuities (Hoek, 2006). Other approaches, defined by several authors, can be used for the GSI evaluation (Miranda, 2007).

Based on experimental data and theoretical knowledge of fracture mechanics, the H-B criterion for rock masses is translated by:

$$\sigma'_1 = \sigma'_3 + \sigma_c \left(m_b \frac{\sigma_3}{\sigma_c} + s \right)^a \tag{2}$$

where σ'_1 and σ'_3 are, respectively, the maximum and minimum effective principal stresses, m_b a reduced value of the m_i parameter which is a constant of the intact rock, and s and a are parameters that depend on characteristics of the rock formation. Serrano *et al.* (2007) extended this failure

Table 7 - Analytical expressions for the calculation of E based in empirical systems (adapted from Miranda, 2007).

System	Expression	Limitations	Reference
RMR	E (GPa) = $10^{(RMR - 10)/40}$	$RMR \leq 80$	Serafim & Pereira (1983)
	E (GPa) = 2RMR - 100	$RMR \geq 50 \wedge \sigma_c \geq 100$ MPa	Bieniawski (1978)
	$E(\text{GPa}) = \frac{\sqrt{\sigma_c}}{10} 10^{(RMR-10)/40}$	$\sigma_c \leq 100$ MPa	Hoek & Brown (1997)
	E (GPa) = $0.3H^{\alpha}$ 10(RMR - 20)/38	$\sigma_c > 100$ Mpa $\wedge H > 50$ m	Verman (1993)
	$E = E_i /100 \times\ 0.0028RMR^2 + 0.9e^{(RMR/22.28)}$	-	Nicholson & Bieniawski (1997)
	$E/E_i = 0.5 \times\ (1 - \cos(\pi \times RMR/100))$	-	Mitri *et al.* (1994)
	E (GPa) = $0.1 \times (RMR/10)^3$	-	Read *et al.* (1999)
Q	E (GPa) = $25 \times \log Q$	$Q \geq 1$	Barton *et al.* (1980)
	E (GPa) = $10 \times Q_c^{1/3}$; $Q_c = Q\sigma_c/100$	$Q \leq 1$	Barton & Quadros (2002)
	E (GPa) = $H^{0.2} \times Q^{0.36}$	$H \geq 50$ m	Singh (1997)
	$E(\text{GPa}) = 7 \pm 3\sqrt{Q'}$	-	Diederichs & Kaiser (1999)
GSI	$E(\text{GPa}) = (1 - D/2)\frac{\sqrt{\sigma_c}}{10} 10^{(GSI-10)/40}$	$\sigma_c \leq 100$ MPa	Hoek *et al.* (2002)
	E (GPa) = $(1 - D/2)\ 10^{(GST - 10)/40}$	$\sigma_c \geq 100$ MPa	Hoek *et al.* (2002)
	$E(\text{GPa}) = E_i \left(\frac{1 - D/2}{1 + \exp((60 + 15D - GSI)/11)} \right)$	-	Hoek & Diederichs (2006)
	$E(\text{GPa}) = 100000 \left(\frac{1 - D/2}{1 + \exp((60 + 15D - GSI)/11)} \right)$	-	Hoek & Diederichs (2006)
	E (GPa) = $E_i\, s^{1/4}$	-	Carvalho (2004)
	E (GPa) = $E_i\, (s^a)^{0.4}$	-	Sonmez *et al.* (2004)

α varies between 0.16 and 0.30 (higher for poorer rock masses); H is depth.

criterion to 3D in order to consider the intermediate principal stress in the failure strength of rock masses.

The H-B criterion has some limitations that should be taken into account and some developments have been introduced (Douglas, 2002; Carter *et al.*, 2007; Carvalho *et al.*, 2007).

Once the value of GSI is determined, the parameters of the H-B criterion can be calculated through the following equations:

$$m_b = m_i \exp\left(\frac{GSI - 100}{28 - 14D}\right)$$
$$s = \exp\left(\frac{GSI - 100}{9 - 3D}\right) \quad (3)$$
$$a = \frac{1}{2} + \frac{1}{6}\left(\frac{GSI - 100}{9 - 3D}\right)$$

where D is a parameter developed for the underground works of the Porto Metro that depends on the disturbance to which the rock mass formation was subjected due to blasting and stress relaxation (Hoek *et al.*, 2002). For $GSI > 25$, m_b can also be calculated through the expression:

$$m_b = m_i s^{1/3} \quad (4)$$

For many cases of foundations on rock and for certain geotechnical software, it is convenient to use the equivalent cohesion (c') and friction angle (φ') to the H-B criterion parameters. The range of stresses should be within $\sigma_{t,mass} < \sigma_3 \leq \sigma'_{3max}$. The value σ'_{3max} should be determined for each specific case:

$$\frac{\sigma'_{3\max}}{\sigma'_{cm}} = 0.47\left(\frac{\sigma'_{cm}}{\gamma H}\right)^{-0.94} \quad (5)$$

where σ'_{cm} is the rock mass strength, γ is the volume weight and H the depth. The equivalent values of φ' and c' are then given by expressions that can be obtained from the publication of Hoek *et al.* (2002).

It is worth mentioning that Data Mining techniques were also applied in order to obtain new models for the strength parameters, namely c' and φ' in granite formations (Miranda, 2007).

3.4. Selection of design geomechanical parameters

In the adoption of shear strength parameter values taken for design purposes are selected rather than determined. The selection of deformability and strength parameters for foundation on rock requires mainly sound engineering judgment and experience based on the results of tests performed and on the use of empirical systems (ASCE, 1996; Wyllie, 1999).

The selection of design shear strength parameters is dependent on the site geological structure taking into consideration the discontinuities, the rock and planes of weakness.

Failure envelopes for upper and lower bounds of shear strength can be determined for the three potential types of failure surfaces, namely for intact rock, clean discontinuities and filled discontinuities. Technical Engineering and Design Guides from US Army Corps of Engineers, n. 16, describes the appropriate selection procedures (ASCE, 1996).

Using the H-B criterion, the publication from Serrano & Olalla (2007), published at the 11th ISRM Congress, presents a synthesis of the applicability of this criterion and the identification of the applicable parameters. The most important hypotheses of the developed work are related to the theory of plasticity.

The deformational response of a deep rock foundation must be assessed in order to estimate the building settlements and the implications in the neighboring structures. Assumptions for deformation and settlements are normally based on the hypothesis that the rock mass behaves as a continuum and the expressions used are based in the theory of elasticity. Therefore, the selection of design parameters normally involves the selection of Poisson's ratio and deformability modulus. For almost all rock masses, Poisson's ratio varies between 0.1 and 0.35 and as a rule, lower values correspond to poorer quality rock masses. The selection of an adequate deformability modulus is most important in order to make reliable predictions of deformations and settlements of deep rock foundations.

4. Design Processes of Rock-Socketed Shafts

4.1. Introduction

The design of deep rock foundations includes the typical bearing capacity and settlement analyses. These analyses are performed to establish the capacity of the foundation to support the loads without bearing failure and without excessive deformations or settlements. Available data should be obtained during design, including geomechanical information of the rock mass as discontinuities, faults and other features; depth of overburden; ground water condition and load conditions (Kulhawy & Carter, 1992a,b; ASCE, 1996).

Rock-socketed shafts or caissons are constructed in drill holes extending below the building to depths where sound rock masses can sustain the applied loads. They are used where structural loads are substantial and allowable settlements small as is the case for tall buildings. Drilled shafts are usually oriented vertically and used to support compressive loads.

Drilled shafts may be installed or drilled through the soil to end bearing on rock or drilled to some depth into the rock. Drilling large diameter holes in rock is expensive and consequently the length and the diameter of the socket should be minimized. An investigation of the ground conditions should be carried out in order to identify the geological features. When dealing with karstic formations it is necessary to perform borings in order to find the optimum depth and plan location of shafts. In these cases the approach for foundation design has to accommodate a high degree of uncertainty.

It is important to obtain information about the compressive strength of the rock in order to determine the bearing capacity and the deformability modulus used to predict settlements. Rock mass deformability modulus can be determined using dilatometer or rock pressuremeter tests, correlated if possible with more accurate *in situ* tests like the PLT. Information on ground water is essential for determination of the construction conditions.

Socketed shafts can be designed to support the loads in side-wall shear comprising adhesion or skin friction on the socket wall; or end bearing on the material below the tip; or a combination of both. When the shaft is drilled some depth into sound rock, a combination of side-wall shear and end bearing can be assumed. Foundation capacity depends on the shaft materials, the geotechnical material where the shaft is founded, the loading and the construction method. The mechanism of load transfer and settlement of the shaft is illustrated in Fig. 10. In the figure, k_s and k_b represent, respectively, the shaft resistance and the bearing end. The support provided in side-wall shear Q_s and end bearing Q_b are equal to the product of the displacement and the applicable spring stiffness ($Q_s = k_s\delta_s$ and $Q_b = k_b\delta_b$).

In the third case presented in Fig. 10, the shaft has been drilled through material with low modulus to end bearing on material with higher deformability modulus. It means that k_b is much greater than k_s. Much of the displacement will occur due to elastic shortening of the shaft and relatively small amount due to deflection of the material below the shaft base. Most of the load is carried in end bearing for this configuration (Wyllie, 1999).

The behavior of rock socketed shafts has been studied through laboratory and *in situ* tests and by using numerical models. The results of this investigation work have shown that the following factors have important influence on the

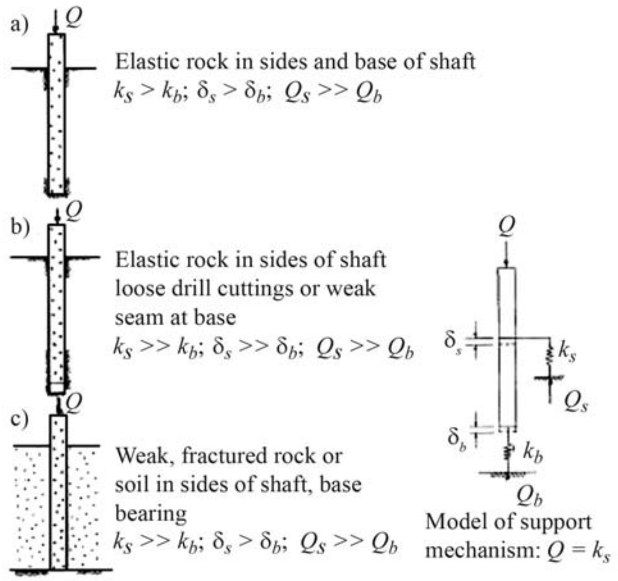

Figure 10 - Simplified support mechanism for socketed shafts (adapted from Wyllie, 1999).

load capacity and settlement of the shaft (Kulhawy & Carter, 1992a; Wyllie, 1999):

• *Socket geometry* - The geometry of a rock socket is defined by the length to diameter ratio and has significant effect on the load capacity of the shaft. As the ratio increases, the load carried in end bearing diminishes and progressively more load is carried in side-wall shear.

• *Rock mass modulus* - The shear stress on the side-walls of a socket is partially dependent on the normal stress acting at the rock mass surface and the magnitude of normal stress related to the stiffness of the surrounding rock formation.

• *Rock mass strength* - The shear strength on the side-walls of the socket and the bearing capacity of the rock mass below the shaft base are related to the strength of the rock mass. Shear strength behavior is different of rough and smooth sockets.

• *End of socket* - If it is assumed that load is carried in end bearing, it is fundamental to assure that the end of socket should be cleaned, because a low modulus material in the socket base will allow considerable displacements of the shaft to take place before end bearing is mobilized. The use of TV cameras can be of assistance in performing the inspection.

• *Rock mass layering* - Layers of weak rock in the socket and at the base may influence the load bearing capacity of the shaft.

• *Creep* - In formations subject to creep, the influence of time can have a great importance. The proportion of the load carried in end loading varied from 15 to 20% of the load at the top of the shaft. While the strain gauges along the shaft showed increasing load with time, the load at the base showed minimal increase.

To predict the strength properties of the rock mass, the use of empirical systems is nowadays very important and the H-B criterion is usually applied. A synthesis of the numerical analysis related to the ultimate bearing capacity and pullout strength force for deep and shallow foundations using the H-B criterion was recently presented (Serrano & Olalla, 2007). The theory associated to the ultimate bearing capacity evaluation at the tip of a pile embedded in rock is also presented in the referenced publication. Figure 11 shows a simplified scheme of the plastic flow net at the tip of a shaft.

The design and construction of deep foundations can be carried out as represented in Fig. 12. Design starts with site investigation and ground parameter evaluation varying in quality and quantity according to the importance and complexity of the project.

Possible foundation schemes are identified based on the results of the investigation, load requirements and local practice. All possible schemes are evaluated relying on load tests. The objectives of these tests are to verify that the shafts' response to loading are in agreement with anticipated response, and to ensure that the ultimate capacities are not less than the calculated ones.

The Osterberg Load tests, also referred to O-cell tests, are commonly used in conjunction with drilled shafts and are often a cost-effective alternative to static load tests. They can be placed anywhere within the shaft (Figs. 13 and 14). In all applications the cell expands to apply equal loads to the portions of the foundation element above and below the cell. Recent history shows a significant increase in maximum loads applied during these tests (England & Cheesman, 2005).

4.2. Design values

Rock socketed shafts can be designed to carry compressive loads in side-wall shear only, end bearing only or combination of both. Important factors affecting the design

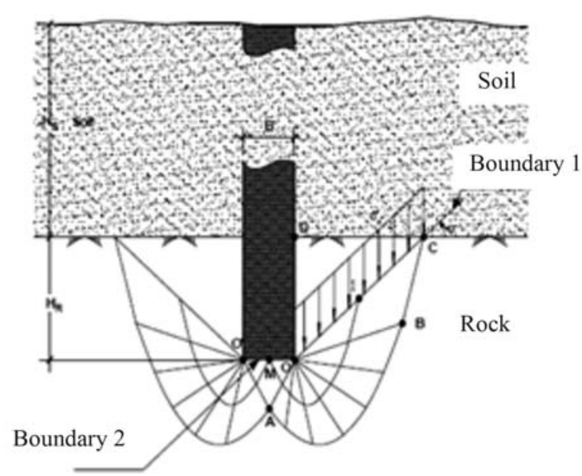

Figure 11 - Simplified scheme of the plastic flow net at the tip of a shaft (Serrano & Olalla, 2007).

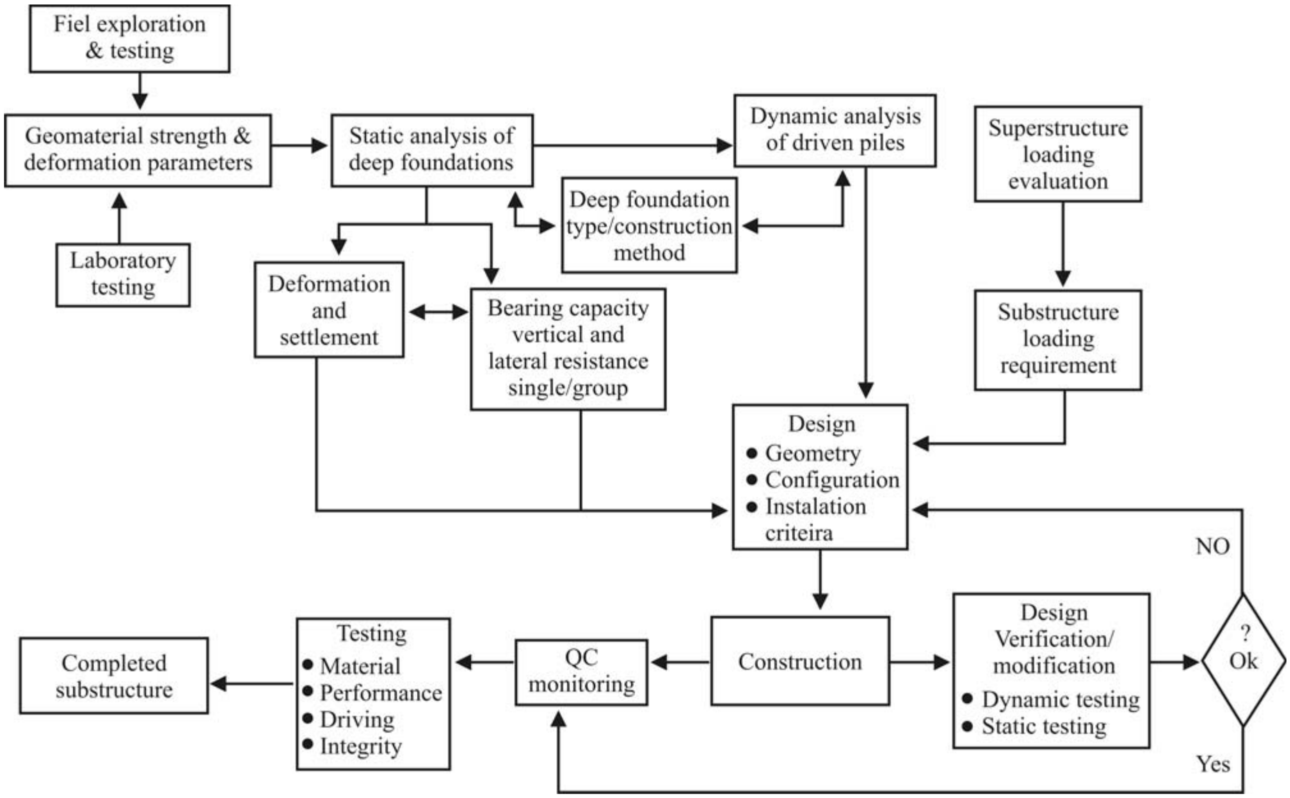

Figure 12 - Design and construction process for deep foundations (Paikowsky, 2004).

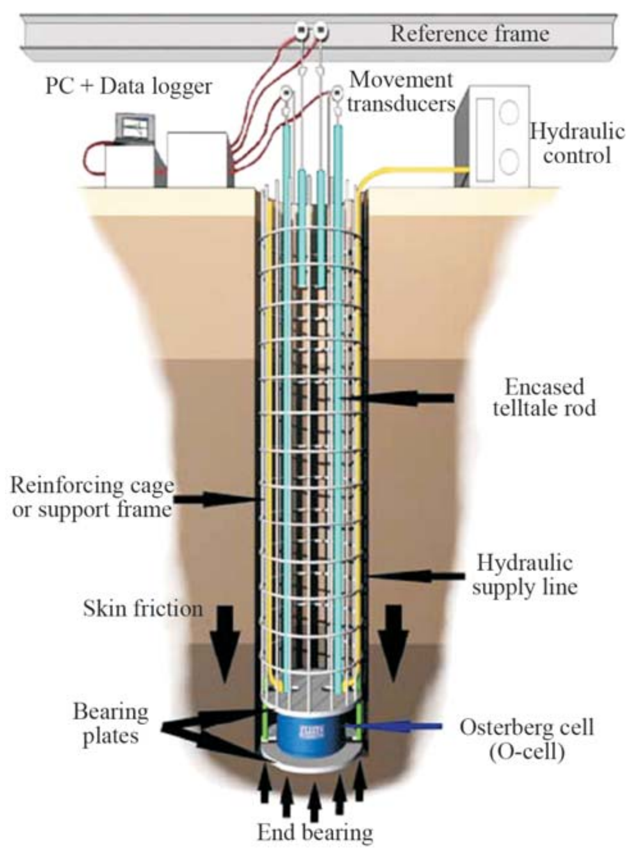

Figure 13 - Bi-direccional test schematic (England & Chessman, 2005).

Figure 14 - High capacity testing with multiple O-cell (England & Chessman, 2005).

are strength, degree of fracturing, E (deformability modulus) of rock mass, condition of walls and base of the socket, and the geometry of the socket.

The load capacity calculation in side-wall shear assumes that shear stress is uniformly distributed in the socket walls and the capacity is given by:

$$Q = \tau_a \pi B L \tag{6}$$

where Q is the total applied load, τ_a is the allowable side-wall shear stress, B and L are the diameter and length of socket, respectively. The diameter is usually determined by the available drilling equipment and the length is selected in order to have a side-wall shear stress not greater than the allowable shear stress and to ensure that the design settlement is not exceeded.

Based on the publication of Wyllie (1999), some design values are presented:

• For clean sockets, with side-wall undulations between 1 and 10 mm deep and less than 10 mm wide:

$$\tau_a = \frac{0.6(\sigma_{u(r)})^{0.5}}{FS} \tag{7}$$

or

$$\tau_a = \frac{(\beta\sigma_{u(r)})}{FS} \tag{8}$$

where $\sigma_{u(r)}$ is the uniaxial compressive strength of the rock for smooth and grooved sockets, FS is safety factor and β the adhesion factor ($\tau/\sigma_{u(r)}$) as defined in a graphic presented in the previous referred publication.

• For clean sockets, with side-wall undulations greater than 10 mm deep and 10 mm wide:

$$\tau_a = \frac{0.75(\sigma_{u(r)})^{0.5}}{FS} \tag{9}$$

Values for the adhesion factor β may be available from test shafts. The factor of safety FS relates the ultimate to the allowable shear resistance. A $FS = 2.5$ relates the ultimate to the allowable stress values in these test shafts. If the rock mass is closely fractured, the values of τ_a should be reduced.

An end-bearing socket may fracture a cone of rock beneath the end of the shaft which will result in excessive settlement. Experience has shown that shafts have been loaded to base pressures as high as three or more the compressive strength of rock without collapse. Test results showed that allowable load capacity Q_a with a FS of about two to three equals:

$$Q_a = \sigma_{u(r)} \frac{\pi B^2}{4} \tag{10}$$

For conditions where the rock below the shaft contains sub-horizontal seams infilled with lower strength material the end-bearing capacity is reduced and the equation is:

$$Q_a = K'\,\omega\sigma_{u(r)} \tag{11}$$

where

$$K' = \frac{3 + \frac{S}{B}}{10\left(1 + 300\frac{t}{s}\right)^{1/2}} \tag{12}$$

ω is a depth factor and is equal to

$$\omega = 1 + \frac{0.4L}{B}$$

for $\omega < 3$. s is the spacing of the seams and t is the thickness of the filled.

4.3. Settlements

Also based on the publication of Wyllie (1999) some expressions for settlement predictions are presented.

For settlements calculation of socketed shafts, a 3-stage process can be developed with the increasing load as follows:

• Deformation starts at shaft with elastic compression and with elastic shear strain at the rock-grout interface. The deformation is small and the major portion of the load is carried in side-wall shear.

• Slippage starts and increasing load is transferred to the pillar base.

• The rock-concrete bond is broken and increasing load is carried in end bearing.

Different socket conditions exist depending on the site geology and construction method (Fig. 15).

The general equation for settlements of socketed shafts that support the load in shear-wall resistance at the surface of a semi-elastic half space is:

$$\delta = \frac{QI}{BE_{m(s)}} \tag{13}$$

$E_{m(s)}$ is the modulus of deformation of rock mass in the shaft and I is a settlement influence factor given by Fig. 16. In this figure R is the ratio between E_c and $E_{m(s)}$. E_c is the deformability modulus of the shaft. Values of rock mass have been back-analyzed and the following equation was proposed:

$$E_{m(s)} = 110\sqrt{\sigma_{u(r)}} \tag{14}$$

It should be noted that the described influence factors assume that the socket is fully bonded from the rock surface. However, influence factors could be reduced where the shaft is recessed below the surface.

When the load is entirely supported in end bearing, the settlement is calculated in a similar manner of a footing near the ground surface. Using reduction factors given by Fig. 17, the equation for settlements of an end bearing shaft is:

$$\delta = \frac{4Q}{\pi B^2}\left[\frac{D}{E_c} + \frac{RF'\,C_d B(1-v^2)}{E_{m(b)}}\right] \tag{15}$$

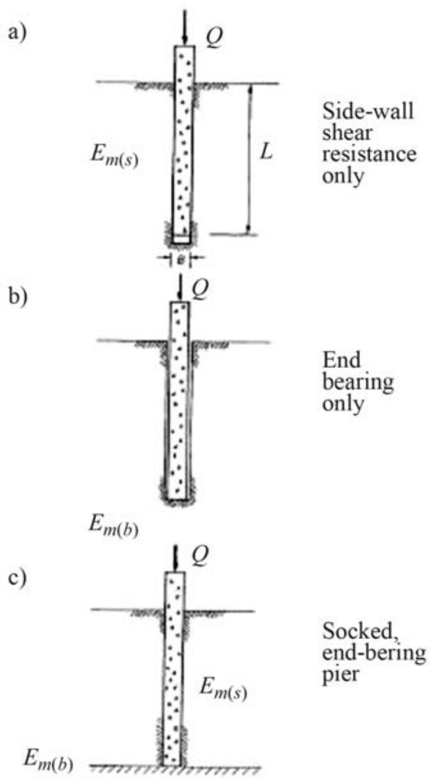

Figure 15 - Summary of calculation methods of settlements (Adapted from Wyllie, 1999).

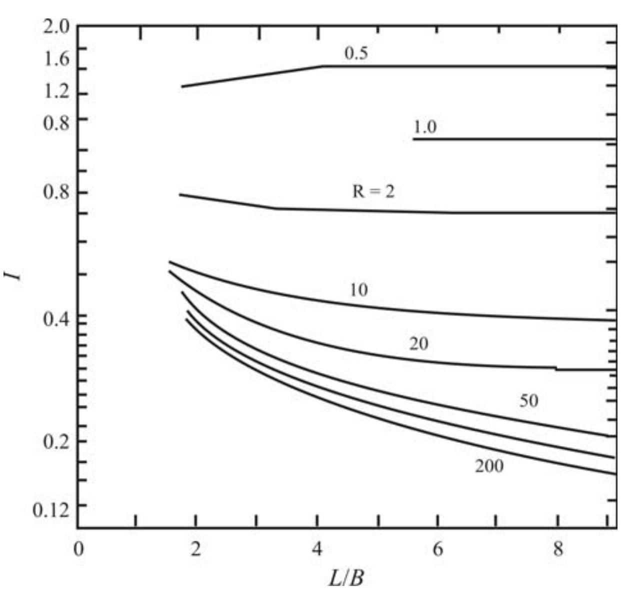

Figure 16 - Elastic settlement factors for side-wall resistance socketed shaft (Adapted from Wyllie, 1999).

where D is the depth of shaft, B the diameter of socket, RF' is a reduction factor given by Fig. 17 and C_d is the shape and rigidity factor as referred in Table 8. Q is the foundation load and $E_{m(b)}$ is the deformation modulus of the rock mass in the shaft base.

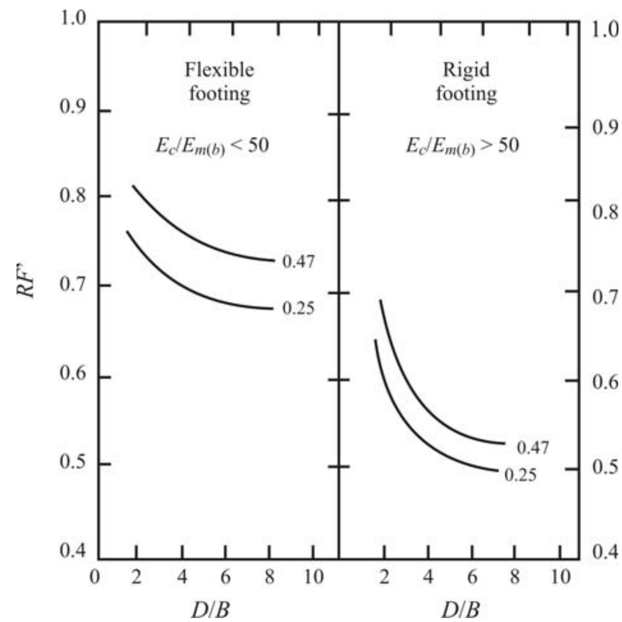

Figure 17 - Reduction factors for calculation of settlement of end bearing sockets (Adapted from Wyllie, 1999).

Table 8 - Shape and rigidity factors C_d.

Shape	Center	Corner	Average
Circle	1.00	0.64	0.64
Circle (rigid)	0.79	0.79	0.79
Square	1.12	0.56	0.76
Square (rigid)	0.99	0.99	0.99
Rectangle: length/width			
1.5	1.36	0.67	0.97
2	1.52	0.76	1.12
3	1.78	0.88	1.35
5	2.10	1.05	1.68
10	2.53	1.26	2.12
100	4.00	2.00	3.60
1000	5.47	2.75	5.03
10000	6.90	3.50	6.50

Also the settlement can be calculated for a mixed situation of the load being carried out by end bearing behavior and along side walls.

5. Analysis of Tall Buildings Foundations

5.1. Empire State Building

The Empire State Building was the tallest building in the world when completed in 1931 as referenced in Table 1. It remained as the world's tallest building until 1972, when the twin towers of the World Trade Center were completed. The most significant statistic of the Empire State was its status as a tall skyscraper and also the extraordinary speed with which it was planned and constructed (Willis, 1998). In reality, six months after setting the first structural column, the steel frame topped off at the eighty-sixth floor. The full building was finished in eleven months, in March 1931.

Figure 18 presents the plan of the ground floor, with a plan area of about 7,796 m^2, and shows a schematic of the foundation layout using 210 shafts.

Based on the publication of Willis (1998), some information about the Empire State is presented. Manhattan bedrock is mostly granite and schist and therefore is capable of supporting high loads. At the site of Empire State Building it ranged to about 23 m below grade, with concrete shafts to transmit loads from the base of the steel columns to the bedrock. Tops of these shafts were reinforced with grillages of steel beams.

Foundation excavation started on January 22, 1930 and finished on March 17, 1931. The excavated material consisted of 6,881 m^3 of soil and 13,303 m^3 of rock material. The concrete poured into 210 shafts totalled about 2,863 m^3. Taking into consideration that shafts have a depth between 9.1 and 12.2 m, an average diameter of about 1.2 m was estimated for each shaft. The excavated rock was soft and it was necessary to go deep in order to get the hard rock necessary to pass tests required by New York City.

The shaft excavation started on February 12, 1930 and first shaft holes satisfied hard rock bottom criteria imposed by City Inspectors and were filled with concrete on February 24.

The first steel columns were set on April 7, 1930 and the building was completely finished on March 1, 1931. The entire project was conceived and successfully executed within twenty-one months.

The theory presented in Section 4 of this article was used to estimate settlements that might have occurred during construction of the Empire State Building.

Considering expression (14), and taking into consideration the average UCS value of 161.4 MPa obtained for granites presented in Table 4, the modulus of deformability $E_{m(s)}$ obtained for the foundation is equal to about 1.4 GPa. This corresponds to a bad geomechanical quality rock mass, with low values for RMR and Q geomechanical indexes. Consequently using this deformability modulus the corresponding RMR value was calculated. According to

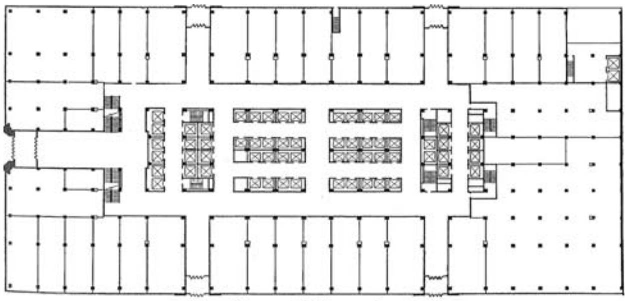

Figure 18 - Empire State Building ground floor plan (Willis, 1998).

our experience and based also on Data Mining applications performed in rock formations (Miranda, 2007), the expressions proposed by Serafim and Pereira (1983) and Hoek and Brown (1997) gave good results in terms of $E_{m(s)}$ calculation. The Serafim and Pereira (1983) expression was adopted due to our experience. The expression takes into consideration in situ tests performed in several countries in Europe, South America and Africa.

Applying that expression, and for the value of E previously calculated, a value of RMR = 16 was obtained. This value is low and corresponds to a class V rock mass according to the RMR empirical system. A higher value of RMR was also adopted (RMR = 30) as more representative of the granite Empire State foundation. The value of E obtained was then equal to 3.2 GPa. These two values (1.4 and 3.2 GPa) were adopted for the analysis of the Empire State foundation.

Considering the hypothesis that all the loads at the foundation are entirely supported by the end bearing of the shafts, Eq. (15) permits estimation of the maximum expected settlement.

A deformability modulus of 50 GPa for E_c was adopted for the composite columns of steel and concrete, and a factor C_d of 0.64 corresponding to the average between center and edge for a circle was chosen. For Poisson's ratio the value of 0.2 was adopted. The diameter of the socket shaft was considered B = 1.2 m and for the depth of the shaft an average value of D = 10.7 m was taken.

The ratio of the modulus E_c to the modulus of the rock mass below the base, for both situations, is equal to 35.7 and 15.6, *i.e.* less than 50, so it can be assumed that the base of the shaft act as a flexible footing. The reduction factor RF' for a flexible footing on a rock with a Poisson's ratio of 0.2 and a depth to diameter ratio, D/B = 10.7/1.2 = 8.9, is about 0.65.

Consequently the settlements are equal to:

1st hypothesis (E = 1.4 GPa),

$$\delta = 0.0491Q \tag{16}$$

2nd hypothesis (E = 3.2 GPa),

$$\delta = 0.0322Q \tag{17}$$

being settlement in cm and Q the applied force per shaft expressed in MN.

The evaluation of Q was obtained applying the International Building Code (IBC, 2006). Live load adopted for hotels and residential areas are equal to 1.915 kPa and for offices are 2.394 kPa. Due to the absence of information, two values were considered for the dead load, equal to and double that of the live load.

The floor area is about 7,800 m^2 and the total number of concrete and steel caissons is 210. It was assumed the existence of 86 floors plus an upper tower. The values for Q in

MN were estimated and presented in Table 9, as well the corresponding settlements.

For the performed simulations, the maximum value obtained for the settlements was 1.3 cm, with a minimum of 0.5 cm. Of course these values could be smaller because the load supported in both side-wall shear of the shafts is not considered. However the calculated settlements do not take creep into consideration.

5.2. Chicago buildings

In this section special reference is made to the IBM building in Chicago and to the Chicago Spire now under construction.

Table 9 - Predicted values for forces and settlements at the foundation.

Calculation	Pressure (kPa)	Q (MN)	Settlement (cm)
C1 (E = 1.4 GPa)	4.309	14.2	0.7
C2 (E = 3.2 GPa)	4.309	14.2	0.5
C3 (E = 1.4 GPa)	7.962	26.2	1.3
C4 (E = 3.2 GPa)	7.962	26.2	0.8

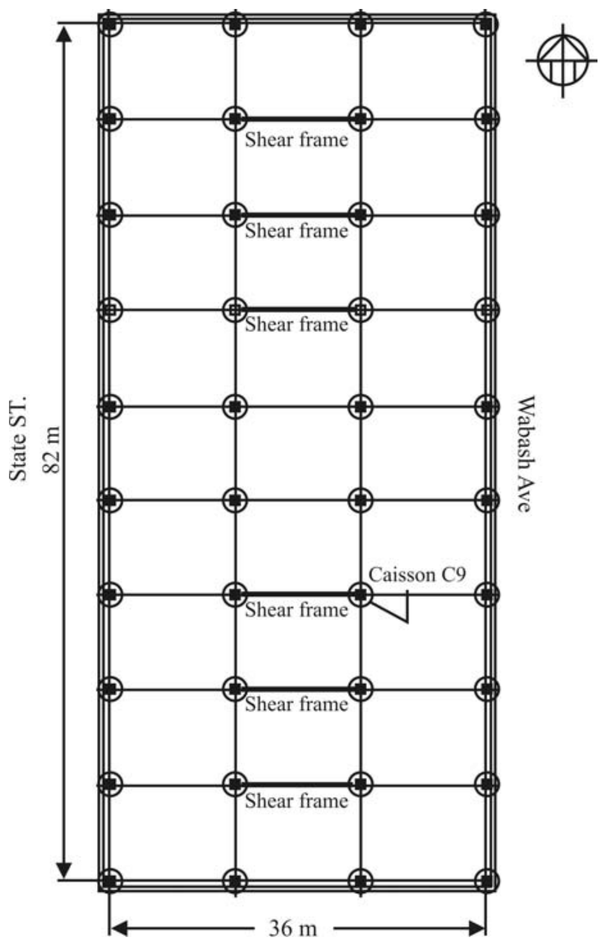

Figure 19 - Caisson and column plan of IBM Chicago Building (Task Force on Foundations, 1972).

The IBM building has 52 stories and rises about 204 m and is supported by 40 caissons. Caisson C9 is instrumented as shown in Fig. 19. The sound rock is represented by a limestone rock formation. The design bearing capacity of the sound limestone was about 12 MPa and the shaft was extended around 0.9 m into sound rock.

The Chicago Committee on High Rise Buildings, formed in 1969, initiated a research for the economic design, construction and maintenance of tall buildings. The Committee decided to analyse the caissons of the IBM building at the time under construction. A new code was proposed recognizing that the steel shell strengthens the caisson allowing an increase the permissible concrete stress (Task Force on Foundations, 1972).

The main purpose of the project was to evaluate the caisson design criteria adopted in 1970, and to check the structure performance to other design criteria used in the Chicago Code. The list of criteria studied was namely related to gravity loads, wind loads, base plate pressure, caisson shell and rock pressure (Task Force on Foundations, 1972).

A borehole was drilled through the caisson and 2.1 m in the bedrock. For the concrete an average values of 41 GPa were obtained for the modulus of elasticity and 40.5 MPa for the compressive strength. Analysis of monitored data was performed in detail once the loading started. The last readings were taken at the end of December, 1971. After that the building was completed and partially occupied.

The evaluation of test measurements was described by the following comments (Task Force on Foundations, 1972):

• Computations were performed considering 65% of dead load and 35% of live load. During construction the loads computed by strain measurements were in good agreement with the design dead load.

• The monitored results show that the total load carried by the steel shell can be evaluated using the theory of elasticity and indicated a rapid transfer of the load from the concrete to the steel shell. Rock sockets should be designed as composite columns

• The study of wind effect was performed during a period in 1971. The magnitude of the load caused by wind agrees reasonably well with the design hypothesis.

• Horizontal tensile stresses were measured in the upper part of the caisson, but compressive stresses are measured in the lower part of the caisson. The effect of Poisson ratio's which causes tensile stresses is counteracted by the horizontal soil pressures.

• Strain meter measurements near the bottom of the steel shell indicate no decrease in steel stress, but indicate a decrease in stress on the concrete. Some of the load is being carried in shear between rock and caisson perimeter.

• It was recommended to increase the ultimate bearing pressure of the rock of about 50% above greater than the previous value, leading to adoption of the value of 28.7 MPa.

The case of the Chicago Spire foundation will provide 34 concrete and steel caissons. A 31.7 m diameter and 23.8 m deep cofferdam will be excavated to create a dry work environment. The caissons will be drilled 36.6 m deep into the bedrock to support the 150-story building's structure. The cofferdam, bathtube-like structure, will serve as the foundation for the building core. The works are taking place near the docks belonging to Chicago Line Cruises (Figs. 5 and 6).

From its many extraordinary features, the Spire will have the world's longest continuous elevator running about 610 m from the underground garage to the 150th floor. The construction of the underground phase will be finished in 2008. The excavations started in June, 2007 (Fig. 20).

The Chicago Spire will be the tallest all-residential structure, will have the most slender profile, and will bear on one of the most tall-building bases ever built. The tower will stand on 34 rock-socketed caissons at a design load of 25.8 MPa, 50% higher than city code allows for large-diameter shafts, and verified to 57.5 MPa using Osterberg cells. The Spire's 33.5 m deep foundations received a special permit in the 2007 summer (Hampton, 2007).

The shafts are arranged in two rings, one 33.5 m in diameter to support a concrete, tapered core that would sit seven levels below grade, and another, 64 m diameter ring of 14 caissons that would hold seven steel perimeter mega-columns at grade. The superstructure contract requires building the core from the bottom up, while excavating a parking garage from the top down.

The Chicago building code section for rock caissons is based on an empirical formula that allows incremental increases in end bearing pressure for each foot of embedment into solid rock, to a maximum value of 19.1 MPa. For maximum design efficiency, a code variance was sought and approved to increase bearing pressure to 23.9 MPa with confirmation load testing by a load test on a 2.4 m rock caisson and in the study conducted by the Chicago Committee on High Rise Buildings (Task Force on Foundations, 1972). The Osterberg cell at the bottom of the rock socket was loaded to its maximum capacity of 23.9 MPa and negligible movement was recorded. The city code also permits higher allowable stress in the rock caisson concrete, provided that it is confined in permanent steel casing of a certain wall thickness.

Figure 20 - Beginning of excavations for the Chicago Spire foundation.

Chicago has surficially some of the youngest geology in the country. The whole Great Lakes landscape was "wiped clean" and replaced with till during the ice age; the most recent glaciation was only 10,000 or so years ago. The rock is about 30.5 m below the surface and usually has a weathered and broken horizon with fractures and clay seams. The unweathered limestone beneath is sound and fairly hard, in the range of 69 to 138 MPa.

The floor area of the Spire is about 278,700 m^2 with 34 rock-socketed caissons, the existence of 150 floors plus the existence of more underground. Therefore expected settlements could be significant (Hampton, 2007).

6. Final Remarks

The study performed for deep rock foundations lead to the following brief comments:

• For skyscrapers suitable bearing surfaces often occur at considerable depths in rock formations. In these cases, socketed shafts or caissons would be required.

• The worldwide tendency is towards living in mega-cities. To accommodate the population the construction of skyscrapers is expected to continue as a major trend, which is corroborated by the impressive tall buildings now in construction.

• The selection of deformability and strength parameters of rock foundation requires sound engineering judgment and experience based on results of tests and the use of empirical systems. Artificial intelligence techniques should be applied in order to develop new geomechanical models.

• A description of design methodologies for deep rock foundations was presented. Better predictions required the use of refined three-dimensional numerical models.

• The analysis of foundations of tall buildings in the USA was performed, considering buildings in New York and Chicago. The existing geomechanical information was scarce. However, reasonable conclusions can be reached.

Acknowledgments

Appreciation is expressed to Lachel Felice & Associates, USA, which supported the preparation of this work.

References

ASCE (1996) Rock Foundations (Technical Engineering and Design Guides as adapted from US Army Corps of Engineers, n. 16). American Society of Civil Engineers, New York, 129 pp.

Babendererde, S.; Hoek, E.; Marinos, P. & Cardoso, S. (2006) Characterization of granite and the underground construction in Metro do Porto. Matos, A.C.; Sousa, L.R.; Kleberger, J. & Pinto, P.L. (eds) Geotechnical Risk in Rock Tunnels, Francis & Taylor, London, pp. 41-51.

Baguelin, F.; Jézéquel, J. & Shields, D. (1978) The Pressuremeter and Foundation Engineering. Trans Tech Publications, Cluasthal, 617 pp.

Barton, N. (2000) TBM Tunnelling in Jointed and Faulted Rock. Balkema, Rotterdam, 172 pp.

Barton, N.; Lost, F.; Lien, R. &Lunde, J. (1980) Application of the Q-system in design decision concerning dimensions and appropriate support for underground installations. Bergman, M. (ed.) Subsurface Space 2, Pergamon, New York, pp. 553-561.

Barton, N. & Quadros, E. (2002) Engineering and hydraulics in jointed rock masses. Symposium EUROCK 2002 - Course A, Funchal.

Bieniawski, Z. (1975) Case studies: Prediction of rock mass behavior by the geomechanical classification. Proc. 2nd Australia-New Zealand Conference Geomechanics, Brisbane, pp. 36-41.

Bieniawski, Z. (1978) Determining rock mass deformability, experience from case histories. Int. Journal of Rock Mechanics and Mining Science, n. 15, p. 237-247.

Bieniawski, Z. (1989) Engineering Rock Mass Classifications. John Wiley & Sons, New York, 251 pp.

Binder, G. (2006) Tall Buildings of Europe, the Middle East and Africa. Images Publishing Group, Victoria, 240 pp.

Cafofo, P. (2006) Projecto hidroeléctrico de Socorridos (Socorridos hydroelectrical project). Final project in Geotechnics, University of Minho, Guimarães, 90 pp.

Carter, T.; Diederichs, M. & Carvalho, J. (2007) A unified procedure for Hoek-Brown prediction of strength and post yield behaviour for rock masses at the extreme ends of the rock competency scale. Proc. 11th ISRM Congress, Lisbon, pp. 161-164.

Carvalho, J. (2004) Estimation of rock mass modulus. Personal communication.

Carvalho, J.; Carter, T. & Diederichs, M. (2007) An approach for prediction of strength and post yield behaviour for rock masses of low intact strength. Proc. 1st Canada USA Rock Symposium, Vancouver, 8 pp.

Christensen, B. (2005) Taipei 101 tower causing earthquakes? www.technovelgy.com.

DFI (2008) Case Foundation Tackles Spire Site. Deep Foundations Institute, Hawthorne, pp. 75.

Diederichs, M. & Kaiser, P. (1999) Stability of large excavations in laminated hard rockmasses: The Voussoir analogue revisited. Int. Journal of Rock Mechanics and Mining Science, v. 36, p. 97-117.

Douglas, K. (2002) The Shear Strength of Rock Masses. PhD Thesis, School of Civil and Environmental Engineering, The University of New South Wales, Sydney, 284 pp.

England, M. & Cheesman, P.F. (2005) Recent experiences with bi-direccional static load testing. http://www.docstoc.com/docs/22682470/recent-experiences-with-bi-directional-static-load-testing 9 pp.

Hampton, H. (2007) Pier pressure may make or break Spire. ENR Engineering News - Record, December. http://www.loadtest.com/loadtest-usa/sidelogs/profiles/ENR1207.pdf.

Hoek, E. (2006) Practical Rock Engineering. www.rocscience.com.

Hoek, E. & Brown, E.T. (1997) Practical estimates of rock mass strength. Int. Journal of Rock Mechanics and Mining Science, n. 34, p. 1165-1186.

Hoek, E.; Carranza-Torres, C. & Corkum, B. (2002) Hoek-Brown failure criterion - 2002 edition. Proc. 5th NARMS Symposium, Toronto, pp. 267-273.

Hoek, E. & Diederichs, M. (2006) Empirical estimation of rock mass modulus. Int. Journal of Rock Mechanics and Mining Science, n. 43, p. 203-215.

IBC (2006) International building code. Code and Commentary, 2 v. http://www.iccsafe.org/Pages/default.aspx.

Judd, W.R. (1969) Statistical Methods to Compile and Correlate Rock Properties and Preliminary Results. Purdue University, Lafayette, 109 pp.

Kulhawy, F. & Carter, J. (1992a) Settlement and bearing capacity of foundations on rock masses. Bell, FG (ed) Eng. in Rock Masses. Butherworth-Heinemann, Oxford, pp. 231-245.

Kulhawy, F. & Carter, J. (1992b) Socketed foundations in rock masses. Bell, FG (ed) Eng. in Rock Masses. Butherworth-Heinemann, Oxford, pp. 509-529.

Kulhawy, F. & Goodman, R.E. (1987) Foundations in rock. In: Ground Engineer’s Reference Book. Butterworth, London, pp. 1-13.

Lima, C.; Resende, M.; Plasencia, N. & Esteves, C. (2002) Venda Nova II hydroelectric scheme powerhouse geotechnics and design. ISRM News Journal, v. 7:2, p. 37-41.

Marinos, P. & Hoek, E. (2005) Estimating the geotechnical properties of heterogeneous rock masses such asch. Bulletin Engineering Geology and Environment, n. 60, p. 85-92.

Miranda, T. (2003) Contribuição para o Cálculo de Parâmetros Geomecânicos na Modelação de Estruturas Subterrâneas em Formações Graníticas (Contribution to the Calculation of Geomechanical Parameters for Underground Structures Modeling in Granite Formations). MSc Thesis, Civil Engineering Department University of Minho, Guimarães, 186 pp.

Miranda, T. (2007) Geomechanical Parameters Evaluation in Underground Structures. Artificial Intelligence, Bayesian Probabilities and Inverse Methods. PhD Thesis, University of Minho, Guimarães, 291 pp.

Miranda, T.; Sousa, L.R. & Correia, A.G. (2008) Bayesian framework for the deformability modulus updating in an underground structure. Proc. 42th U.S. Rock Mechanics Symposium, San Francisco, 7 p CD-ROM).

Mitri, H.; Edrissi, R. & Henning, J. (1994) Finite element modeling of cable bolted stopes in hard rock underground mines. SME Annual Meeting, Albuquerque, pp. 14-17.

Nicholson, G. & Bieniawski, Z. (1997) A non-linear deformation modulus based on rock mass classification. Int. Journal of Mining and Geology Engineering, n. 8, p. 181-202.

Paikowsky, S. (2004) Load and resistance factor design (LRFD) for deep foundations. National Cooperative Highway Research Program, Report 507, Washington, 74 pp.

Plasencia, N. (2003) Underground Works - Aspects of the Engineering Geology Contribution and Design. MSc Thesis, Technical University of Lisbon, Lisbon (in Portuguese).

Post, N. (2008a) Building sector needs reeducation. ENR Engineering News - Record, March, pp. 10-12. http://enr.ecnext.com/coms2/article_nebuar080312a.

Post, N. (2008b) 650-plus meters skyward, crews are already. Out of this world. ENR Engineering News - Record, May, pp. 26-33. http://enr.ecnext.com/coms2/article_febiar080430-1.

Read, S.; Richards, L. & Perrin, N. (1999) Applicability of the Hoek-Brown failure criterion to New Zeland greywacke rocks. Proc. 9th ISRM Congress, Paris, pp. 655-660.

Reina, P. (2006) Final height on 'on deck' tallest tower shrouded in secrecy. ENR Engineering News - Record, June. http://enr.construction.com/features/_covers/2006/06-default1.asp.

Rocha, M. (1971) Rock Mechanics (in Portuguese). LNEC, Lisbon, 276 pp.

Serafim, J.L. & Pereira, J. (1983) Considerations of the geomechanics classification of Bieniawski. Proc. of the Int. Symposium of Engineering Geology on Underground Construction, Lisbon, pp. II.33-II.42.

Serrano, A. & Olalla, C. (2007) Bearing capacity of shallow and deep foundations in rock with the Hoek and Brown failure criteria. Proc. 11th ISRM Congress, Lisbon, v. 3, pp. 1379-1392.

Singh, S. (1997) Time Dependent Modulus of Rocks in Tunnels. MSc Thesis, Civil Engineering Department, University of Roorkee, 153 pp.

Sonmez, H.; Gokceoglu, C. & Ulusay, R. (2004) Indirect determination of the modulus of deformation of rock masses based on the GSI system. Int. Journal of Rock Mechanics and Mining Science, n. 41, p. 849-857.

Sousa, L.R.; Leitão, N.S. & Monteiro, G. (1999) Observed behavior of the structures for the power increase of the Miranda hydroelectric project. Proc. 9th ISRM Congress, Paris, pp. 1603-1612.

Sousa, L.R.; Nakamura, A.; Yoshida, H.; Yamaguchi, Y.; Kawasaki, M. & Satoh, H. (1997) Evaluation of the deformability of rock masses for dam foundations. Analysis of deformability investigation results in heterogeneous bedrock. Technical Memorandum n. 3514, Public Works Research Institute, Tsukuba, 45 pp.

Stephens, S. (2004) Imagining Ground Zero. Official and Unofficial Proposals for the World Trade Center Site. McGraw-Hill Construction, NewYork, 224 pp.

STS (2006) Viewpoint 5, STS Consultants.

Task Force on Foundations (1972) Strain measurements in rock-socketed caisson. Chicago Committee on High Rise Buildings, Report n. 3, Chicago, 50 pp.

Verman, M.; Singh, B.; Viladkar, M. & Jethwa, J. (1997) Effect of tunnel depth on modulus of deformation of rock mass. Rock Mech. Rock Engng., v. 30:3, p. 121-127.

Willis, C. (1998) Building the Empire State. Skyscraper Museum, New York, 190 pp.

Wyllie, D. (1999) Foundations on Rock. E & FN Spon, London, 401 pp.

Yufin, S.; Lamonina, E. & Postolskaya, O. (2007) Estimating of strength and deformation parameters of jointed rock masses. Proc. 5th Int. Work. on Applications of Computational Mechanics in Geotechnical Engineering, Guimarães, pp. 3-15.

List of Symbols and Acronyms

α: Modulus reduction factor

β: adhesion factor

γ: volumic weight

δ: settlement

σ_1', σ_3': Maximum and minimum effective principal stresses

σ_c: uniaxial compressive strength

σ'_{cm}: rock mass strength

$\sigma_{t,mass}$: tensile strength of the rock mass

$\sigma_{u(r)}$: unconfined compressive strength for smooth and grooved sockets

φ': effective friction angle

τ_a: Allowable side-wall shear stress

B, L: diameter and length of the socket, respectively

c': effective cohesion

C_d: Shape and rigidity factor

D: disturbance factor of the GSI system

E: deformability modulus of the rock mass

E_c: deformability modulus of concrete

E_i: deformability modulus of the intact rock

$E_{m(s)}$: deformability modulus of the rock mass in the shaft

$E_{m(b)}$: deformability modulus of the rock mass in the base

H: depth
I: settlement influence factor
m_b, s, a: strength parameters of the Hoek and Brown strength criterion for the rock mass
m_i: strength parameter of the Hoek and Brown strength criterion for the intact rock
k_s, k_b: shaft and end bearing resistance of piles
Q: applied load to the pile
Q_a: allowable load capacity of the pile
RF': reduction factor
S: spacing of the seams
t: thickness of the filled
ASCE: American Society of Civil Engineers
DFI: Deep Foundations Institute
DM: Data Mining
FS: Safety factor
GSI: Geological Strength Index
H-B: Hoek and Brown
ISRM: International Society of Rock Mechanics
LFJ: Large Flat Jack test
PLT: Plate Load Test
Q: Q system index value
RMR: Rock Mass Rating
SFJ: Small Flat jack test
STS: STS Consultants
STT: LNEC Strain Tensor Tube
UCS: Uniaxial compressive strength

Theoretical and Experimental Evaluation of the Influence of the Length of Drill Rods in the SPT-T Test

Anna Silvia Palcheco Peixoto, Luttgardes de Oliveira Neto, Valéria Borin Antenor

Abstract. The influence of soil drill rod length on the *N* value in the SPT-T test has been studied extensively by Mello (1971), Schmertmann & Palacios (1979), Odebrecht *et al.* (2002) and Cavalcante (2002). This paper presents an analysis of the Standard Penetration Test supplemented with torque measurement (SPT-T). A theoretical study of the resistance of the rod material to torsion and bending indicated that the shear stress caused by the rod self-weight represents less than 1% of that caused by the torsional moment. An experimental study with electric torquemeters attached to a horizontal rod system, as well as two field tests in the vertical direction, were also carried out to compare and substantiate the results. The purpose of these tests was to analyze changes along the length of the rod in response to successive increments at 1-meter intervals. Torque measurements were taken at each increment of the length to ascertain the accuracy of the theoretical data. The difference between the applied torque and the measured torque at the end of rod system was lower than the minimum scale of mechanical torquemeters used in practice.

Keywords: SPT-T, torque measurement, torquemeter, rod length.

1. Introduction

The standard penetration test (SPT) is commonly used in the design of pile and shallow foundations in Brazilian foundation construction practices. Mayne (2001), who questioned the notion that just one number (an N-value) suffices to estimate a wide range of soil parameters, recommended the use of *in situ* testing with hybrid devices. Ranzini (1988) proposed supplementing the conventional SPT test with torque measurements required to turn the split-spoon sampler after driving.

A simple test can be performed by drilling, following the Brazilian ABNT NBR 6484 (2001) standard. After penetration of the split-spoon sampler, keeping count of the hammer blows, an adapter is attached to the anvil, onto which the torquemeter is attached. A centralizing device should be placed either on the top of the hole or inside the pipe to prevent the rod from shifting off-center in the hole during the application of torque. The rod-sampler set is then turned, using the torquemeter. The maximum torque is measured and turning continues to be applied until the torque remains constant, at which point the residual torque value is determined.

Torque is measured at the top of the rod-sampler system, Fig. 1a, but friction, as proposed by Ranzini (1994), is calculated considering only adhesion at the sampler-soil interface, Eq. (1):

$$f_T = \frac{T}{(41.336 \times h - 0.032)} \quad (1)$$

where f_T is sampler-soil adhesion, kPa; T is the measured torque, kN.m; and h is the depth of penetration of the sampler, m.

The constants in this equation are based on sample dimensions. In this paper, the Raymond split-spoon sampler is considered (ABNT NBR 6484-2001).

The influence of rod length on the torque measurements should be checked, since the readings are taken at the upper end of the sampler-rod system, while the actual load is borne by the sampler. This paper describes the first study in which the rod system is considered in a horizontal position (Fig. 1b) to allow for control of the applied torque. The experimental findings are preceded by a theoretical study of simple torsion, bending and bending-torsion concepts in a thin-walled tubular steel shaft.

Electric torquemeters designed by Peixoto (2001) were used here. These torquemeters were equipped with a data acquisition system coupled to a horizontal rod system to control the applied torque, Fig. 1b. The purpose of these tests was to analyze 1-meter to 20-meter long rods, with the torque measured at the ends of the rod system to ensure the accuracy of the data.

The SPT-T tests were carried out vertically, but experimental loading must be done with the rods in the horizontal position to allow for control of the applied torque, since the results of field tests depend on soil resistance. Moreover, field tests enable one to evaluate how and to what extent the rod's instability affects the accuracy of the SPT-T test.

The theoretical study that preceded the experimental tests was fundamental in understanding the behavior of

Anna Silvia Palcheco Peixoto, D.Sc., Assistant Professor, Departamento de Engenharia Civil, Faculdade de Engehraria, Universidade Estadual Paulista, Bauru, SP, Brazil. e-mail: anna@feb.unesp.br.
Luttgardes de Oliveira Neto, D.Sc., Assistant Professor, Departamento Engenharia Civil, Faculdade de Engenharia, Universidade Estadual Paulista, Bauru, SP, Brazil. e-mail: lutt@feb.unesp.br.
Valéria Borin Antenor, Civil Engineer, Consórcio Queiroz Galvão/Odebrecht, São Paulo, SP, Brazil. e-mail: valeria_antenor@hotmail.com.
Submitted on January 30, 2008; Final Acceptance on July 17, 2009; Discussion open until September 30, 2010.

rods during the SPT-T test, clarifying the difference between the torque applied at the upper part of the rod system and the torque at the sampler-soil interface.

2. Methodology

The present study aimed to determine the influence of rod length on the *N* value in the SPT-T test. Therefore, a theoretical study was first made to provide the necessary background for analyzing soil drill rod behavior, in order to gain a better understanding of how experimental tests are performed in practical engineering.

2.1. Theoretical background

Concepts of materials resistance and buckling phenomena are necessary for theoretical analyses and comparisons with experimental results.

Based on the concept of free torsion (or uniform torsion) as a type of load in which all the cross sections of a rod are loaded only by a torsional moment, any other kind of internal load such as the bending moment, normal load or shear load is equal to zero. An initial hypothesis is that the cross sections undergo free warping, but their projections remain undeformed. This phenomenon does not occur with *in situ* SPT test rods that have a circular thin-walled section.

However, in the initial phase of this research, which was conducted in the laboratory, thin-walled section rods were subjected to normal stresses caused only by the bending moment. The rods were placed in a horizontal position and loaded with metal weights, as illustrated in Fig. 1b. The diagram in Fig. 2 depicts a beam with a vertical load P and its respective load diagrams.

In the second phase, which consisted of field tests, the rods were positioned vertically and the buckling phenomenon was examined, which occurs when a structure is subjected to the action of external compression and bending. According to Schiel (1984), this phenomenon is not a problem of structural strength. The factor that determines whether the structure will be subjected to this phenomenon is its cross section dimensions (elastic buckling).

Elastic buckling is determined by analyzing the phenomenon in an axially compressed prismatic bar, as shown

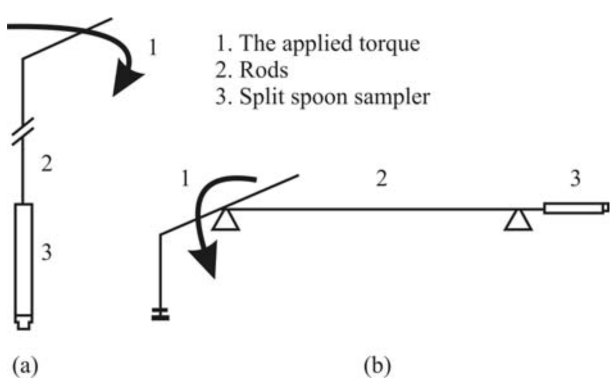

Figure 1 - (a): SPT-T test load; (b): Laboratory experimental load.

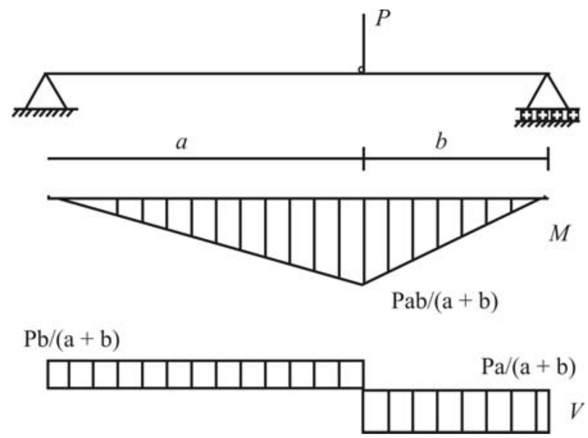

Figure 2 - Beam load diagrams.

in Fig. 3. In this figure, the deformation of the bar is represented by the elastic curve, with the y axis representing the displacement of the cross section.

The critical buckling load (Euler's Load) is presented in Eq. (2),

$$\frac{\pi^2}{L^2} = \frac{P}{EI} \rightarrow P_{cri} = \frac{\pi^2 EI}{L^2} \tag{2}$$

where $L = L_{fl}$ is the critical length; I is the moment of inertia of the cross section; and E is Young's modulus.

However, the goal here is to study the influence of weight on the buckling phenomenon in a bi-jointed column, which probably best represents SPT-T rods in field tests. The real elastic deformation of the bar to meet the new boundary conditions depicted in Fig. 4 is obtained by Eq. (3),

$$y = \delta \sin\left(\frac{\pi x}{L}\right) \tag{3}$$

which results in

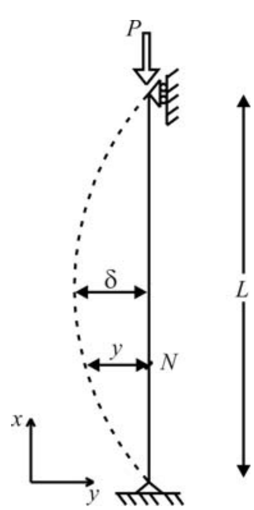

Figure 3 - Static scheme of axially compressed bar.

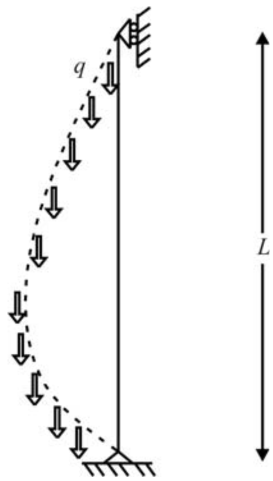

Figure 4 - Probable deformation of a bi-jointed column under its own weight.

Figure 5 - Strain gauges attached to the rod.

$$\left\{\{q \to 0.\}, \left\{q \to \frac{61.661EI}{L^3}\right\}\right\} \tag{4}$$

where q represents the Critical Distributed Buckling Load.

Mathematica (Wolfram, 2003) software was used to solve the equation that theoretically determines the critical rod length.

To verify the theoretical calculation of the Euler load experimentally, a 2-meter length rod used in the SPT-T test was subjected to an axial compression test in the Structures Laboratory, School of Engineering, São Paulo State University, Bauru City, Brazil.

The rod was placed in a metallic frame and loaded, using a load cell and a hydraulic jack, ensuring that the ultimate buckling load would not be reached. The hydraulic jack was connected to the load cell and a data acquisition system was used to control the applied load and record the strain values.

Four strain gauges were attached vertically around the rod section at mid-length, which is the critical area for the occurrence of maximum deformations, Fig. 5.

Figure 6a shows the strain gauge arrangement, while Fig. 6b illustrates a strain gauge attached to the rod. This test was conducted to confirm Euler's critical load, since a test that could analyze only the rod's self-weight could not be performed.

2.2. Laboratory tests

The influence of length rod on the buckling phenomenon was studied using the SPT device recommended by the Brazilian NBR6484 (2001) standard. The theoretical weight of the rod was 32 N/m, its external diameter was 33.4 mm ± 2.5 mm, and its internal diameter was 24.3 mm ± 5 mm.

The laboratory tests were performed to control the applied torque without soil resistance. The calibration system

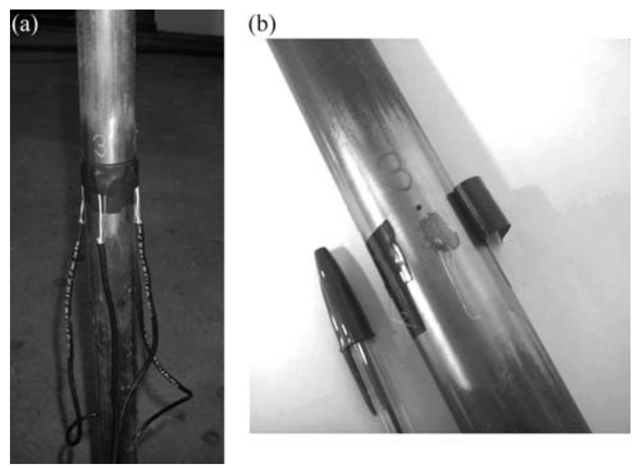

Figure 6 - Strain gauge details.

represents the field operator applying the torque, but with the rods in a horizontal position, as illustrated in Fig. 7. The results were recorded by two electric torquemeters positioned at the extremities of the rod system.

The rods were positioned horizontally and their length varied from 1 m to 20 m. Tripods equipped with roller bearings were used to reduce the friction between the rods and tripods, Fig. 8.

2.3. Field tests

The purpose of the field tests was to verify the influence of rod length on practical SPT-T tests. These tests were performed in winter (July 2006) at the Experimental Foundation Site, School of Engineering, São Paulo State University, Bauru City, São Paulo State, Brazil, Fig. 9.

Two different tests were carried out. The first was in a borehole, as performed in a standard SPT test, while the second one was carried out inside a pit with a diameter of 0.80 m, in which it was possible to execute a test similar to

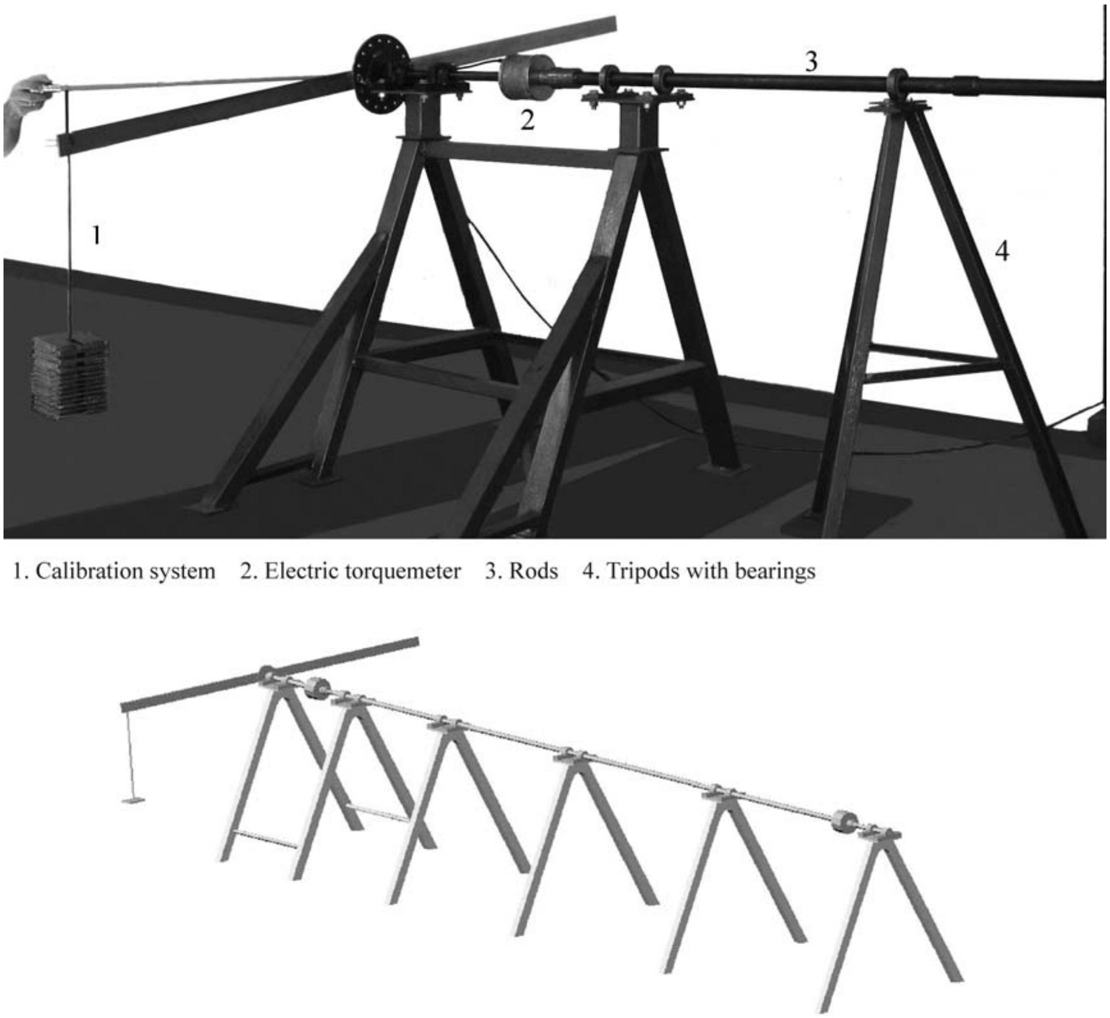

Figure 7 - Rod system.

Figure 8 - Roller bearing.

the laboratory test, *i.e.*, using two electric torquemeters, the first attached to the upper end of the rod system and the second between the sampler and the rod system.

Figure 10 illustrates the two test configurations, including previous *in situ* tests carried out in this area.

3. Results and Analysis

This analysis is essential, since rod instability may impair the practical results. The presentation of this analysis is followed by an analysis of the laboratory and field tests.

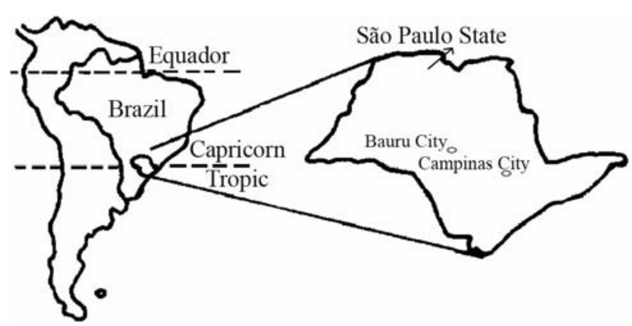

Figure 9 - Site location.

3.1. Theoretical analyses

In the static scheme, Fig. 11, the rod's self-weight is considered as a transversally distributed load (q = 32 N/m) and the applied torsion moment, M_t = 500 N.m, is greater

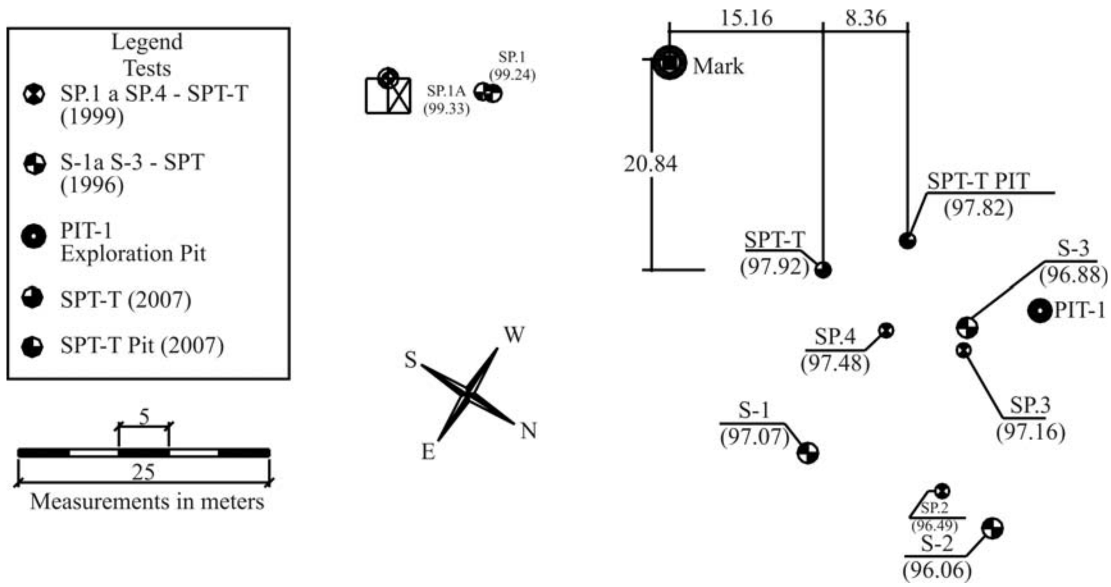

Figure 10 - Configuration of the tests conducted at the Experimental Foundation Site of UNESP's Faculty of Engineering at Bauru.

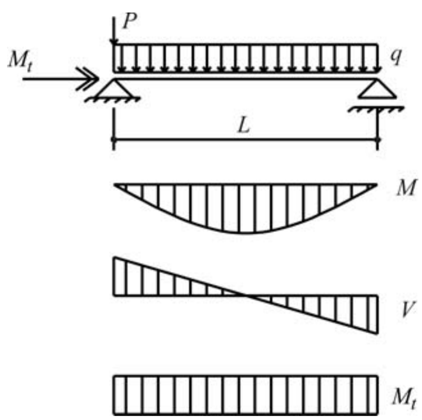

Figure 11 - Static scheme showing the rod's self-weight load and torsion moment.

than the usual field test loads. The rod's geometric properties are listed in Table 1.

As can be seen in Table 2, the shear stress (τ_V) caused by bending was less than 1% of the shear stress caused by the torsional moment, τ_{Mt}, Eq. (5), since it is 20 m long in the rod system.

$$\tau_{Mt} = \frac{M_t}{2tA_m} \tag{5}$$

where τ_{Mt} is the torsion shear stress at the cross section, MPa; t is the cross section thickness, m; and A_m is the area enclosed by the medium curve, m^2.

3.1.1. Buckling

Based on the theoretical expressions, Table 4 illustrates the critical load results for the columns with articulated ends. The Critical Buckling Load (Euler load), P_{cri}, is obtained by Eq. (2) and the Critical (Self-Weight) Distributed Buckling Load, q_{cri}, is obtained by Eq. (4). The Equivalent Critical Load ($P_{cri,eq}$) is calculated by multiplying the Critical Self-Weight Buckling Load (q_{cri}) by the corresponding rod length (L). It is then possible to compare those values with the theoretical Critical Buckling Load (P_{cri}, far right column, Table 4).

Since the rod's weight is 32 N/m, note that the *self-weight* is not a limiting factor for the occurrence of buckling up to 20 m (as shown in the q_{cri} column, Table 4). These results indicate that the influence of the column's

Table 1 - Cross section dimensions and properties.

d_{in} (m)[1]	d_{out} (m)[2]	d_m (m)[3]
$2.390.10^{-2}$	$3.355.10^{-2}$	$2.8725.10^{-2}$
A_{cross} (m^2)[4]	t (m)[5]	A_m.(m^2)[6]
$4.3542.10^{-2}$	$4.8250.10^{-3}$	$6.4805.10^{-4}$
I_t (m^4)[7]	I (m^4)[8]	r (cm)[9]
$1.089.10^{-4}$	$7.3034.10^{-8}$	1.030

[1]Internal diameter; [2]External diameter; [3]Medium diameter; [4]Cross section area; [5]Cross section thickness; [6]Area enclosed by the medium curve; [7]Torsion inertial momentum; [8]Bending inertial momentum; [9]Radius of gyration.

Table 2 - General stress.

τ_V (MPa)[1]	τ_{Mt} (MPa)[2]	σ (MPa)[6]
$7.35.10^{-1}$	79.95	0.82

[1]Bending shear stress; [2]Torsion shear stress at cross section; [6]Bending stress.

Table 3 - Shear stress caused by bending (τ_V) and torsional (τ_{Mt}) moments.

L (m)	V (N)	τ_V (MPa)	τ_{Mt} (MPa)	$\frac{\tau_V}{\tau_{Mt}}$ (%)
1	16	0.037	79.95	0.046
5	80	0.184	79.95	0.230
10	160	0.367	79.95	0.460
15	240	0.551	79.95	0.689
20	320	0.735	79.95	0.919

self-weight does not affect the buckling phenomenon in the STT-T test.

Even admitting, hypothetically, that the weight of the SPT operator with a magnitude of 772.1 N (column 4, Table 4) is applied axially to the upper extremity of the rod during the *in situ* test, this would be considered a critical load for a rod with over 11 m of free length. Considering depths of more than 11 m, this influence may cause lateral instability of the rod system, given that critical loads diminish.

Table 4 - Critical Buckling Load q_{cri} as a function of the rods' length.

Length L (m)	Critical self-weight buckling load q_{cri} (N/m), Eq. (4)	Equivalent critical load $P_{cri,eq}$ (N)	Critical buckling load (Euler load) P_{cri} (N), Eq. (2)
1	583706.3	583706.3	93423.0
2	72963.3	145926.6	23355.7
3	21618.8	64856.3	10380.3
4	9120.4	36481.6	5838.9
5	4669.7	23348.3	3736.9
6	2702.3	16214.0	2595.1
7	1701.8	11912.4	1906.6
8	1140.1	9120.4	1459.7
9	800.7	7206.2	1153.4
10	583.7	5837.1	934.2
11	438.6	4824.1	772.1
12	337.8	4053.5	648.8
13	265.7	3453.8	552.8
14	212.7	2978.1	476.7
15	173.0	2594.3	415.2
16	142.5	2280.2	364.9
17	118.8	2019.8	323.3
18	100.1	1801.6	288.3
19	85.1	1616.9	258.8
20	73.0	1459.2	233.6

It is also possible to conclude that the self-weight is less critical than the axial load the operator applies at the upper extremity of the rod. Therefore, the column's slenderness must be taken into account when defining a safety limit for the rod's free length in order to ensure the good performance of the SPT-T, considering an axially compressed column.

Table 5 shows the slenderness (λ) of the rod column calculated as a function of length and obtained by the ratio of the buckling length (L) to the radius of gyration (r).

According to the Brazilian ABNT NBR 8800/1986 code, the maximum admissible slenderness of a prismatic steel bar subjected to axial compression is 200. Considering the results found in Table 5, the critical buckling length in the rod column test is 2 m (λ = 194,2). This means that in tests conducted at deeper depths, intermediary spacers must be added at 2-meter intervals to satisfy the slenderness limit. The goal is to diminish the rod's free length, avoiding buckling and large lateral displacements of the rod column, thereby improving the efficiency of the test.

Figure 12 depicts the instant when buckling occurs in a compressed rod under the application of the critical load. The cross section at mid-span shows the maximum transversal displacement.

Considering $L_{fl} = L/\sqrt{2} = 0.7L$ for a joint-clamp bar scheme according to the ABNT NBR 8800/86 standard, it is possible to estimate the buckling load. Based on theoretical calculations (Eq. (11)), the buckling load was 46 kN. Figure 13 depicts the load *vs.* time curve obtained during the buckling test, showing a maximum load of 48.5 kN was obtained, which means a difference of about 5% over the expected value.

An analysis of Fig. 14 reveals that when the buckling load was almost attained, two pairs of the four strain gauges exhibited major deformations, distension and contraction.

Table 5 - Slenderness as a function of length.

Length (m)	λ	Length (m)	λ
1.0	97.1	11.0	1068.1
2.0	194.2	12.0	1165.2
3.0	291.3	13.0	1262.3
4.0	388.4	14.0	1359.4
5.0	485.5	15.0	1456.5
6.0	582.6	16.0	1553.6
7.0	679.7	17.0	1650.8
8.0	776.8	18.0	1747.9
9.0	873.9	19.0	1845.0
10.0	971.0	20.0	1942.1

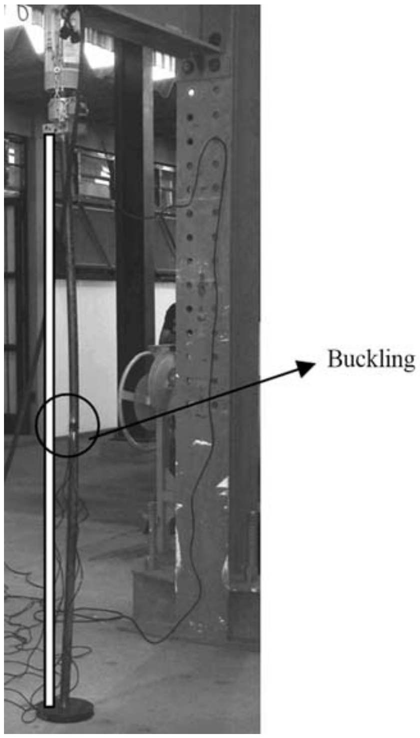

Figure 12 - Instant when buckling occurred.

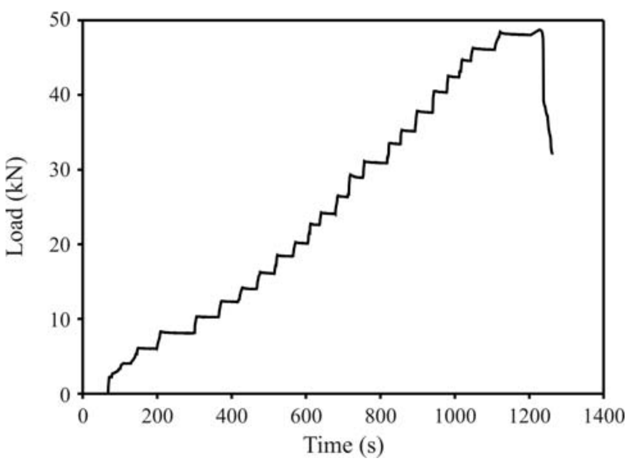

Figure 13 - Load *vs.* time curve.

3.2. Laboratory tests

The two graphs below display the values of torque obtained at the extremity close to the point where torque was applied, and the differences between the first and second torque values. In Fig. 15, the ordinate axis represents the ratio between the torque applied at the beginning (T_b) and the torque received at the end of rod system (T_e). The ordinate axis in Fig. 16 shows the values of the differences between the two torquemeters. Note that although the applied torque increases the ratio between the applied torque and the received torque, the minimum value remains constant (Fig. 15).

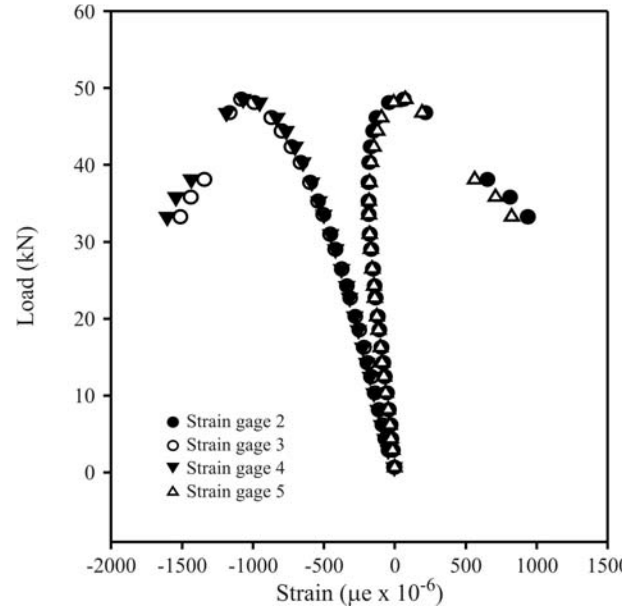

Figure 14 - Strain *vs.* load.

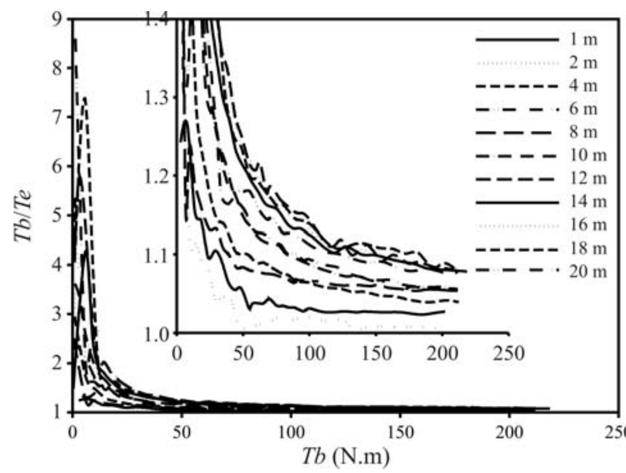

Figure 15 - *Tb*/*Te* analysis.

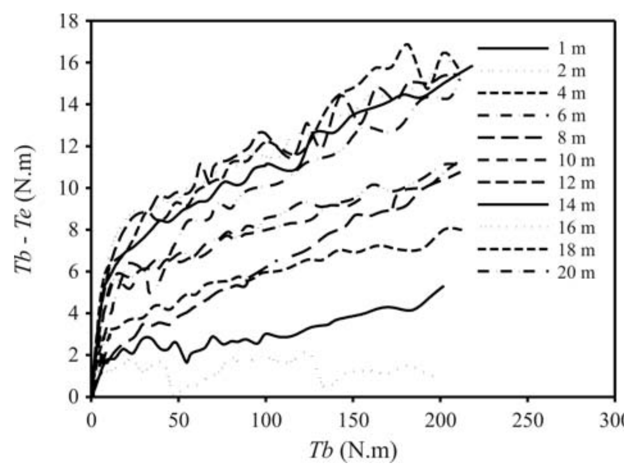

Figure 16 - (*Tb* - *Te*) *vs. Tb*.

3.3. Field tests

Figure 17 depicts the data recorded by the data acquisition system, showing the torque values from both torquemeters and the substantial differences between those values.

Table 6 lists the maximum torques recorded by the torquemeters used in the field tests. As can be observed, the differences between the two values, T_b and T_e, (on average around 16 N.m) are below the normal minimum torquemeter scale (20 N.m). These results confirm the data obtained in the laboratory tests.

4. Conclusions

Based on the laboratory and field tests, it is possible to ensure that the torque difference through rod length is lower than the minimum scale of mechanical torquemeters that are used on practical engineering (20 N.m). That way, the influence of the drill rod length is not significant considering the practical results.

Following the theoretical analyses, it can be concluded that the rod's self-weight is not the limiting factor for the buckling phenomenon. The most important rod characteristic is the column's slenderness in order to preserve the rods' stability during field tests.

As stated earlier herein, the column's slenderness should be kept to the 200 limit, which corresponds to two

Table 6 - Differences in the applied torques recorded by the two torquemeters.

Rod length (m)	Depth (m)	T_b (N.m)	T_e (N.m)	T_b - T_e (N.m)
2	1	50.2	36.9	13.3
3	2	60.2	57.6	2.6
4	3	57.7	42.6	15.1
5	4	96.8	78.9	17.9
6	5	98.6	80.7	17.9
7	6	158.7	146.4	12.3
8	7	99.5	81.2	18.3
9	8	289.9	272.0	17.9
10	9	192.9	164.2	28.7
16	15	290.7	273.2	17.5
		Average (N.m)		16.2

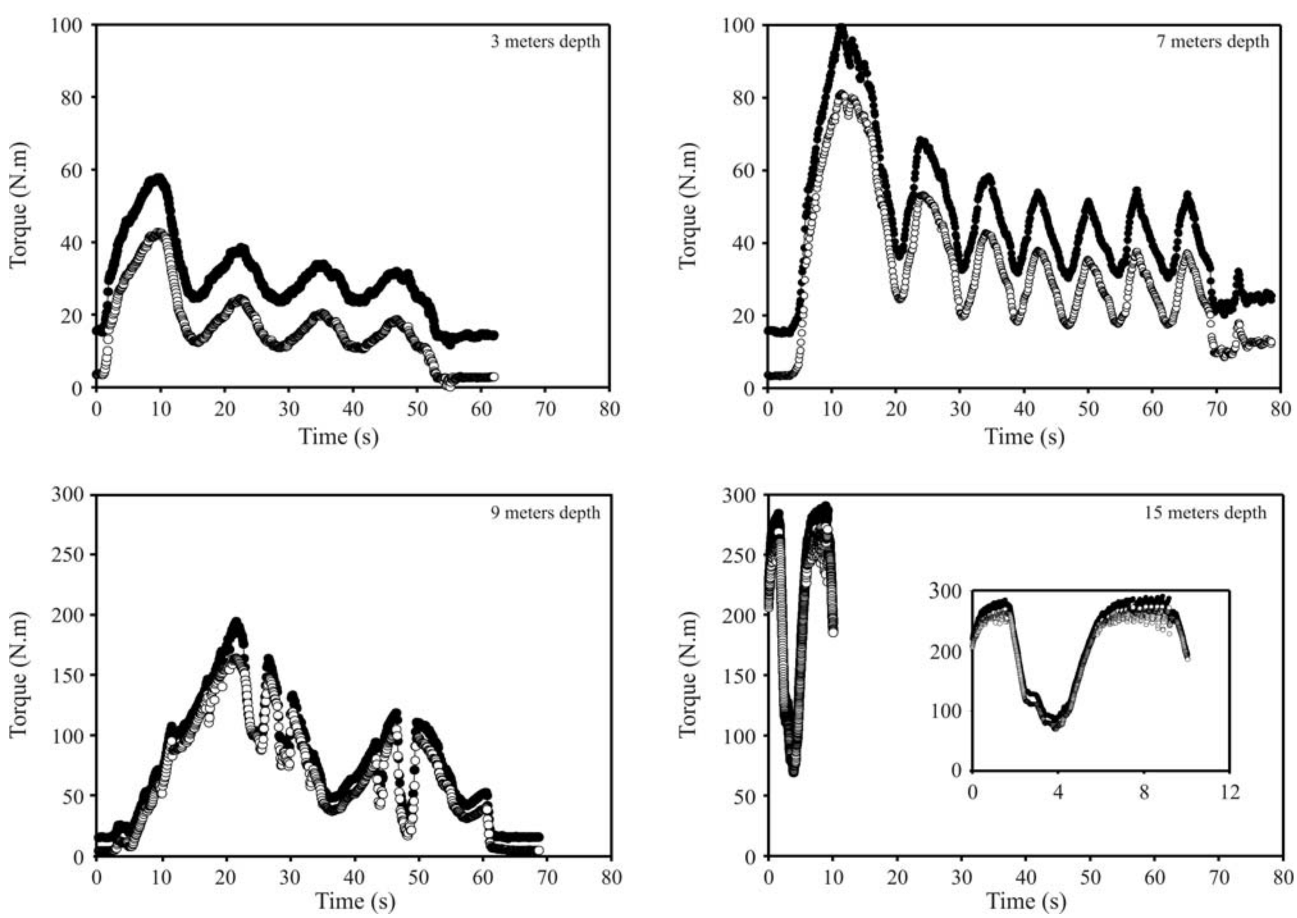

Figure 17 - Torque *vs.* time.

meters of free rod length. Intermediate spacers should be placed along the rod's entire length to avoid free rod lengths from exceeding two meters and thereby reducing the efficiency of the test.

Moreover, with regard to the sampler's penetration in response to the falling hammer, this load can be considered to have no influence down to a depth of around 12 m. However, this dynamic effect could not be eliminated, since determining it is the goal of the test.

Some important aspects to be considered are that the real column is not bi-articulated at its extremities and also that it has eccentricities along its length, neither of which are considered in the theoretical formulation. All the above described details confirm the idea that the rod's free length should be diminished by using intermediate spacers.

Acknowledgments

The authors acknowledge the financial support of the Brazilian research funding agency FAPESP (Fundação de Amparo à Pesquisa do Estado de São Paulo).

References

ABNT (2001) NBR 6484 - Execução de Sondagens de Simples Reconhecimento dos Solos, 12 pp.

ABNT (1986) Projeto e Execução de Estruturas de Aço em Edifícios, NBR 8800, 198 pp.

De Mello, V.F.B. (1971) The Standard Penetration Test. Pan-American Conference on Soils Mechanics and Foundation Engineering, Porto Rico, v. 1. 86 pp.

Cavalcante, E.H.; Danziger F.A.B.; Danziger, B.R. & Bezerra R.L. (2002). Medida de Energia do SPT: Instrumentação para Registro de Força e de Velocidade nas Hastes. XII COBRAMSEG – Congresso Brasileiro de Mecânica dos Solos e Engenharia Geotécnica, São Paulo, v. 1, pp. 97-106.

Wolfram, S. (2003) Mathematica Book, 5 th ed. Wolfram Media, Champaign, 1464 pp.

Mayne, P.W. (2001) Strain-strenght-flow parameters from enhanced *in-situ* tests. In-Situ 2001, Bali, pp. 21-48.

Odebrecht, E.; Rocha, M.M.; Bernardes, G.P. & Schnaid, F. (2002) Medidas de energia no ensaio SPT. Proc. XII COBRAMSEG – Congresso Brasileiro de Mecânica dos Solos e Engenharia Geotécnica, São Paulo, v. 1, pp. 107-118.

Peixoto, A.S.P. (2001) Estudo do ensaio SPT-T e sua Aplicação na Prática de Engenharia de Fundações (Study of SPT-T test and its application on Foundation Engineering). PhD Thesis, Universidade Estadual de Campinas.

Ranzini, S.M.T. (1994) SPTF: 2ª parte. Soils and Rocks, v. 17:3, p. 189-190.

Ranzini, S.M.T. (1988) SPTF. Soils and Rocks, v. 11:1, p. 29-30.

Schiel, F. (1984) Introdução à Resistência dos Materiais, 3ª ed. Editora Harper & Row do Brasil Ltda, São Paulo, 395 pp.

Schmertmann, J.H. & Palacios, A. (1979) Energy Dynamics of SPT. Journal of the Geotechnical Engineering Division, v. 105:GT8 p. 909-926.

Timoshenko, S. (1981) Resistência dos Materiais, 1ª ed. Livro Técnicos e Científicos Editora S.A., Rio de Janeiro, 518 pp.

Influence of Geogrid Geometrical and Mechanical Properties on the Performance of Reinforced Veneers

Helber N.L. Viana, Ennio M. Palmeira

Abstract. Some types of geosynthetics have been traditionally used as reinforcement in several types of geotechnical projects. They can also be used as reinforcement to increase the stability of cover soils in slopes of waste disposal areas. This paper investigates the influence of some geometrical and mechanical properties of geogrids on the stability of cover soils using a large scale ramp test. Tests were performed with a sand and different combinations of geosynthetics, involving the use of geogrids, a nonwoven geotextile and rough and smooth geomembranes. The elevation of the geogrid in the cover soil was varied in the test programme. The results obtained show a marked influence of the presence of geogrid reinforcement in the cover soil on the stability of the system and on the reduction of tensile forces mobilised in the geomembrane during the test in tests with smooth or rough geomembranes. The beneficial effect of the presence of the geogrid in the cover soil was a function of its geometrical and mechanical properties.

Keywords: geosynthetics, veneers, reinforcement, ramp test, cove soil stability.

1. Introduction

The stability of veneers on slopes of waste disposal areas or in protective works against slope erosion has to be carefully evaluated to avoid failures that may cause significant cost and time to repair. Works in the literature (Dwyer *et al.* 2002, Gross *et al.* 2002, Blight 2007) have reported failures of cover soils of slopes of waste disposal areas or of final covers of landfills due to low adherence between soils and geosynthetics or due to tensile failure of the geosynthetic layer caused by excessive mobilization of tensile forces. Figures 1(a) and (b) show some examples of such failures. The occurrence of these types of failure mechanisms can be avoided or minimised with the use of geosynthetic reinforcement in the cover soil (Palmeira & Viana 2003, Palmeira *et al.* 2008).

Several authors have reported the use of geogrid layers installed directly on the geomembrane to increase the stability of cover soils and to reduce tensile forces mobilised in geomembranes (Chouery-Curtis & Butchko 1991, Quinn & Chandler 1991, Chiado & Walker 1993, Fox 1993, Wilson-Fahmy & Koerner 1993, Baltz *et al.* 1995, Sperling & Jones 1995, Palmeira *et al.* 2002, Palmeira & Viana 2003, for instance). Palmeira & Viana (2003) performed large scale ramp tests to study the behaviour of reinforced cover soils where the reinforcement layer was installed parallel to the slope surface but at varying elevations above the geomembrane. Palmeira *et al.* (2008) reports the use of horizontal reinforcement layers to increase the stability of cover soils in landfills. The arrangement with the reinforcement installed parallel to the slope is more practical than the use of horizontal reinforcement layers, but stronger and stiffer reinforcements are required, particularly for long slopes. In either case, the presence of the reinforcement increases the stability conditions of the cover soil and reduces its deformability, as well as the tensile loads mobilised in the geomembrane (Palmeira & Viana 2003, Palmeira 2009).

Direct shear tests, pull-out tests and ramp or inclined plane tests are usual testing techniques to evaluate the adherence between soils and geosynthetics. The advantage of the latter with respect to direct and pull-out tests is that tests under very low normal stresses can be performed, which is consistent with the actual low stress levels at the soil-geosynthetic or geosynthetic-geosynthetic interfaces in slope veneers. The use of conventional direct shear tests under such low stress levels or the extrapolation of results of direct shear tests carried out under higher stress levels can yield to unsafe values of interface strength parameters, as reported by Girard *et al.* (1990), Giroud *et al.* (1990) and Gourc *et al.* (1996), for instance.

Ramp tests to evaluate adherence between different materials have been performed by several researchers (Girard *et al.* 1990, Giroud *et al.* 1990, Koutsourais *et al.* 1991, Girard *et al.* 1994, Gourc *et al.* 1996, Izgin & Wasti 1998, Lalarakotoson *et al.* 1999, Lima Junior 2000, Lopes *et al.* 2001, Mello 2001, Wasti & Özdüzgün 2001, Palmeira *et al.* 2002, Viana 2003, Viana 2007, Aguiar 2003, Palmeira & Viana 2003, Viana 2007, Aguiar 2008). Palmeira *et al.* (2002) report the results of tests on different interfaces using a large scale ramp test device. The advantage of a large ramp apparatus is that the distribution of normal stresses on the interface can be more uniform than that in a smaller apparatus and there is less influence of the boundary conditions on the results obtained.

Helber N.L. Viana, PhD., Ministry of National Integration, Secretariat of Water Infrastructure, SIH, 70067-901, Brasília, DF, Brazil. e-mail: helber@unb.br.
Ennio M. Palmeira, PhD., Professor, University of Brasília, Department of Civil and Environmental Engineering, FT, 70910-900 Brasília, DF, Brazil. e-mail: palmeira@unb.br.
Submitted on December 17, 2008; Final Acceptance on May 6, 2009; Discussion open until September 30, 2010.

(a) Dwyer *et al.* (2002).

(b) Gross *et al.* (2002).

Figure 1 - Cover soil failures in landfills. (a) Dwyer *et al.* (2002). (b) Gross *et al.* (2002).

This paper examines the influence of reinforcement in cover soils using a large ramp test device. The study focus on the influence of geometrical and mechanical properties of geogrid reinforcement on the performance of reinforced cover soils.

2. Experimentals

2.1. Equipment used in the tests

A large ramp test apparatus was used in the experimental programme. Figures 2 and 3 show the apparatus and the test arrangement (Palmeira & Viana 2003). Boxes with varying heights were used to confine the soil and the box heights could be chosen according to the soil sample height and reinforcement elevation (y in Fig. 3). The internal dimensions of the boxes were 1920 mm (length) and 470 mm (width) and the total height of the soil sample (H in Fig. 3) in the present series of tests was equal to 200 mm. The geosynthetic layers tested were fixed to the ramp by clamps connected to load cells for the measurement of mobilised tensile loads at the geosynthetic end during testing (Fig. 3). The roughness of the surface of the ramp in the present series of tests was reduced using double layers of plastic films and oil, yielding to an interface friction angle between ramp surface and the smooth HDPE geomembrane used in the tests of approximately 6°. Displacement transducers allowed the measurement of relative displacements between the soil sample and the ramp. The methodology of the test consisted on increasing the inclination of the ramp to the horizontal direction (α, in Fig. 3) until sliding of the top soil block occurred.

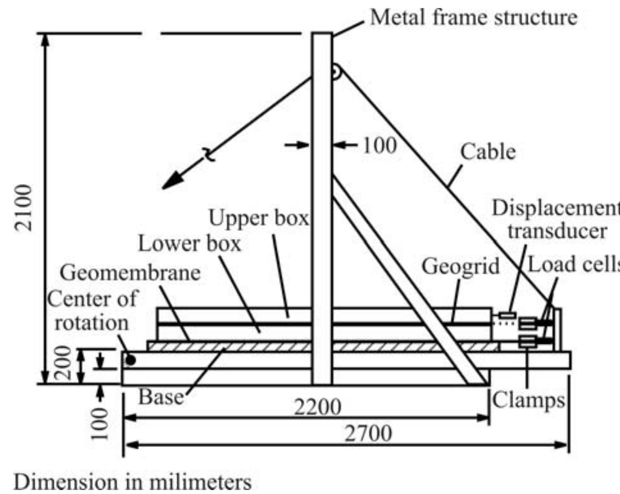

Figure 2 - Large ramp test apparatus.

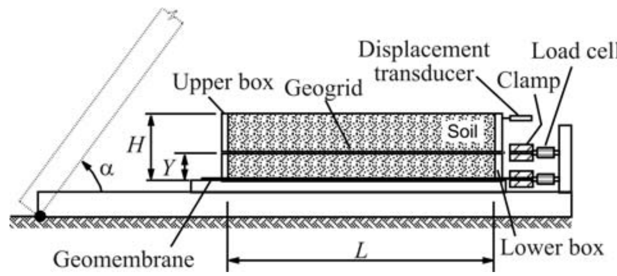

Figure 3 - Test setup.

The values of the elevation (y) of the reinforcement layer inside the cover soil used were 0, 0.05 m, 0.10 m and 0.15 m. Tests with reinforcement at varying elevations and a nonwoven geotextile layer directly on the geomembrane were also carried out. A geotextile layer on the geomembrane is a common measure to minimise the risk of mechanical damage to the geomembrane or to reduce the shear loads transferred to the geomembrane by the cover soil.

2.2. Materials tested

The soil used in the tests was a uniform coarse sand, with particle diameters varying between 0.6 mm and 2 mm.

Table 1 summarises the main properties of this sand. The sand was compacted in the testing box in 5 cm thick layers by tamping using a compaction energy per unit volume of soil of 1.56 kN.m/m^3, to reach a target relative density of 57%.

The geosynthetic materials used in the tests comprised two geomembranes, a nonwoven geotextile and several geogrids. Table 2 presents the main properties of the geosynthetics used. Geomembrane GMS is a smooth HDPE geomembrane, whereas geomembranes GMR-A and GMR-B are rough HDPE geomembranes, respectively, with different roughness conditions. Figures 4(a) and (b) show the surface characteristics of these geomembranes. The roughness of the surface of geomembrane GMR-A is not uniform and consists of a succession of rough rib-like bumps, which locally interacts with soil by bearing, on a rather smooth surface. The roughness of the geomembrane GMR-B can be considered as uniform and similar to a sandpaper surface. The nonwoven geotextile (code GTNW) was a needle-punched product, made of polypropylene, with a mass per unit area of 200 g/m^2. The several geogrid geometries tested were obtained by cutting longitudinal or transverse members of two reference geogrids (GG-A and GG-H, Fig. 5), made of polyester, to obtain the geometrical patterns of the other grids (GG-B to GG-G and GG-I to GG-O). By cutting transverse and/or longitudinal members of such grids, one can vary the grid solid surface per unit area, the bearing load capacity of the grid and/or its tensile strength and stiffness. The removal of grid trans-

Table 1 - Properties of the sand used in the tests.

Property$^{(1)}$	
D_{10} (mm)	0.63
D_{60} (mm)	1.00
CU	1.61
G_s	2.57
ϕ (degrees)	37$^{(2)}$

Notes: (1) D_{10} = diameter for which 10% of the soil in mass have particles smaller than that diameter, D_{60} = diameter for which 60% of the soil in mass have particles smaller than that diameter, CU = soil coefficient of uniformity, G_s = soil particle density and ϕ = soil friction angle; (2) Friction angle obtained from tests on the sand using the ramp test equipment under similar stress level as that in the ramp tests with geosynthetics.

Table 2 - Geosynthetics tested.

Geosynthetic	Code	$M_A$$^{(2)}$ (g/m^2)	$t_G$$^{(3)}$ (mm)	$T_{max}$$^{(4)}$ (kN/m)	$\varepsilon_{max}$$^{(5)}$ (%)	J$^{(6)}$ (kN/m)	N$^{(7)}$	Aperture$^{(8)}$ (mm)
Geotextile (PP)$^{(1)}$	GTNW	200	2.2	12	60	22	—	—
Geomembranes (HDPE)$^{(1)}$	GMS	950	1.0	20/33$^{(9)}$	12/700$^{(9)}$	260	—	—
	GMR-A	950	1.0	20/33$^{(9)}$	12/700$^{(9)}$	260	—	—
	GMR-B	940	2.0	29/21$^{(9)}$	12/100$^{(9)}$	300	—	—
Geogrids (PET)$^{(1)}$	GG-A	250	1.1	20	12.5	200	96	20 x 20
	GG-B	233	1.1	10	12.5	100	96	20 x 40
	GG-C	227	1.1	5	12.5	50	96	20 x 80
	GG-D	168	1.1	2.5	12.5	25	96	20 x 160
	GG-E	228	1.1	20	12.5	200	48	40 x 20
	GG-F	213	1.1	20	12.5	200	24	80 x 20
	GG-G	205	1.1	20	12.5	200	12	160 x 20
	GG-H	760	1.6	200	12.0	1670	10	200 x 40
	GG-I	739	1.6	100	12.0	835	10	200 x 80
	GG-J	719	1.6	50	12.0	417.5	10	200 x 160
	GG-L	699	1.6	25	12.0	208.75	10	200 x 320
	GG-M	748	1.6	200	12.0	1670	5	400 x 40
	GG-N	737	1.6	200	12.0	1670	2	800 x 40
	GG-O	726	1.6	200	12.0	1670	1	1600 x 40

Notes: (1) PP = polypropylene, HDPE = high density polyethylene, PET = polyester; (2) M_A = mass per unit area; (3) t_G = thickness; (4) T_{max} = tensile strength from wide strip tensile tests; (5) ε_{max} = maximum tensile strain from wide strip tensile tests; (6) J = tensile stiffness from wide strip tensile tests; (7) N = number of grid transverse members; (8) Value on the left is parallel to the grid longitudinal member and value on the right is parallel to the transverse members; (9) Value on the left is at yielding and on the right at rupture.

verse members will also influence the amount of interference among these members (Palmeira and Milligan 1989, Palmeira 2004 and 2009).

(a) Smooth geomembrane surface.

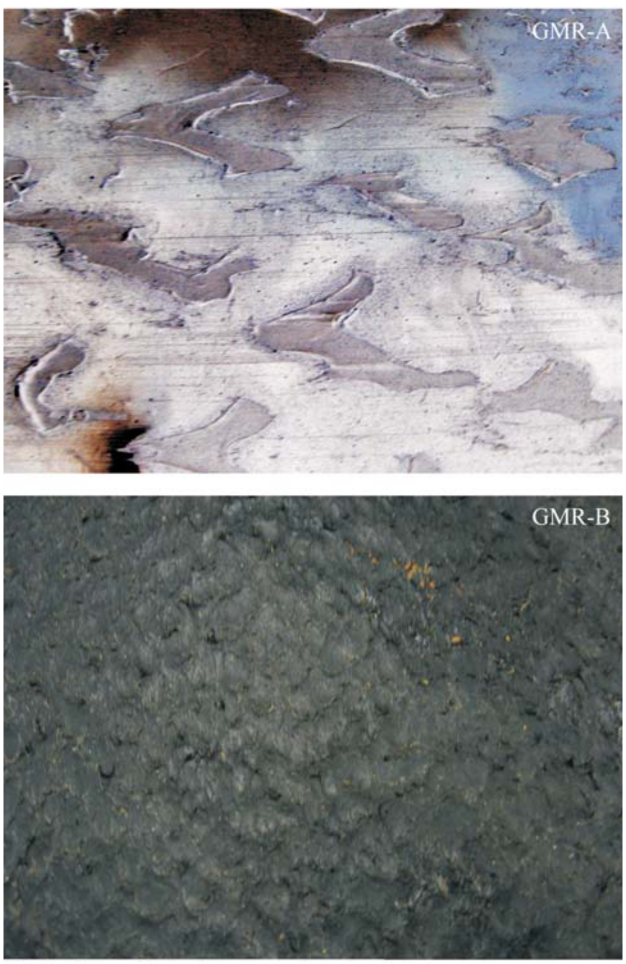

(b) Surfaces of rough geomembranes.

Figure 4 - Surface characteristics of the geomembranes tested. (a) Smooth geomembrane surface. (b) Surfaces of rough geomembranes.

3. Results Obtained

3.1. Tests with geomembranes only

The results obtained for ramp tests with the geomembranes only are presented in Figs. 6(a) and (b). Sliding of the cover soil on the geomembrane occurred for ramp inclinations of 26° for geomembrane GMS, 29° for geomembrane GMR-B and 31° for geomembrane GMR-A (Fig. 6a).

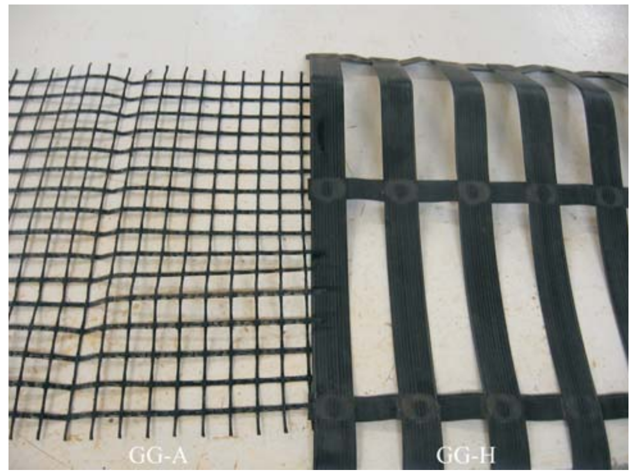

Figure 5 - Reference grids GG-A and GG-H.

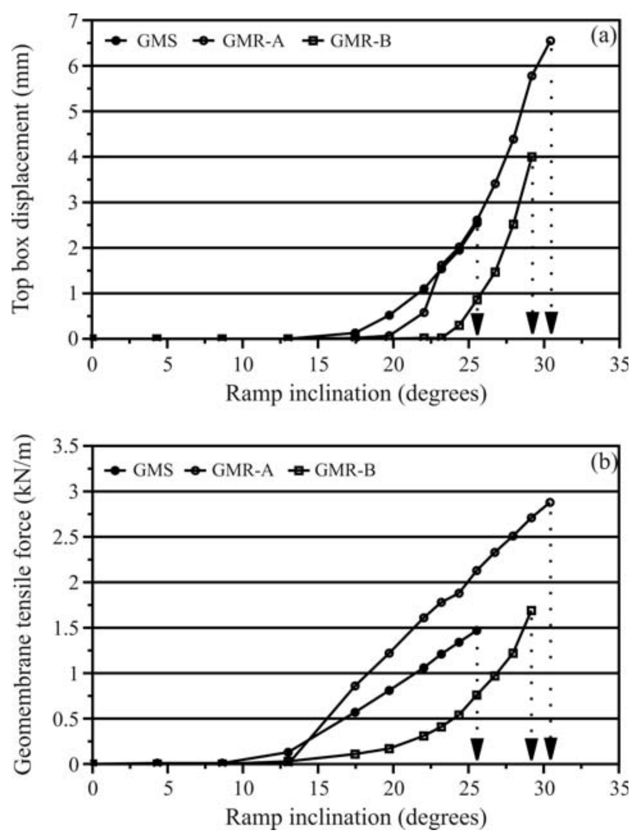

Figure 6 - Ramp tests on geomembranes. (a) Top box displacement *vs.* ramp inclination. (b) Geomembrane tensile force *vs.* ramp inclination.

These results show the influence of roughness on the adherence between cover soil and geomembrane. It is interesting to note that the development of box displacements for tests with geomembranes GMS and GMR-A was similar up to box displacements of 26°(failure of the sand-GMS interface). To some extent, this can be explained by the characteristics of the surface of geomembrane GMR-A (discrete bumps on a smooth surface), as described before. Thus, sliding must have occurred first in the smooth parts of the geomembrane followed by bearing failure at the bumps, the latter being responsible for the increase of 5° on ramp inclination at failure in comparison with the result obtained for geomembrane GMS.

The mobilisation of tensile forces in the geomembranes during the test are shown in Fig. 6(b). The pattern of tensile force during ramp inclination was very distinct among the geomembranes. One should bear in mind that the mobilisation of tensile forces in the geomembrane also depends on the adherence between geomembrane and ramp surface. The progressive failure mechanism developed in this type of test (Palmeira *et al.* 2002, Fox & Kim 2008 and Palmeira 2009) also influences the pattern of force mobilisation in the geomembrane.

3.2. Influence of the presence of geogrid and geotextile on reinforced veneer behaviour

3.2.1. Tests with the smooth geomembrane

Figures 7(a) and (b) show the results obtained for tests with the smooth geomembrane (GMS) and the reference geogrids GG-A and GG-H positioned at different elevations regarding top box displacements *vs.* ramp inclination. It can be seen that for both geogrids a marked increase on the ramp inclination at failure was obtained with respect to the test on the unreinforced cover soil. The presence of the geogrid causes failure to take place along the soil-geogrid interface, rather than along the soil-geomembrane interface. Under these circumstances, the ramp inclination at failure was closer to the sand friction angle (37°). The results also show that the systems with the geogrid directly on the geomembrane (y = 0) presented a very distinct behaviour in comparison to the cases where the geogrid was located some distance above the geomembrane. The elevation of the geogrid influenced the development of top box displacement with largest displacements for y = 0. The elevation of the geogrid affected less the ramp inclination at failure, except for the case with y = 0 and particularly for geogrid GG-H, where the ramp inclination at failure was significantly smaller than those observed for y > 0. It is also interesting to note that for y > 0 the presence of the geogrid in the cover soil yielded values of ramp inclination at failure in tests with the smooth geomembrane greater that those obtained for the tests with the rough geomembranes GMR-A and GMR-B only (Figs. 6a and b). Therefore, for the materials tested and test conditions the presence of the geogrid compensated for the smoothness of geomembrane GMS, regarding ramp inclination at failure.

The presence of a geotextile layer on the geomembrane reduced even further the displacements of the top box during ramp inclination, as seen in Fig. 8(a) for tests with y = 0.1 m. The presence of the geotextile also slightly increased the ramp inclination at failure. The mobilised tensile forces in the smooth geomembrane GM-S were also reduced due to the presence of the geotextile, as shown in Fig. 8(b). Independent on the geogrid considered, a significant reduction on forces in the geomembrane can be noted, with the test with GG-H presenting slightly less geomembrane forces than the test with GG-A. However, the presence of the geotextile layer on the geomembrane had a more significant effect on the test with geogrid GG-H.

3.2.2. Tests with rough geomembranes

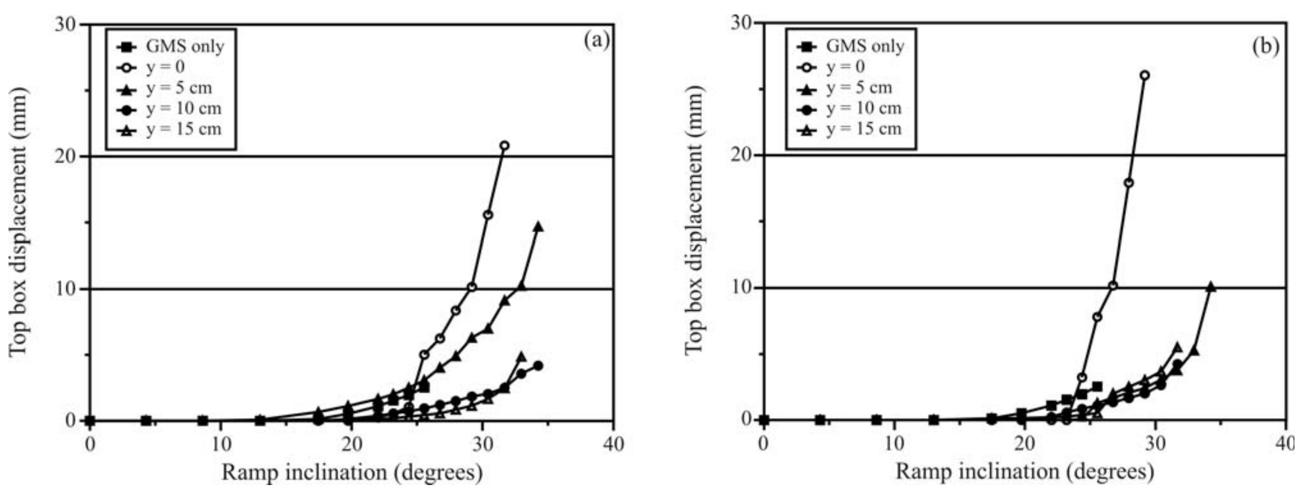

Figure 7 - Results of tests on cover soils reinforced with geogrids at varying elevations – geomembrane GMS. (a) Tests with geogrid GG-A. (b) Tests with geogrid GG-H.

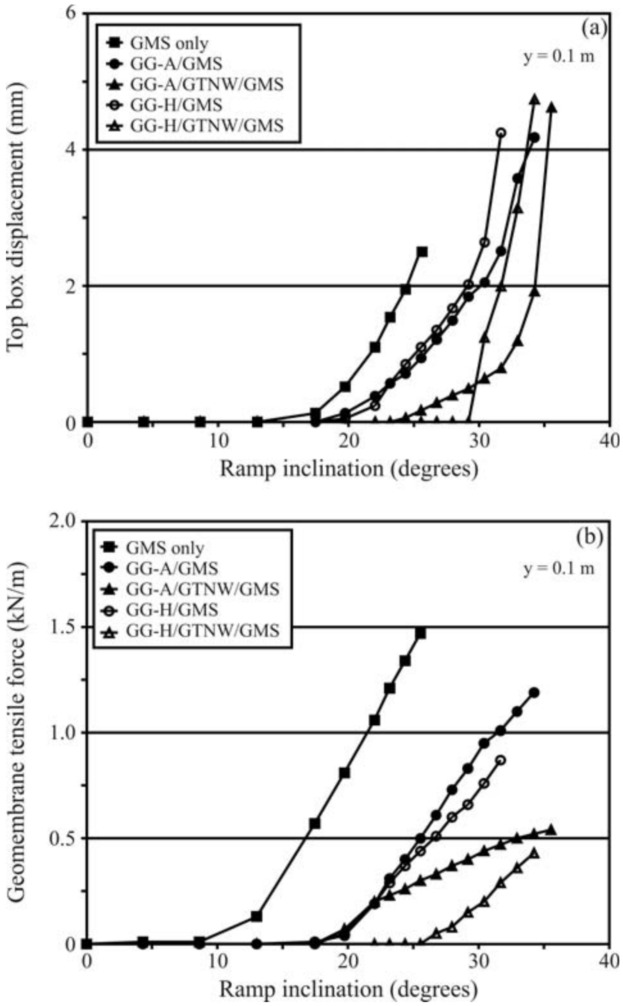

Figure 8 - Influence of the presence of a geotextile on the smooth geomembrane. (a) Top box displacement *vs.* ramp inclination. (b) Geomembrane tensile force *vs.* ramp inclination.

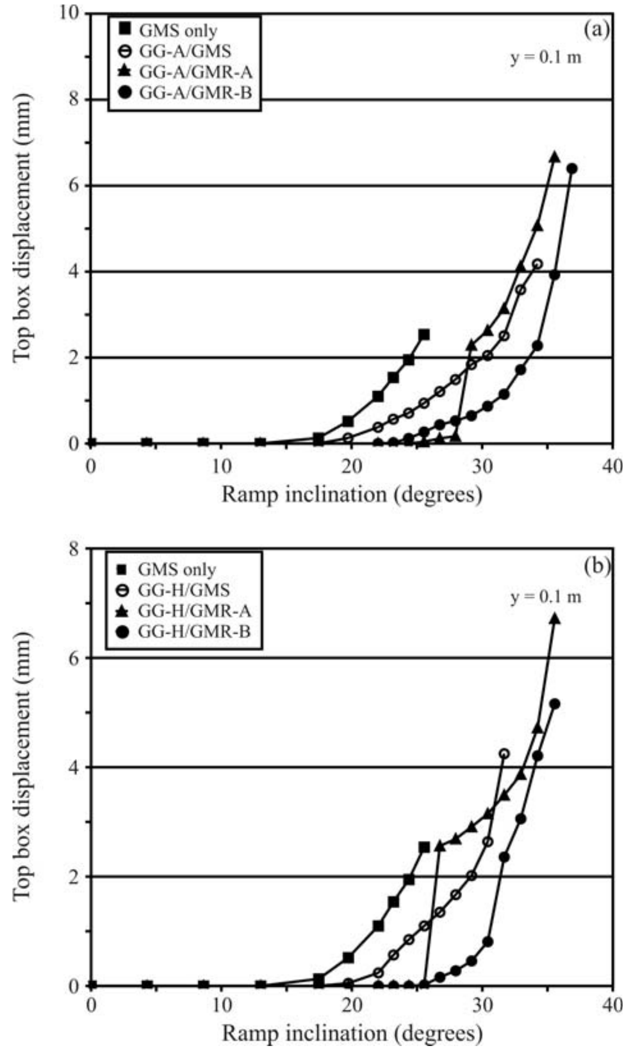

Figure 9 - Tests with rough geomembranes GMR-A and GMR-B. (a) Tests with geogrid GG-A. (b) Tests with geogrid GG-H.

Results of top box displacement *vs.* ramp inclination obtained in tests on unreinforced and reinforced (y = 0.1 m) cover soils with rough geomembranes GMR-A and GMR-B and geogrids GG-A and GG-H are presented in Figs. 9(a) and (b). Again, the presence of the geogrid in the cover soil caused a marked increase on the ramp inclination at failure. Interesting features are the sudden increase of top box displacements for the tests with geomembrane GMR-A at ramp inclinations of 28 degrees for geogrid GG-A and 26 degrees for geogrid GG-H. This occurrence was more intense in the test with geogrid GG-H and influenced the variation of mobilised tensile load in the geomembrane with ramp inclination, as shown in Fig. 10, although the forces in the geomembranes in the tests with grid reinforcement in the cover soil remained considerably lower than those in the tests without reinforcement (Fig. 10).

The sudden increases of top box displacement and geomembrane forces mentioned above are certainly associated with the characteristics of the surface of geomembrane

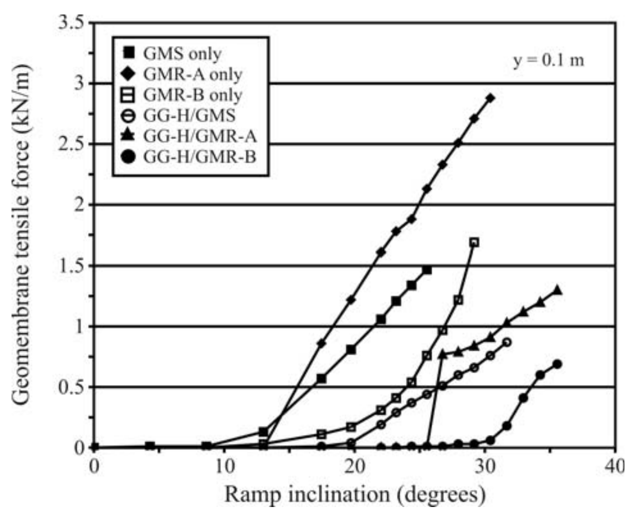

Figure 10 - Geomembrane tensile forces in tests with geogrid GG-H.

GMR-A, commented before. This type of behaviour was neither observed in the tests with the uniformly roughened geomembrane GMR-B nor in the tests with GMR-A only (Fig. 6). It is interesting also to note that the sudden increase on top box displacement and geomembrane tensile force occurred at ramp inclinations (26° and 28° for geogrids GG-H and GGA, respectively) close or slightly greater than the value at failure for the test with the smooth geomembrane. It is likely that sliding of the sand on the smoother parts of the surface of geomembrane GMR-A will increase the passive resistance at the rib-like bumps and cause dilation at the sand-geomembrane interface. The presence of the geogrid in the cover soil will inhibit dilation and increase confinement on the geomembrane. The results obtained show that the presence of the geogrid reinforcement caused a complex interaction mechanism with the rough geomembrane GMR-A. As it was observed in the tests with the smooth geomembrane, the presence of the geogrid also increased markedly the ramp inclination at failure and reduced the tensile loads mobilised in the rough geomembranes.

Figures 11 and 12 show the influence of the presence of a nonwoven geotextile layer on the rough geomembranes for tests with geogrids GG-A and GG-H, respectively. The presence of the geotextile layer did not influence significantly the development of top box displacement during the tests with geomembrane GMR-B (Figs. 11a and 12a). More important influence on box displacement was observed for the test with geomembrane GMR-A and geogrid GG-H (Fig. 12a). In this case the presence of the geotextile attenuated the sudden increase in top box displacements observed for the tests with geogrid in the cover soil only. The presence of the geotextile further reduced the tensile force mobilised in the geomembranes for both grids (Figs. 11b and 12b) and attenuated the sudden increase in geomembrane force observed in tests with the geogrids only, particularly for the case of geogrid GG-H (Fig. 12b).

Figures 13(a) to (c) show the reductions on tensile force in the geomembrane in tests with geogrid and/or geotextile, with respect to the force mobilised in the geomembrane in the tests without geogrid and geotextile, when sliding of the cover soil occurred (y = 0.1 m). Reductions of forces over 50% can be observed in all cases, with greater reductions when geogrid in the cover soil and geotextile on the geomembrane were used. This was particularly so for tests with geomembrane GMR-B (Fig. 13c). These results show that the benefit brought by the presence of the geotextile layer on the geomembrane is twofold. First, it

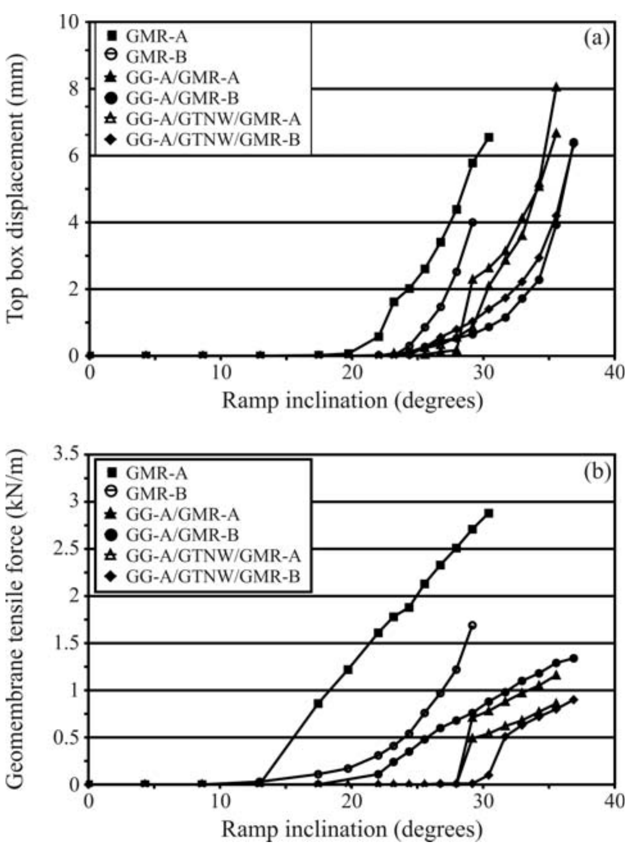

Figure 11 - Influence of the presence of geotextile in tests with rough geomembranes – Tests with and without geogrid GG-A. (a) Top box displacements. (b) Mobilised tensile forces in the geomembrane.

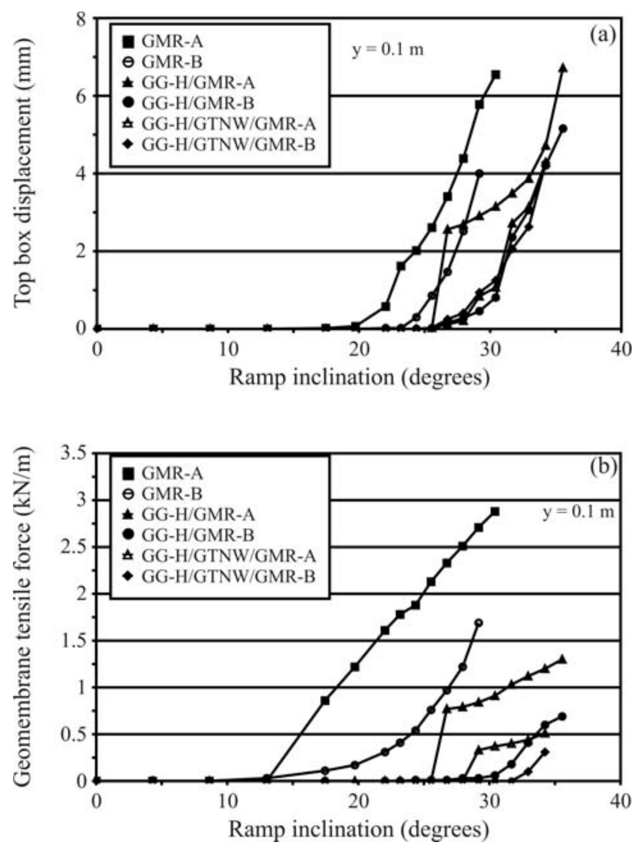

Figure 12 - Influence of the presence of geotextile on top box displacements in tests with rough geomembranes – Tests with geogrid GG-H. (a) Top box displacements. (b) Mobilised tensile forces in the geomembrane.

reduces the possibility of mechanical damage of the geomembrane and second it may reduce even further the tensile force mobilised in the geomembrane.

3.3. Influence of reducing the number of grid longitudinal members

By removing grid longitudinal members, one can reduce the geogrid tensile stiffness (J). The removal of such members not only reduces grid stiffness but also the skin friction between grid and soil and changes grid geometry, increasing aperture size and reducing bending stiffness of transverse members. Palmeira & Viana (2003) presented a preliminary study on the effects of the reduction of longitudinal and transverse members of geogrids on the stability of cover systems, but on a limited basis in comparison to the present study, regarding the variety of geosynthetics products and characteristics investigated. Figures 14(a) and (b) show the effects of altering geogrid aperture size (reductions of up to 80% on the reference grid GG-A original stiffness, J_o) on top box displacements and geomembrane mobilised tensile forces (for y = 0.1 m). As the number of longitudinal members removed increases, so does the displacement of the top box close to failure (Fig. 14a). The ramp inclination at failure was less influenced by the removal of the grid longitudinal members. With the exception of the test with grid GG-D ($J = 0.125J_o$), whose results were close to those of the unreinforced test, the development of top box displacement up to a value of ramp inclination of 32° were similar for grids GG-A to GG-C. The influence of the removal of grid longitudinal members was more significant on the tensile force in the geomembrane (Fig. 14b), but with little difference among results obtained for grids GG-B to GG-D. As the grid aperture increases, greater loads are expected to be transferred to the geomembrane.

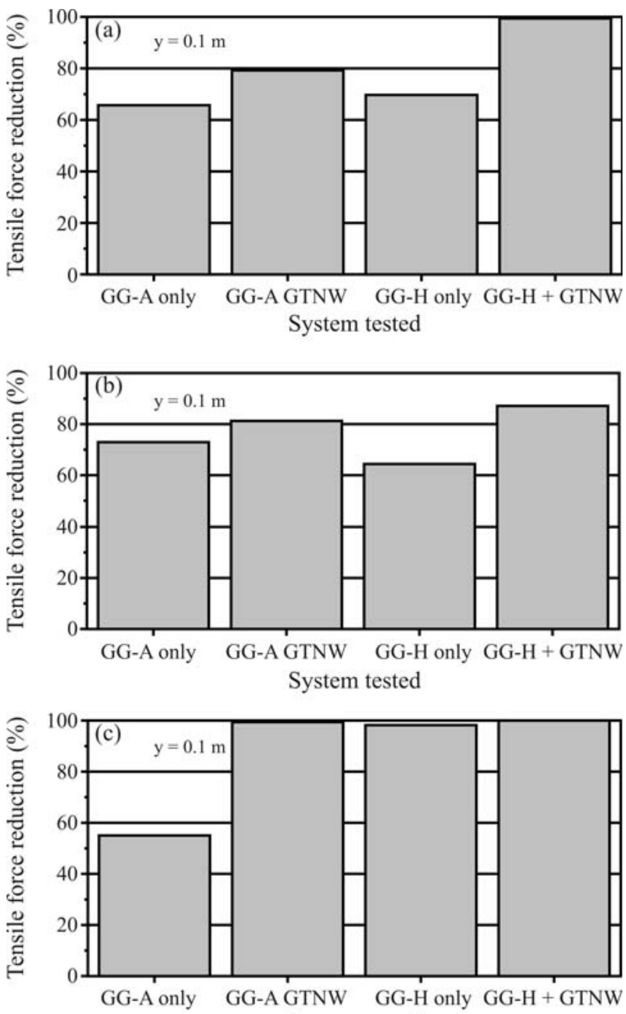

Figure 13 - Reductions on geomembrane tensile force for the ramp inclination of the unreinforced system at failure. (a) Tests with smooth geomembrane GMS. (b) Tests with rough geomembrane GMR-A. (c) Tests with rough geomembrane GMR-H.

Figures 14(a) and (b) also present the result of tests with geogrid GG-C ($J = 0.25J_o$) and the nonwoven geotextile on the geomembrane (test code GG-C/GTNW in Figs. 14a and b). Again these results show a beneficial effect of the geotextile presence in as far as that the test with the combination GG-C/GTNW presented results very close

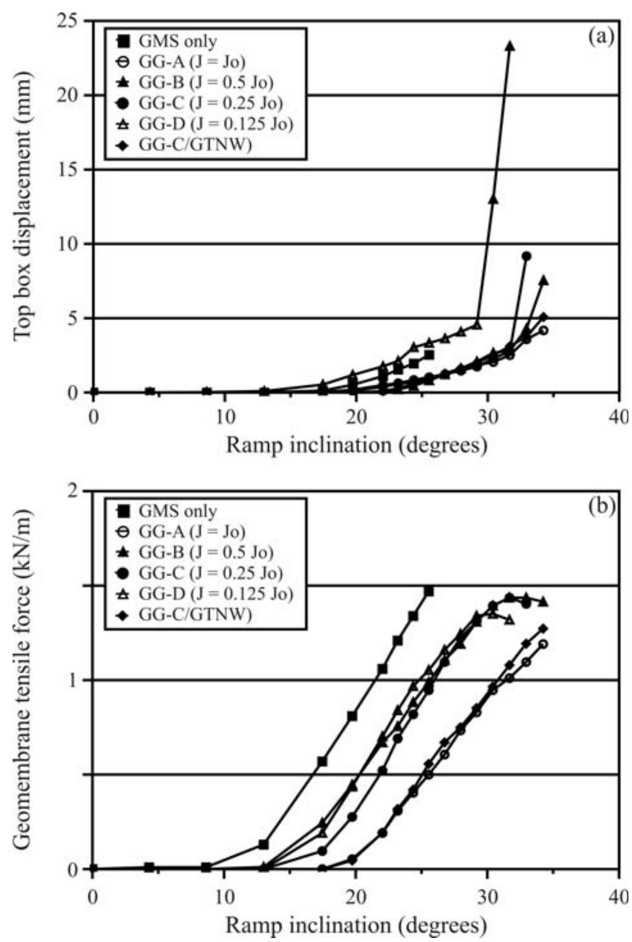

Figure 14 - Influence of the reduction of grid longitudinal members – Geogrid GG-A. (a) Top box displacement *vs.* ramp inclination. (b) Mobilised tensile forces in the geomembrane.

to those obtained in the test with the reference geogrid GG-A. Therefore, the presence of the geotextile compensated for the reduction of geogrid tensile stiffness and increase of geogrid open area.

The effects of the removal of longitudinal members of grid GG-H are shown in Figs. 15(a) and (b) (y = 0.1 m – geogrids GG-I to GG-L), where in this case J_o is the tensile stiffness of the reference grid GG-H. Again, the ramp inclination at failure was not much affected by the changes in grid geometry, but the influence of these changes was slightly more clearly noticed for the grids resulting from the removal of members of grid GG-H than for those resulting from the removal of members of grid GG-A. Again, the combination of a less stiff and more opened geogrid (geogrid GG-J, $J = 0.25J_o$) and geotextile on the geomembrane (test code GG-J/GTNW in Figs. 15a and b) improved the performance of the system, with respect to the test with the geogrid only.

3.4. Influence of reducing the number of grid transverse members

The removal of grid transverse members reduces the amount of soil-grid interaction by bearing as well as skin friction between soil and geogrid. The influence of reducing the number (N) of grid bearing members was assessed by carefully cutting transverse members from the original reference grids GG-A and GG-H, yielding to grids (GG-E to GG-G and GG-M to GG-O, respectively – Table 2) with up to eight times less transverse members than the reference grids. In this series of tests, the elevation of the grid layer was also kept constant and equal to 0.1 m.

Figures 16(a) and (b) show top box displacements and mobilised tensile loads in the geomembrane *vs.* ramp

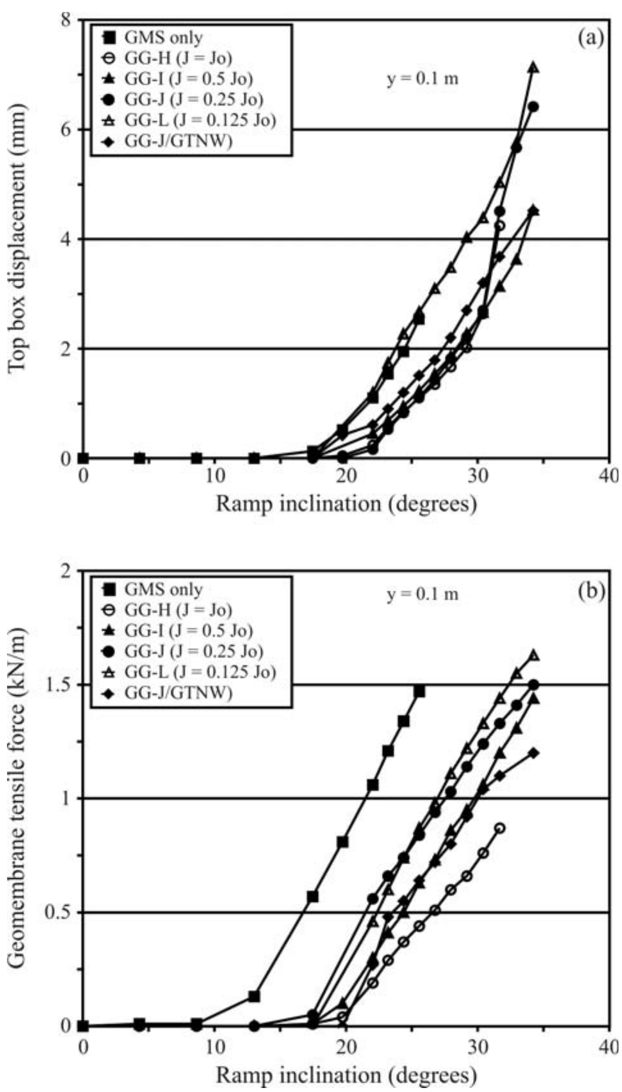

Figure 15 - Influence of the reduction of grid longitudinal members – Geogrid GG-H. (a) Top box displacement *vs.* ramp inclination. (b) Mobilised tensile forces in the geomembrane.

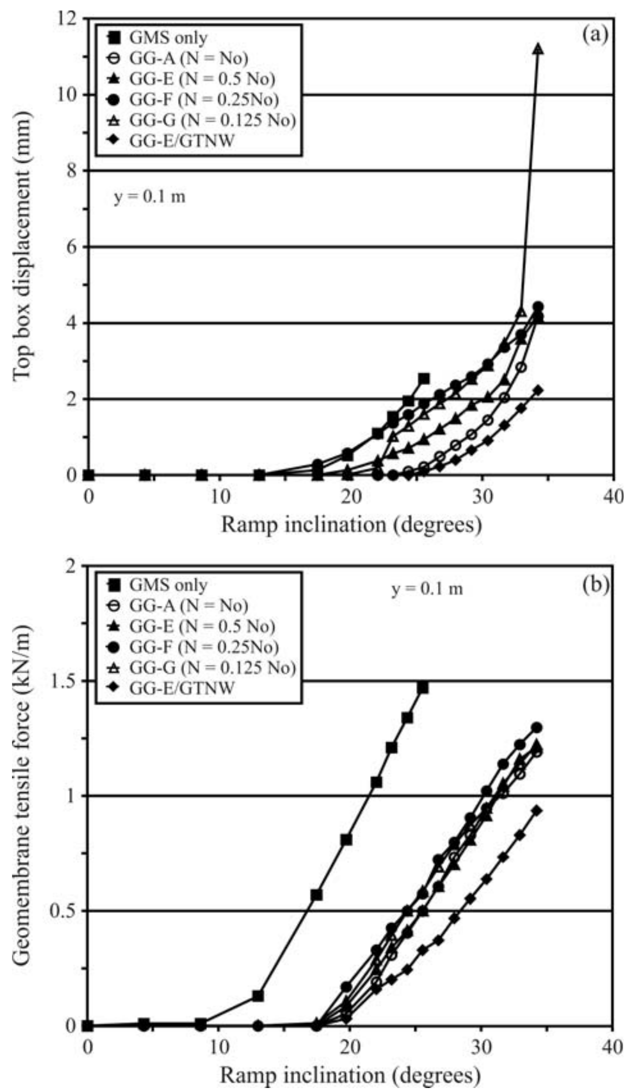

Figure 16 - Influence of the reduction of grid transverse members – Geogrid GG-A. (a) Top box displacement *vs.* ramp inclination. (b) Mobilised tensile forces in the geomembrane.

inclinations for tests with geomembrane GM-S and geogrids GG-E to GG-G, produced by cutting transverse members from the reference geogrid GG-A, for which the number of transverse members is equal to N_o in Figs. 16(a) and (b). It can be noted that the deformability of the system increases with the reduction of the number (N) of transverse members (Fig. 16a). The ramp inclination at failure was not affected by the reduction of transverse members. Failure occurs along the upper interface between soil and geogrid, and the results suggest that the reduction of skin friction between grid surface and soil caused by the removal of transverse members was not significant. The same applies to the mobilised tensile force in the geomembrane, as shown in Fig. 16(b). For the range of values of N tested, the grid was still capable of carrying a considerable amount of load that otherwise would be transferred to the geomembrane. The combination of geogrid GG-E ($N = 0.5N_o$) and geotextile on the geomembrane (test code GG-E/GTNW in Figs. 16a and b) yielded to the best performance in terms of top box displacements and geomembrane tensile forces.

Figures 17(a) and (b) present the influence of the number of transverse members in tests with geogrids (GG-I to GG-L) formed by the reduction of the number (N) of transverse members of the reference grid GG-H (for which $N = N_o$). In this series of tests geomembrane GM-S was used and the grid elevation was equal to 0.1 m. The removal of transverse members increased a little the ramp inclination at failure observed for grid GG-H and had a marked effect on the deformability of the system (Fig. 17a). This was due to the fact that the reduction of the number of transverse members increased the soil to soil contact area (less geogrid solid surface – greater grid apertures). The smaller the number of grid transverse members the smaller the top box displacements at failure. However, less transverse members increased the load transferred to the geomembrane, as can be seen in Fig. 17(b). The removal of transverse members of geogrid GG-H (Fig. 17b) was more influential to geomembrane mobilised tensile loads than the removal of transverse members of geogrid GG-A (Fig. 16b). The smaller the number of transverse members the smaller the ramp inclination for which the geomembrane started to be tensioned and the greater the tensile load mobilised in the geomembrane for a given ramp inclination. The combination of geogrid GG-M ($N = 0.5N_o$) and geotextile on the geomembrane was also beneficial to the reduction of tensile forces in the geomembrane (Fig. 17b), but less influential on the top box displacements (Fig. 17a).

4. Conclusions

This paper presented a study on the influence of the presence of geogrid in the cover soil on the stability of veneers using the ramp test. The main conclusions obtained are summarised as follows.

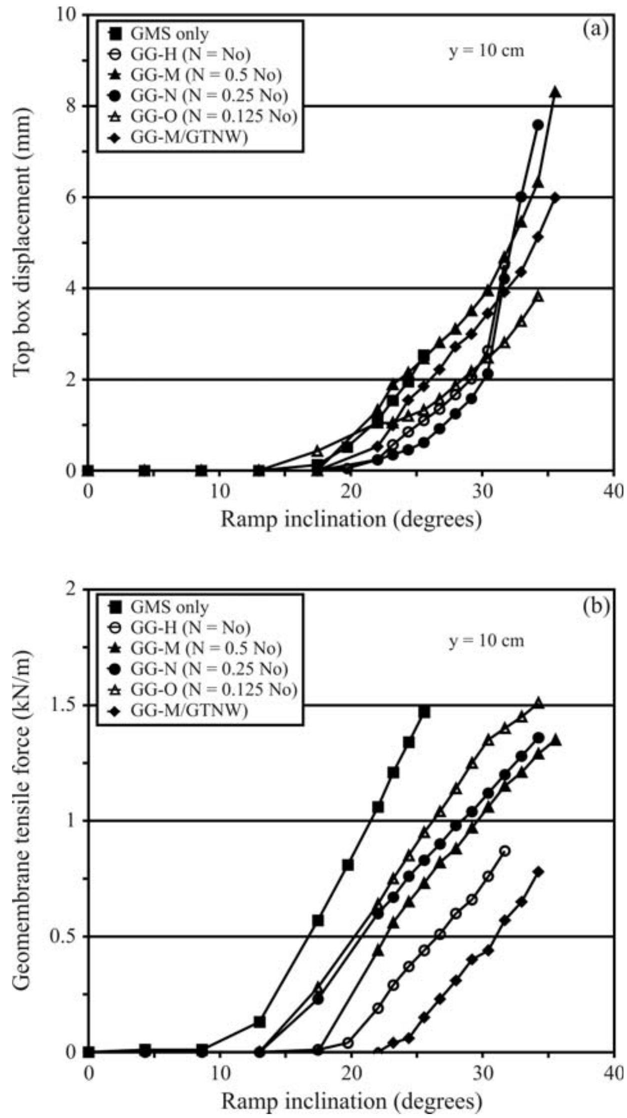

Figure 17 - Influence of the reduction of grid transverse members – Geogrid GG-H. (a) Top box displacement *vs.* ramp inclination. (b) Mobilised tensile forces in the geomembrane.

• The ramp test proved to be a suitable experimental technique for the investigation of soil-geosynthetic interaction under low stress levels, which are typical in cover soils of landfills and waste disposal areas.

• The presence of a geogrid layer in the cover soil increased the ramp inclination at failure and reduced significantly the tensile forces mobilised in the geomembrane. This was observed for both smooth and rough geomembranes.

• The type of roughness of the geomembrane influenced the ramp inclination at failure, development of displacements of the top box and development of tensile forces in the geomembrane.

• The variation of grid geometrical characteristics complicates the interpretation of test results, as the variation of the number of grid members (transverse or longitudinal) also causes variations of grid open area (reduction of soil-geogrid skin friction) and of interference among grid transverse members. These factors can yield to complex modes of interaction among the different materials present in the veneer (soil, grid, geotextile and geomembrane). In general, for the materials and test conditions of the present study, the reduction of the number of grid longitudinal or transverse members increased the deformability of the system and the tensile load mobilised in the geomembrane but had negligible influence on the ramp inclination at failure.

• The presence of a geotextile layer on the geomembrane, besides protecting the latter against mechanical damages, can increase the stability conditions of the system a bit further and reduces the forces transferred to the geomembrane.

• It should be pointed out that the level of contributions due to the presence of geogrid in the cover soil and geotextile on the geomembrane observed in the tests, although encouraging, should be viewed with due care because of the limitations of the testing procedure used, boundary conditions and development of progressive failure mechanisms, for instance. Despite a large scale equipment having been used, the dimensions of the problem in the field are larger and other factors that may play important roles to the stability of actual veneers were not considered in this work. Nevertheless, the results obtained suggest important contributions of geogrid reinforcement to the stability of veneers.

Acknowledgments

The authors are indebted to the following institutions for their contributions to this work: University of Brasília, CNPq (National Council for Scientific and Technological Development) and CAPES, Brazilian Ministry of Education.

References

Aguiar, V.R. (2003) Ensaios de Rampa para o Estudo da Resistência de Interface Solo-Geossintético (Ramp Test for the Study of Soil-Geosynthetic Interface Strength). MSc. Dissertation, Pontifical University of Rio de Janeiro, Rio de Janeiro (in Portuguese), 105 pp.

Aguiar, V.R. (2008) Equipamento para Ensaios de Resistência de Interfaces Solo-Geossintético (Apparatus for Testing Soil-Geosynthetic Interface Strength). PhD. Thesis, Pontifical University of Rio de Janeiro, Rio de Janeiro (in Portuguese).

Baltz, J.F.; Zamojski, L. & Reinknecht, D. (1995) Design and construction of a geogrid-reinforced landfill cap. Geosynthetics'95, NAGS/IFAI/IGS, Nashville, v. 2, pp. 759-769.

Blight, G.E. (2007) Failures during construction of a landfill lining: a case analysis. Waste Management Research, v. 25, p. 327-333.

Chiado, E.D. & Walker, S.D. (1993) Use of increased frictional resistance in landfill liner system design and construction. Geosynthetics'93, NAGS/IFAI/IGS, Vancouver, v. 3, p. 1215-1228.

Chouery-Curtis, V.E. & Butchko, S.T. (1991) Structural geogrids used to stabilize soil veneer covers. Geosynthetics'91, NAGS/IFAI/IGS, Atlanta, v. 1, pp. 125-143.

Dwyer, S.F.; Bonaparte, R.; Daniel, D.E.; Koerner, R.M. & Gross, B. (2002) Technical guidance for RCRA/CERCLA final covers. US Environmental Protection Agency, Office of Solid Waste and Emergency Response, Washington, DC, 287 pp.

Fox, G. (1993) Geogrid provides design solution at Midway landfill. Geosynthetics'1993, NAGS/IFAI/IGS, Vancouver, v. 3, pp. 1229-1241.

Fox, P.J. & Kim, R.H. (2008) Effect of progressive failure on measured shear strength of geomembrane/GCL interface. Journal of Geotechnical and Geoenvironmental Engineering, v. 134:4, p. 459-469.

Girard, H.; Berroir, G.; Gourc, J.P. & Matheu, G. (1994) Frictional behaviour of geosynthetic and slope stability of lining systems. Proc. 5th International Conference on Geotextiles, Geomembranes and Related Products, Singapore, v. 1, pp. 339-342.

Girard, H.; Fisher, S. & Alonso, E. (1990). Problems of friction posed by the use of geomembranes on dam slopes-examples and measurements. Geotextiles and Geomembranes, v. 9:2, p. 129-143.

Giroud, J.P.; Swan, R.H.; Richer, P.J. & Spooner, P.R. (1990) Geosynthetic landfill cap: laboratory and field tests, design and construction. Proc. 4th International Conference on Geotextiles, Geomembranes and Related Products, The Hague, v. 2, pp. 493-498.

Gourc, J.P.; Lalarakotoson, S.; Müller-Rochholtz, H. & Bronstein, Z. (1996) Friction measurements by direct shearing or tilting process – Development of a European standard. Proc. 1st European Conference on Geosynthetics – EUROGEO 1, Maastricht, v. 1, pp. 1039-1046.

Gross, B.A.; Bonaparte, R. & Giroud, J.P. (2002) Appendix F, assessment and recommendations for optimal performance of waste containment systems. In: Waste Containment Systems: Problems and Lessons Learned. EPA, USA, 214 p.

Izgin, M. & Wasti, Y. (1998) Geomembrane-sand interface frictional properties as determined by inclined board and shear box tests. Geotextiles and Geomembranes v. 16:4, p. 207-219.

Koutsourais, M.M.; Sprague, C.J. & Pucetas, R.C. (1991) Interfacial friction study of cap and liner components for landfill design. Geotextiles and Geomembranes, v. 10:5-6, p. 531-548.

Lalarakotoson, S.; Villard, P., Gourc & J.P. (1999) Shear strength characterization of geosynthetic interfaces on inclined planes. Geotechnical Testing Journal, v. 22:4, GTJODJ, p. 284-291.

Lima Junior, N.R. (2000) Estudo da Interação Solo-Geossintético em Obras de Proteção Ambiental com o uso do Equipamento de Plano Inclinado (Study on Soil-Geosynthetic Interaction in Environmental Protection Works Using the Inclined Plane Test). MSc. Dissertation, Graduate Programme of Geotechnics, University of Brasília, Brasília (in Portuguese).

Lopes, P.C.; Lopes, M.L. & Lopes, M.P. (2001) Shear behaviour of geosynthetics in the inclined plane test – Influence of soil particle size and geosynthetic structure. Geosynthetics International, v. 8:4, p. 327-342.

Mello, L.G.R. (2001) Estudo da Interação Solo-Geossintético em Taludes de Obras de Disposição de Resíduos (Study on Soil-Geosynthetic Interaction in Slopes of Waste Disposal Works). MSc. Dissertation, Graduate Programme of Geotechnics, University of Brasília, Brasília (in Portuguese).

Palmeira, E.M. (2004) Bearing force mobilisation in pull-out tests on geogrids. Geotextiles and Geomembranes, v. 22:6, p. 481-509.

Palmeira, E.M. (2009) Soil-geosynthetics interaction: Modelling and analysis – Mercer Lecture 2007-2008. Geotextiles and Geomembranes, v. 27:5, p. 368-390.

Palmeira, E.M.; Lima Junior, N.R. & Mello, L.G.R. (2002) Interaction between soil and geosynthetic layers in large scale ramp tests. Geosynthetics International, v. 9:2, p. 149-187.

Palmeira, E.M. & Milligan, G.W.E. (1989) Scale and other factors affecting the results of pull-out tests of grids buried in sand. Geotechnique, v. 39:3, p. 511-524.

Palmeira, E.M.; Tatsuoka, F.; Bathurst, R.J.; Stevenson, P.E. & Zornberg, J.G. (2008) Advances in geosynthetics materials and applications for soil reinforcement and environmental protection works. Electronic Journal of Geotechnical Engineering, v. 13, pp. 1-38.

Palmeira, E.M. & Viana, H.N.L. (2003) Effectiveness of geogrids as inclusions in cover Soils of slopes of waste disposal areas. Geotextiles and Geomembranes, v. 21:5, p. 317-337.

Quinn, M. & Chandler, M. (1991) Landfill liner side slope design to minimize geomembrane tensile stress. Geosynthetics'91, NAGS/IFAI/IGS, Atlanta, v. 1, pp. 113-123.

Sperling, T. & Jones, A. (1995) Application of geosynthetics at Victoria's Hartland landfill. Geosynthetics'95, NAGS/IFAI/IGS, Nashville, v. 2, pp. 707-718.

Viana, H.N.L. (2003). Estabilidade de Taludes de Áreas de Disposição de Resíduos Revestidos com Geossintéticos: Influência da Presença de Geogrelhas (Stability of Slopes of Waste Disposal Areas with Geosynthetics: Influence of the Presence of Geogrids). MSc. Dissertation, University of Brasília, Brasília (in Portuguese).

Viana, H.N.L. (2007) Estudo da Estabilidade e Condutividade Hidráulica de Sistemas de Revestimento Convencionais e Alternativos para Obras de Disposição de Resíduos (A Study on the Stability and Hydraulic Conductivity of Conventional and Alternative Veneers for Waste Disposal Works). PhD Thesis, University of Brasília, Brasília (in Portuguese).

Wasti, Y. & Özdüzgün, Z.B. (2001) Geomembrane-geotextile interface shear properties as determined by inclined board and direct shear box tests. Geotextiles and Geomembranes, v. 19:1, p. 45-57.

Wilson-Fahmy, R.F. & Koerner, R.M. (1993) Finite element analysis of stability of cover soil on geomembrane-lined slopes. Geosynthetics'93, NAGS/IFAI/IGS, Vancouver, v. 3, pp. 1425-1437.

Technical Note

Soils and Rocks
v. 33, n. 1

Determination of Depth Factors for the Bearing Capacity of Shallow Foundations in Sand

Armando Nunes Antão, Mário Vicente da Silva, Nuno M. da Costa Guerra

Abstract. The bearing capacity of shallow foundations is a traditional problem in geotechnical engineering. Many authors have contributed to the solution of this problem using an equation valid under ideal conditions, such as strip foundation under vertical and centred loading and assuming the superposition of the separate effects of self-weight and surcharge. Successive corrections are made to this equation using factors which take into account conditions different from the ideal ones. Among these corrections are the depth factors, which consider the resistance of the soil above the foundation level. In this work, the shallow foundation is considered in sand, and its strength is modelled by an associated Mohr-Coulomb criterion. Approximations to the depth factors are determined using a finite element formulation based on a strict implementation of the upper bound limit analysis theorem, which allows to obtain an optimal failure mechanism and to determine the limit loads. A comparison with previously published solutions is presented, and values for the depth factors are proposed. Following proposals by other authors, depth factors which take into account the superposition of effects of the bearing capacity equation are presented.

Keywords: bearing capacity, depth factors, upper bound limit analysis, sand.

1. Introduction

The bearing capacity of a strip footing in sand deposit acted upon by a vertical centred load can be expressed by (Terzaghi, 1943):

$$q_u = 0.5\gamma B N_\gamma + q N_q \tag{1}$$

where γ is the soil unit weight below the footing base level, B is the footing width, q is the surcharge at the footing base level and N_γ and N_q are bearing capacity factors which depend on the soil friction angle ϕ'. If the soil above 47-52ting base has the same unit weight and the footing is embedded to a depth D, the surcharge q is equal to γD.

Equation (1) is an approximation:

• it assumes that the bearing capacity in the described conditions is the sum of the bearing capacity in two idealised situations: the first one ($0.5\gamma B N_\gamma$) assumes that the surcharge q is null; the second one considers the soil unit weight below the footing base level equal to zero; the superposition of both effects is not theoretically correct, but this is a traditional solution;

• it does not consider the resistance of the soil above the footing base level, which means that this soil is considered in the calculations by its weight only ($q = \gamma D$).

An exact value of the bearing capacity factor N_q is known (Brinch Hansen, 1970), assuming an associated flow rule:

$$N_q = \tan^2\left(\frac{\pi}{4} + \frac{\phi'}{2}\right) e^{\pi \tan\phi'} \tag{2}$$

but there is not a known exact solution for N_γ. Recently, some excellent approximations have been found (Hjiaj *et al.*, 2005; Martin, 2005). The values obtained by Hjiaj *et al.* (2005) can be approximately determined by the following equation, proposed by them:

$$N_\gamma = e^{\frac{\pi + 3\pi^2 \tan\phi'}{6}} (\tan\phi')^{\frac{2}{5}\pi} \tag{3}$$

The second of the assumptions presented above can be addressed by using depth factors d_γ and d_q:

$$q_u = 0.5\gamma B N_\gamma d_\gamma + q N_q d_q \tag{4}$$

These depth factors account for the resistance of the soil above the footing base and several proposals have been made. Amongst these proposals, are (Meyerhof, 1963):

$$d_\gamma = d_q = 1 + 0.1 \tan\left(\frac{\pi}{4} + \frac{\phi'}{2}\right)\frac{D}{B} \tag{5}$$

and from Brinch Hansen (1970) and Vesic (1973):

$$d_\gamma = 1 \tag{6}$$

$$d_q^{\frac{D}{B} \le 1} = 1 + 2\tan\phi'(1 - \sin\phi')^2 \frac{D}{B} \tag{7}$$

$$d_q^{\frac{D}{B} > 1} = 1 + 2\tan\phi'(1 - \sin\phi')^2 \tan^{-1}\frac{D}{B} \tag{8}$$

In the present work the depth factor d_γ will be considered equal to 1. This was assumed by Brinch Hansen and by Vesic and seems to be the appropriate theoretical value for this factor.

Armando Nunes Antão, Assistant Professor, UNIC, DEC, Faculdade de Ciências e Tecnologia, Universidade Nova de Lisboa, Portugal. e-mail: “amna@fct.unl.pt.
Mário Vicente da Silva, Assistant Professor, UNIC, DEC, Faculdade de Ciências e Tecnologia, Universidade Nova de Lisboa, Portugal. e-mail: vicente.silva@fct.unl.pt.
Nuno M. da Costa Guerra, Associate Professor, UNIC, DEC, Faculdade de Ciências e Tecnologia, Universidade Nova de Lisboa, Portugal. e-mail: nguerra@fct.unl.pt.
Submitted on March 25, 2009; Final Acceptance on August 12, 2009; Discussion open until September 30, 2010.

In fact, if depth factors take into account the resistance of the soil above the footing base, the first part of Eq. (4), being obtained using $q = 0$, should need no depth correction.

The paper will, then, deal with the depth factor d_q and its determination.

2. Using Limit Analysis for Determining Bearing Capacity of Footings

The bearing capacity calculations which will lead to the determination of depth factors d_q that are used in this paper are performed using numerical limit analysis.

A finite mixed element formulation which implements the upper bound theorem of limit analysis was used. External forces are considered in two types: fixed forces and variable ones, which are affected by a collapse load multiplier. Scaling the mechanism by setting the work rate of the variable external forces equal to one, the optimisation algorithm performs the minimisation of the difference between the plastically dissipated work rate and the work rate of the fixed external forces. The calculations of the present paper were made using a parallel implementation of the above mentioned tool (Vicente da Silva & Antão, 2008), which allows the use of very fine meshes and, therefore, good approximations of the collapse loads.

As is traditionally considered in the determination of depth factors, only 2D analysis were performed. The influence of the length of the footing on the bearing capacity expression is usually considered by the use of shape factors s_γ and s_q, which are not covered in this work.

Initial calculations are performed to evaluate the accuracy of the method and of the level of refinement of the finite element mesh. These calculations considered the situation presented in Fig. (1a), using a null unit weight for the soil. The bearing capacity $q_{u,a}^{UB}$ was numerically determined for $q = 1$ $[FL^{-2}]$, $B = 2[L]$ and for ϕ' equal to 25, 30, 35, 40 and 45°. This made it possible to determine the values of the bearing capacity factor N_q using the second part of Eq. (1):

$$N_q = \frac{q_{u,a}^{UB}}{q} \tag{9}$$

In these calculations, as in all other presented in this work, the footing was considered rigid and the contact of the base of the footing with the soil below was assumed as rough (Fig. 2). In these initial calculations there is no soil above the footing base.

The mechanism represented in Fig. 3(a) for $D/B = 0$ is the one obtained from those calculations for the case $\phi' = 35°$. The obtained results of N_q for all analysed values of ϕ' are presented in Fig. 4 and show a very good agreement with the theoretical values given by Eq. (2).

Calculations for the determination of depth factors d_q assumed the geometry presented in Fig. 1(b). Soil below the footing base was considered weightless ($\gamma_1 = 0$), and soil above this base had a unit weight $\gamma_2 = 20$ $[FL^{-3}]$, therefore corresponding to a surcharge $q = \gamma_2 D$. The ratios D/B were considered in the range [0.1;2]. Contact between the footing and the soil was assumed as in Fig. 2: rough at the base and smooth laterally.

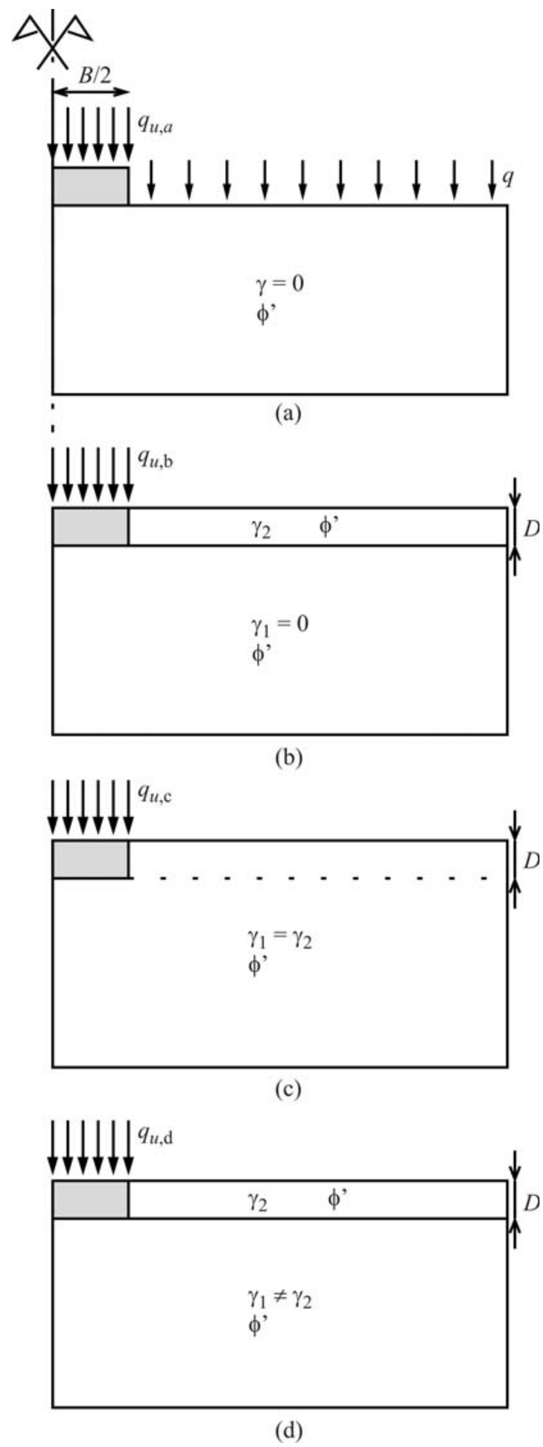

Figure 1 - Geometry considered in the calculations.

In all calculations about 10^6 3-noded triangular linear finite elements were used. The size of the analysed soil was adapted in function of the *D*/*B* ratio and friction angle in order to adapt the size of the mesh to the size of the plastic zones when failure is obtained.

Later in the paper the situations presented in Figs. 1(c) and (d) will also be considered for comparison with other results.

3. Results

For the cases shown in Fig. 1(b) the bearing capacity $q_{u,b}^{UB}$ was determined in the calculations and the second part of Eq. (4) was used to determine the depth factor d_q:

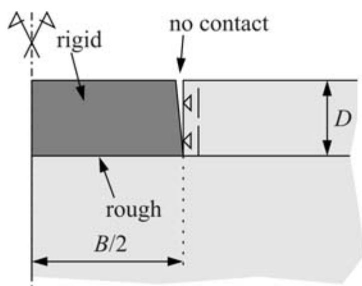

Figure 2 - Details of the footing-soil contact modelling.

$$d_q = \frac{q_{u,b}^{UB}}{qN_q} \tag{10}$$

The theoretical values of the bearing capacity factor N_q given by Eq. (2) were used in this equation. Results of

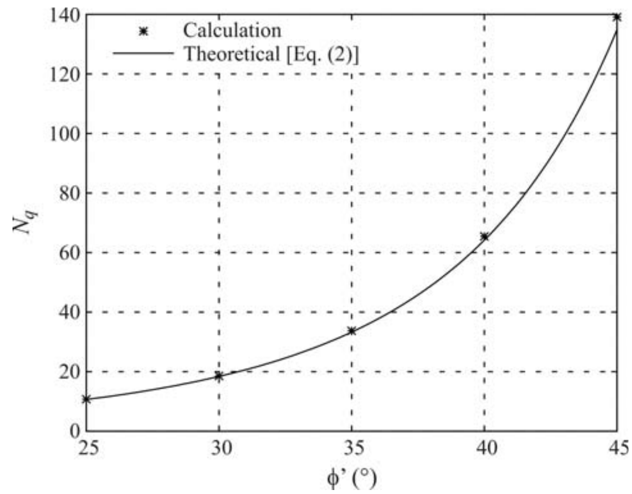

Figure 4 - Comparison between the values of the bearing capacity factor N_q obtained from limit analysis calculations and the theorical ones.

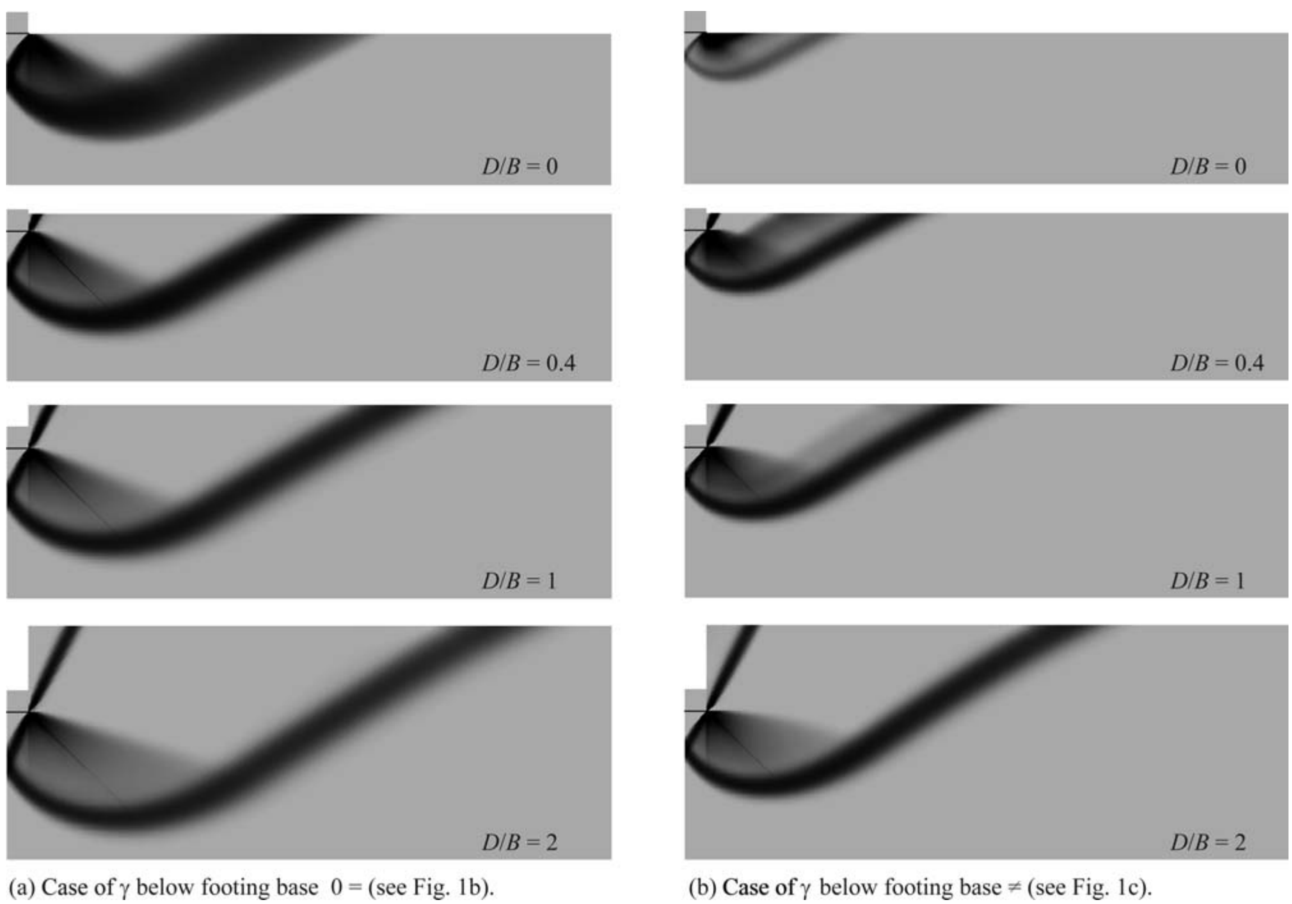

Figure 3 - Failure mechanisms for different *D*/*B* ratios and for ϕ' = 35° [note: for figure (a) *D*/*B* = 0 a surcharge *q* was applied on the soil surface].

the depth factor d_q are presented in Fig. 5. Figure 5(a) compares the results obtained for two values of the soil friction angle (25° and 45°) with classical solutions and Fig. 5(b) presents values for all friction angles analysed in the present study.

Analysis of Fig. 5 allows the following remarks:

• Meyerhof's values are consistently greater than those obtained by the numerical calculations performed for this work, and therefore they seem to be unsafe, particularly for lower values of the friction angle;

• Brinch Hansen's values are closer to those obtained by the numerical calculations; however, for D/B less than 1 they also give unsafe results; this is also particularly true for the lower values of the friction angle;

• For a given value of D/B, numerical results are less variable with the friction angle of the soil than the ones obtained by either method (Meyerhof or Brinch Hansen);

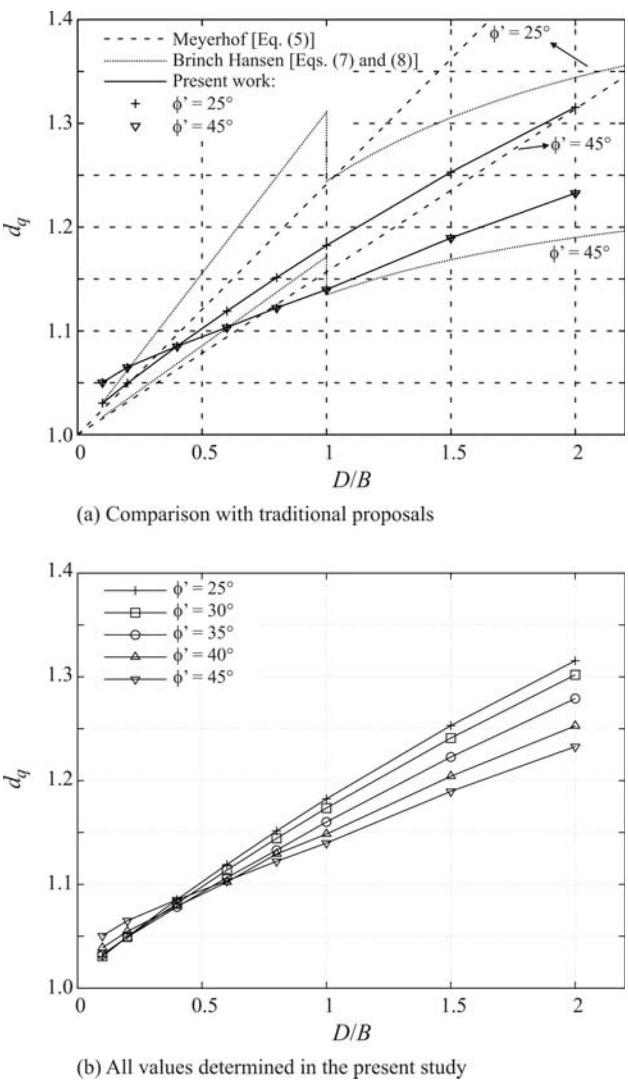

Figure 5 - Values of the depth factor d_q obtained from calculations.

• The depth factor d_q is greater for greater values of the ratio D/B; it is close to the unity for D/B close to zero and can reach 1.3 for ϕ' = 25° and D/B = 2;

• The depth factor d_q is greater for lesser values of the friction angle.

The influence of the D/B ratio on the depth factor d_q can also be observed by analysing the failure mechanisms for a given value of friction angle. This is represented in Fig. 3(a), for the case of ϕ' = 35°. It should be noticed that the graphics in this figure are for representation purposes and were obtained using a simplified finite element mesh (of about 10^5 elements) and the width of the mesh was kept constant.

The analysis of this figure makes it possible to see that there is a clear influence of the D/B ratio on the failure mechanism. This influence is not only and most obviously seen on the soil above the footing plane but also on the soil below: a greater D/B ratio results on a wider failure mechanism (even below the footing plane) but also on a deeper one. It should, however, be noticed that this influence is moderate: in fact, for the case represented (ϕ' = 35°), the mechanism for D/B = 2 is only about 15% wider (below the footing base) and 20% deeper than the one for D/B = 0. This can probably explain the more or less linear dependence of the depth factor from the D/B ratio.

4. Comments on the Validity of the Superposition of Effects

Equations (1) and (4) are approximations which consider the superposition of the effects given by the first and the second portions of the sum. It is well known that this approximation underestimates the collapse load of the problem represented in Fig. 1(c) (Terzaghi & Peck, 1967). This situation was also considered in a new set of calculations, so that a collapse load $q^{UB}_{u,c}$ could be obtained.

The failure mechanisms for this situation is shown (for ϕ' = 35°) in Fig. 3(b). It can be seen that the failure mechanisms are clearly not the same as those obtained for the determination of d_q. Their width and depth are lower than the ones previously obtained. The influence of D/B is much more clear in the mechanism: for D/B = 2 is about 75% wider (below the footing base) and deeper than the one for D/B = 0.

Figure 6 shows the results obtained by these calculations divided by the sum of $q^{UB}_{u,b}$ with the first portion of Eq. (4):

$$\chi_c = \frac{q^{UB}_{u,c}}{q^{UB}_{u,b} + 0.5\gamma_1 B N_\gamma} \tag{11}$$

where N_γ was determined using Eq. (3). It can be seen that values of χ_c range between 1.16 and 1.31 for the cases analysed. It should be noticed that χ_c - 1 can be interpreted as a measure of the error of Eq. (4) if the values of d_q determined in this paper and shown in Fig. 5 are used. This means, therefore, that bearing capacity obtained from the numerical cal-

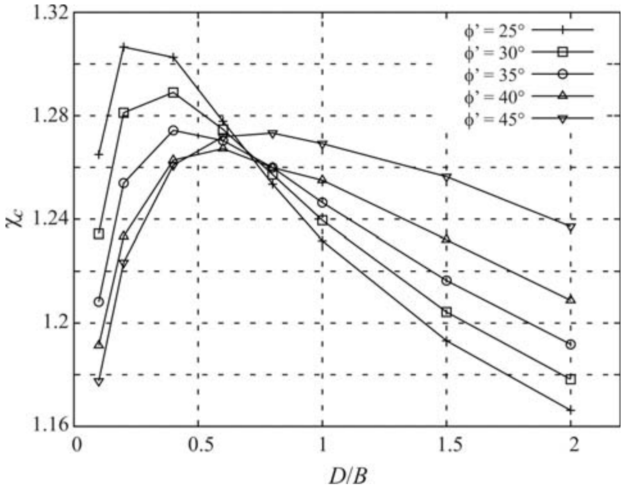

Figure 6 - Ratio χ_c obtained from Eq. (11).

culations are about 15 to 30% greater than the one estimated by Eq. (4). It is interesting to notice that *D/B* has a greater influence on this error estimation for the lower values of the friction angle and that it decreases with increasing *D/B* from a value of 0.2 to 0.8, depending on the friction angle (Fig.6). An approach where a depth factor (in the present work d_q^* will be used) takes into account the superposition effects (Lyamin *et al.*, 2007) can also be considered. This was achieved by using the following equation:

$$d^*_{q,c} = \frac{q^{UB}_{u,c} - 0.5\gamma_1 B N_\gamma}{q N_q} \quad (12)$$

Figure 7 presents the comparison between the results obtained from this equation using the (upper bound) calculations from the present study and the results obtained from published upper bound solutions (Lyamin *et al.*, 2007). It should be noticed that those authors performed both upper bound and lower bound calculations.

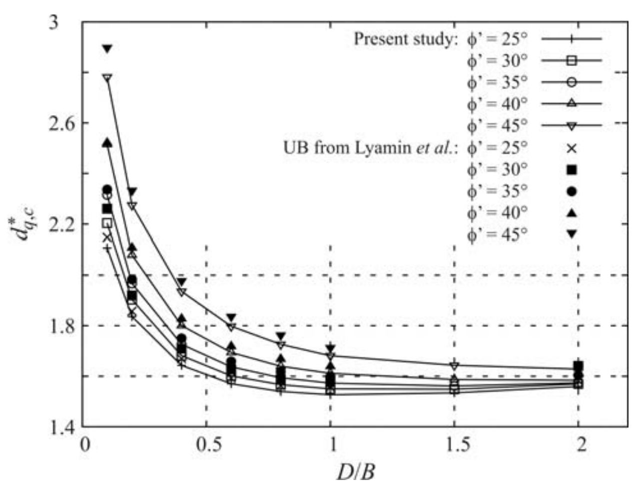

Figure 7 - Comparison between depth factor $d^*_{q,c}$ (Eq. 12) obtained from the calculations of the present work and the upper-bound ones from Lyamin *et al.* (2007).

It can be seen from the analysis of this figure that results are very similar, with a slight improvement in the results from the present work.

Figures 6 and 7 were obtained for the case presented in Fig. 1(c), where $\gamma_1 = \gamma_2$. Results for $\gamma_1 \neq \gamma_2$ will be different and will depend on the ratio between the two unit weights. Soils, however, do not usually have significant differences in the unit weight and, therefore, an idealized model where γ_1 would be much different from γ_2 is not realistic, except for the case where the water level is coincident with the footing base. For this situation calculations can be made using γ_1 equal to the effective unit weight of the submerged soil. The following results assume that γ_1 = 10 [FL^{-3}] and γ_2 = 20 [FL^{-3}] and case (d) of Fig. 1 was considered for the determination of the bearing capacity. New values of χ can, therefore, be computed using the following equation:

$$\chi_d = \frac{q^{UB}_{u,d}}{q^{UB}_{u,b} + 0.5\gamma_1 B N_\gamma} \quad (13)$$

and results are compared in Fig. 8 with the previously obtained ones. It can be seen that values of χ_d are lesser than those of χ_c. This could be expected, as results obtained with a smaller value of γ_1 will naturally be closer to the one obtained using γ_1 = 0, which means that the values of χ are closer to the unity. In fact, bearing capacity obtained from the numerical calculations for this case are about 10 to 30% greater than the estimate given by Eq. (4).

Obtaining new values of the bearing capacity for the case γ_1 = 10[FL^{-3}] also means that new values of d_q^* can be obtained:

$$d^*_{q,d} = \frac{q^{UB}_{u,d} - 0.5\gamma_1 B N_\gamma}{q N_q} \quad (14)$$

Results of this depth factor are presented in Fig. 9, where they can be compared with those previously obtained.

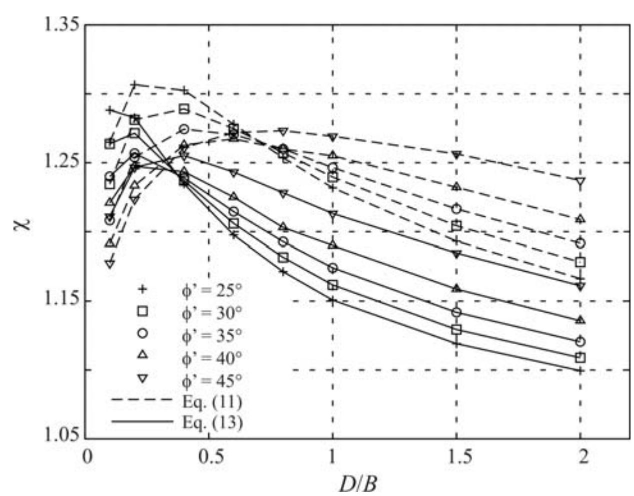

Figure 8 - Comparison between ratios χ obtained from Eq. (11) for γ_1 = 20[FL^{-3}], and Eq. (13), for γ_1 = 10[FL^{-3}].

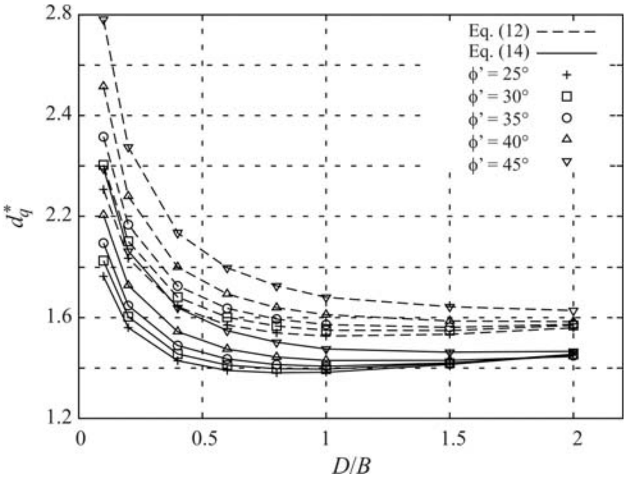

Figure 9 - Comparison between depth factor d_q^* obtained in the present work using Eq. 12, for $\gamma_1 = 20[FL^{-3}]$, and Eq. (14), for $\gamma_1 = 10[FL^{-3}]$.

It can be seen that results now obtained for this factor are significantly lower than the ones previously determined, which shows the influence of the value of the soil unit weight.

5. Conclusions

Resistance of the soil above the footing base can be taken into account by using depth factors, d_γ and d_q which correct, for practical purpuses, the bearing capacity formula for this effect. Commonly used proposals for these factors have been made by Meyerhof (1963) and Brinch Hansen (1970) and Vesic (1973).

Following previous proposals, depth factor d_γ was assumed equal to 1. Using two-dimensional upper bound numerical limit analysis, a proposal for depth factor d_q was presented and compared with the classical ones.

Further analysis made it possible to assess the validity of the superposition of effects classically assumed in bearing capacity formulas. For the analysed situations, bearing capacity is about 10 to 30% greater than the one determined by those formulas.

The same calculation results also allowed to determine values for a different depth factor d_q^* – originally defined by other authors – which correct the underestimation of the classic bearing capacity formula. The results obtained for the case where soil below and above the footing base have the same unit weight are quite similar to the ones obtained using upper bound methods by other authors, slightly improving them.

It could also be established that, for the case of submerged soil below the footing base, lower values should be used and were determined.

Acknowledgments

The authors would like to thank the financial contributions given to this paper by Fundação para a Ciência e Tecnologia (Project PTDC/ECM/70368/2006).

References

Brinch Hansen, J. (1970) A revised and extended formula for bearing capacity. Bulletin of The Danish Geotechnical Institute, v. 28 p. 5-11.

Hjiaj, M.; Lyamin, A.V. & Sloan, S.W. (2005) Numerical limit analysis solutions for the bearing capacity factor N_γ. International Journal of Solids and Structures, v. 42:5-6, p. 1681-1704.

Lyamin, A.V.; Salgado, R.; Sloan, S.W. & Prezzi, M. (2007) Two- and three-dimensional bearing capacity of footings in sand. Géotechnique, v. 47:8, p. 647-662.

Martin, C.M. (2005) Exact bearing capacity calculations using the method of characteristics. Proc. 11th Int. Conf. IACMAG, Turin, v. 4, pp. 441-450.

Meyerhof, G.G. (1963) Some recent research on bearing capacity of foundations. Canadian Geotechnical Journal, v. 1:1, p. 16-26.

Terzaghi, K. (1943) Theoretical Soil Mechanics, 2nd ed. John Wiley and Sons, New York, 510 pp.

Terzaghi, K. & Peck, R.B. (1967) Soil Mechanics in Engineering Practice, 2nd ed. John Wiley and Sons, New York, 729 pp.

Vesic, A.S. (1973) Analysis of ultimate loads of shallow foundations. ASCE Journal of Soil Mechanics and Foundation Division, v. 99:1, p. 45-73.

Vicente da Silva, M. & Antão, A.N. (2008) Upper bound limit analysis with a parallel mixed finite element formulation. International Journal of Solids and Structures, v. 45:22-23, p. 5788-5804.

Symbols

B: footing width
d_γ, d_q: depth factors
d_q^*: depth factor taking into account the superposition of effects, as defined by Lyamin *et al.* (2007)
$d_{q,c}^*$, $d_{q,d}^*$: depth factor taking into account the superposition of effects for the cases of Figs. 1(c) and 1(d).
D: depth of the footing base
N_γ, N_q: bearing capacity factors
q: surcharge at the footing base level
q_u: bearing capacity
$q_{u,a}^{UB}$, $q_{u,b}^{UB}$, etc.: upper bound bearing capacity calculation for the case of Figs. 1(a) and 1(b), etc.
s_γ, s_q: shape factors
χ_c, χ_d: ratio between $q_{u,c}^{UB}$, $q_{u,d}^{UB}$ and the bearing capacity determined by the classical bearing capacity equation
ϕ': soil friction angle
γ: soil unit weight
γ_1: soil unit weight below the footing base level
γ_2: soil unit weight above the footing base level

SOILS and ROCKS
An International Journal of Geotechnical and Geoenvironmental Engineering

Publication of

ABMS - Brazilian Association for Soil Mechanics and Geotechnical Engineering
ABGE - Brazilian Association for Engineering Geology and the Environment
SPG - Portuguese Geotechnical Society

Volume 33, N. 1, January-April 2010

Author index

Instructions to Authors

Category of the Papers

Soils and Rocks is the scientific journal edited by the Brazilian Society of Soil Mechanics and Geotechnical Engineering (ABMS) and by the Brazilian Society of Engineering and Environmental Geology (ABGE). The journal is intended to the divulgation of original research works from all geotechnical branches.

The accepted papers are classified either as an Article paper, a Technical Note, a Case Study, or a Discussion according to its content. An article paper is an extensive and conclusive dissertation about a geotechnical topic. A paper is considered as a technical note if it gives a short description of ongoing studies, comprising partial results and/or particular aspects of the investigation. A case study is a report of unusual problems found during the design, construction or the performance of geotechnical projects. A case study is also considered as the report of an unusual solution given to an ordinary problem. The discussions about published papers, case studies and technical notes are made in the Discussions Section.

When submitting a manuscript for review, the authors should indicate the category of the manuscript, and is also understood that they:

a) assume full responsibility for the contents and accuracy of the information in the paper;

b) assure that the paper has not been previously published, and is not being submitted to any other periodical for publication.

Manuscript Instructions

Manuscripts must be written in English. The text is to be typed in a word processor (MS Word or equivalent), using ISO A4 page size, left, right, top, and bottom margins of 25 mm, Times New Roman 12 font, and line spacing of 1.5. All lines and pages should be numbered. The text should be written in the third person.

The fist page of the manuscript is to include the title of the paper in English, followed by the names of the authors with the abbreviation of the most relevant academic title. The affiliation, address and e-mail is to be indicated below each author's name. An abstract of 200 words is to be written in English after the author's names. A list with up to six keywords at the end of the abstract is required.

Although alteration of the sequence and the title of each section may be required, it is suggested that the text contains the following sections: Introduction, Material and Methods, Results, Discussions, Conclusion, Acknowledgements, References and List of Symbols. A brief description of each section is given next.

Introduction: This section should indicate the state of the art of the problem under evaluation, a description of the problem and the methods undertaken. The objective of the work is to be clearly presented at the end of the section.

Materials and Methods: This section should include all information needed to the reproduction of the presented work by other researchers.

Results: In this section the data of the investigation should be presented in a clear and concise way. Figures and tables should not repeat the same information.

Discussion: The analyses of the results should be described in this section. **Conclusions**: The text of this section should be based on the presented data and in the discussions.

Acknowledgenments: If necessary, concise acknowledgements should be written in this section.

References: References to other published sources are to be made in the text by the last name(s) of the author(s), followed by the year of publication, similarly to one of the two possibilities below:

"*while Silva & Pereira (1987) observed that resistance depended on soil density*" or "*It was observed that resistance depended on soil density (Silva & Pereira, 1987).*"

In the case of three or more authors, the reduced format must be used, *e.g.*: Silva *et al.* (1982) or (Silva *et al.*, 1982). Two or more citations belonging to the same author(s) and published in the same year are to be distinguished with small letters, *e.g.*: (Silva, 1975a, b, c.). Standards must be cited in the text by the initials of the entity and the year of publication, *e.g.*: ABNT (1996), ASTM (2003).

Full references shall be listed alphabetically at the end of the text by the first author's last name. Several references belonging to the same author shall be cited chronologically. Some examples are listed next:

Papers: Bishop, A.W. & Blight, G.E. (1963) Some aspects of effective stress in saturated and unsaturated soils. Géotechnique, v. 13:2, p. 177-197.

Books: Lambe, T.W & Whitman, R.V. (1979) Soil Mechanics, SI Version, 2nd ed. John Wiley & Sons, New York, p. 553.

Book with editors: Sharma, H.D.; Dukes, M.T. & Olsen, D.M. (1990) Field measurements of dynamic moduli and Poisson's ratios of refuse and underlying soils at a landfill site. Landva A. & Knowles, G.D. (eds) Geotechnics of Waste Fills - Theory and Practice, American Society for Testing and Materials - STP 1070, Philadelphia, p. 57-70.

Proceedings (printed matter or CD-ROM): Jamiolkowski, M.; Ladd, C.C.; Germaine, J.T & Lancellotta, R. (1985) New developments in field and laboratory testing of soils. Proc. 11th Int. Conf. on Soil Mech. and Found. Engn., ISSMFE, San Francisco, v. 1, pp. 57-153.(specify if CD – ROM)

Thesis and dissertations: Lee, K.L. (1965) Triaxial Compressive Strength of Saturated Sands Under Seismic Loading Conditions. PhD Dissertation, Department of Civil Engineering, University of California, Berkeley, 521 p.

Standards: ASTM (2003) Standard Test Method for Particle Size Analysis of Soils - D 422-63. ASTM International, West Conshohocken, Pennsylvania, USA, 8 p.

Internet references: Soils and Rocks available at http://www.abms.com.br.

On line first publications must also bring the digital object identifier (DOI) at the end.

Figures shall be either computer generated or drawn with India ink on tracing paper. Computer generated figures must be accompanied by the corresponding digital file (.tif, .jpg, .pcx, etc.). All figures (graphs, line drawings, photographs, etc.) shall be numbered consecutively and have a caption consisting of the figure number and a brief title or description of the figure. This number should be used when referring to the figure in text. Photographs should be black and white, sharp, high contrasted and printed on glossy paper.

Tables shall be numbered consecutively in Arabic and have a caption consisting of the table number and a brief title. This number should be used when referring to the table in text. Units should be indicated in the first line of the table, below the title of each column. Abbreviations should be avoided. Column headings should not be abbreviated. When applicable, the units should come right below the corresponding column heading. Any necessary explanation can be placed as footnotes.

Equations shall appear isolated in a single line of the text. Numbers identifying equations must be flush with the right margin. International System (SI) units are to be used. The symbols used in the equations shall be listed in the List of Symbols. It is recommended that the used symbols be in accordance with Lexicon in 8 Languages, ISSMFE (1981) and the ISRM List of Symbols.

The text of the submitted manuscript (including figures, tables and references) intended to be published as an article paper or a case history should not contain more than 30 pages formatted according to the instructions mentioned above. Technical notes and discussions should have no more than 15 and 8 pages, respectively. Longer manuscripts may be exceptionally accepted if the authors provide proper explanation for the need of the required extra space in the cover letter.

Discussion

Discussions must be written in English. The first page of a discussion paper should contain:

• The title of the paper under discussion in the language chosen for publication;

• Name of the author(s) of the discussion, followed by the position, affiliation, address and e-mail. The discusser(s) should refer himself (herself, themselves) as "the discusser(s)" and to the author(s) of the paper as "the author(s)".

Figures, tables and equations should be numbered following the same sequence of the original paper. All instructions previously mentioned for the preparation of article papers, case studies and technical notes also apply to the preparation of discussions.

Editorial Review

Each paper will be evaluated by reviewers selected by the editors according to the subject of the paper. The authors will be informed about the results of the review process. If the paper is accepted, the authors will be required to submit a version of the revised manuscript with the suggested modifications. If the manuscript is refused for publication, the authors will be informed about the reasons for rejection. In any situation comprising modification of the original text, classification of the manuscript in a category different from that proposed by the authors, or refusal for publication, the authors can reply presenting their reasons for disagreeing with the reviewers' comments

Submission

The author(s) must submit for review:

1. A hard copy of the manuscript to Editors - Soils and Rocks, Av. Prof. Almeida Prado, 532 – IPT, Prédio 54 – DEC/ABMS, 05508-901 - São Paulo, SP, Brazil. The first page of the manuscript should contain the identification of the author(s), or

2. The digital file of the manuscript, omitting the authors' name and any information that eventually could identify them, should be sent to **abms@ipt.br**. The following must be written in the subject of the e-mail message: "*Paper submitted to Soils and Rocks*". The authors' names, academic degrees and affiliations should be mentioned in the e-mail message. The e-mail address from which the digital file of the paper was sent will be the only one used by the editors for communication with the corresponding author.

Follow Up

Authors of manuscripts can assess the status of the review process at the journal website (www.soilsandrocks.com.br) or by contacting the ABMS secretariat.

Volume 33, N. 1, January-April 2010

Table of Contents